ADVANCED TECHNOLOGY LABORATORIES

DESIGN CRITERIA FOR ZERO-LEAKAGE CONNECTORS FOR LAUNCH VEHICLES, VOL. 5, PRESSURE ENERGIZED SEALS

Edited by
B.T. FANG

CONTRACT NAS 8-4012

MARCH 15, 1963

GENERAL ELECTRIC

FINAL REPORT FOR FIRST CONTRACT PERIOD

(March 1962 through February 1963)

DESIGN CRITERIA
FOR ZERO-LEAKAGE CONNECTORS
FOR LAUNCH VEHICLES

Contract NAS 8-4012

VOLUME 5
PRESSURE-ENERGIZED SEALS

Edited by B.T. Fang

March 15, 1963

PREPARED FOR: Propulsion and Vehicle Engineering Division
George C. Marshall Space Flight Center
National Aeronautics and Space Administration
Huntsville, Alabama

PREPARED BY: Advanced Technology Laboratories
General Electric Company
Schenectady, New York

SPONSORED BY: Missile and Space Division
General Electric Company
Philadelphia, Pennsylvania

N.A.S.A. TECHNICAL MANAGER: C.C. Wood (M-P&VE-PT)

CONTENTS

51. CANTILEVER-TYPE PRESSURE-ENERGIZED SEALS

by

J. Wallach

12391

51.0 Summary

Pressure-energized static seals are used between the flanges of a flanged joint to form a leak-tight seal between the flanges and maintain this seal as the internal pressure is increased and the flanges tend to separate. The characteristics and design of the cantilever type of pressure-energized seals are presented in this section. O-ring type seals are discussed in Section 52.

The geometry and materials of many of the seals used in the missile industry are similar enough to allow their analysis using a small number of generalized mathematical models. Each model is analyzed and curves of its characteristics calculated for a set of typical dimensions. The designer can compare his requirements with the characteristics of the various types of seals and choose the most appropriate one. Then he completes the detailed design of the seal by using the design formulas in the section for that particular seal.

The derivations of the design formulas are in the appendix, Section 51.5. Included in these derivations are other formulas of less frequent interest. Section 51.5.8 of the appendix is devoted to the justification of the use of beam theory in the derivation of the design formulas.

51.1 Introduction

Static seals for use with pipe flanges where high internal pressures are encountered are usually pressure-energized. High internal pressures cause flange separation and unless the initial bolting stresses are very high may reduce the seal-to-flange face contact pressure to a point where leakage occurs. The use of high bolt stresses means larger bolts and flanges and a resultant increases in weight. In order to avoid this weight increase and maintain a sufficiently large seal-to-flange sealing pressure, the seal is designed so that an increase in pressure results in an increase in the sealing force.

The flanges are designed to preload the seal to furnish a minimum seal-to-flange sealing force for zero internal pressure. Otherwise the effect of the flange on the seal is minimized. A typical design has the seal sitting in a recess in the flange, see Fig. 51.1. The difference between the free height of the seal and restrained height results in a preloading of the seal. The restrained height is also affected by the bolt load and resulting compression in the flange faces. However, this effect is small as compared to the difference between the free height and the depth of the recess.

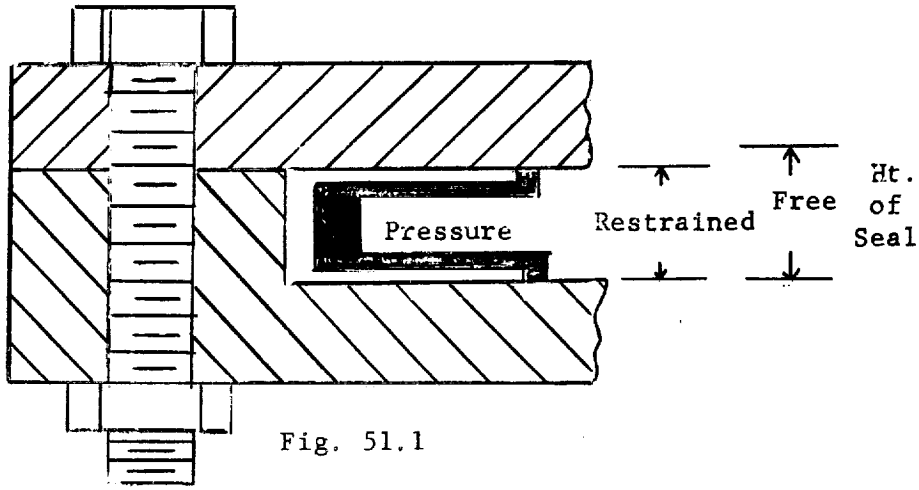

Fig. 51.1

INSTALLATION OF CANTILEVER-TYPE PRESSURE ENERGIZED SEAL

Therefore, the effect of the bolt load on the seal is secondary. The bolt pre-load need only be sufficient to keep the flange faces in contact under all loading conditions.

The sealing of the fluid depends primarily on the seal-to-flange sealing force. As the flange and seal are usually both made of a high-strength metal, the seal lip contacting the flange is often covered with a softer material such as Teflon. The plastic flow of this softer material effects the seal. The minimum sealing force required is determined by the properties of this material.

An analysis is needed to determine the sealing force characteristics for various types of pressure-energized seals. In this section various seal designs are analized to determine the deflection, stress, and sealing force, and to generate design formulas and methods. A number of generalized designs

are chosen which are representative of the seals in use in the missile industry. The mathematical models combine simplicity and design accuracy. Because of the recessed flange face the seal analysis considers only the seal and neglects the surrounding structure.

51.2 Nomenclature

		Units
a,b	Constants	
A	Amplitude of edge deflection variation	inches
d	$12(1-\nu^2)/E$	$inch^2/lb$
D	Flexural rigidity $Eh^3/12(1-\nu^2)$	inch-lb
E	Modulus of elasticity	psi
F	Force	lb/in
h	Thickness of seal leg	inches
H_F	Free height of seal	inches
H_R	Restrained height of seal	inches
I_c	Area moment about the centroid	in^4
k	Axial distance from seal centerline to outside surface of seal leg	inches
K	Constants of integration	
ℓ	Length of seal leg	inches
L	Axial length	inches
m	Reciprocal Poisson's ratio	
M	Moment	inch lb/in
n	Length of seal lip	inches
p	Pressure	psi
r	Radius of seal	inches
R	Edge load or reactive load	lb/in
R_s	Sealing force	lb/in
Q	Shear	lb/in
t	Web thickness	inches
V	Total edge shear	lb/in
w	Circumferential length	inches
x	Length along beam (seal leg)	inches
y	Transverse deflection	inches
z	Circumferential linear coordinate	inches
δ_A	Axial deflection	inches
δ_m	Membrane deflection (radial)	inches
δ_r	Radial deflection	inches
ϵ	Percent error	
μ	Coefficient of friction	
ν	Poisson's ratio	
σ	Stress with subscripts b - using beam theory m - maximum p - using plate theory s - using shell theory	psi
ϕ	Angle	radians

51.3 Design of Seals

Three general types of pressure-energized seals are analyzed and discussed in this section. For each type of seal considered, a design procedure, design equations, and curves for a typical seal showing the seal's characteristics are presented. The analysis for each seal is given in the appendix, Section 51.5, as noted by the references. In addition to the design equations, included in the appendix, Section 51.5 are the equations for the seal leg deflection and stress, and the seal-to-flange sealing force.

The seal cross-section, as shown below, consists of a web and two legs with a small lip on the end of each leg. All of the cross-sectional dimensions are usually much smaller than the inside radius of the seal, and the seal legs are much more flexible than the web. Therefore, the seal is analyzed as three separate parts: Two identical legs and the web. The web designs considered are represented by one model, and the legs are represented by three different models:

1. Seal with Straight Leg of Constant Width (Section 51.3.1)
2. Seal with Straight Leg of Linearly Varying Thickness (Section 51.3.2)
3. Seal with Straight Leg of Constant Width without Lip (Section 51.3.3)

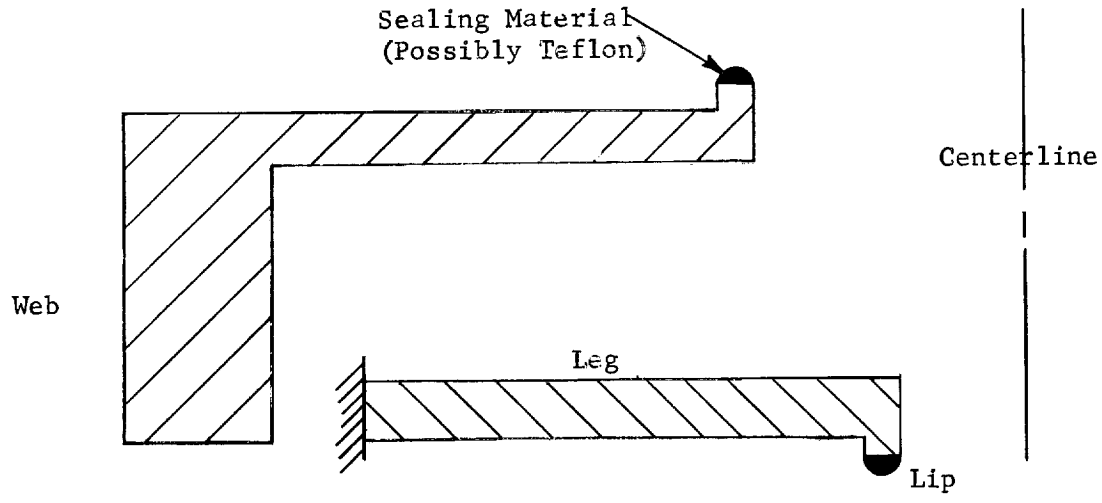

FIGURE 51.2 Cross-section of Cantilever Type Pressure Energized Seal

The characteristics of each of these models have been analyzed and with the use of typical dimensions are illustrated in Section 51.3.6. Based on the needs of a particular application, one of the seal leg designs may be chosen by a comparison of their characteristics.

The chosen seal configuration may then be designed by using the design procedures as outlined in this section. In each case it is assumed that the seal body material and its properties, the required sealing force, the maximum allowable stress, and the inside seal radius are known. The seal body materials used are usually steel or aluminum for their structural properties, provided they are compatible with the fluid contained. In any case the material could be specified and its modulus of elasticity and Poisson's ratio either known or readily determined. The required sealing force is determined from a consideration of the flange faces, sealing material on the seal lip, and pressure and properties of the retained fluid. The method of determining this sealing force is discussed in Volume 3 of this report. The maximum allowable stress is determined by the designer based on the seal material and application. The inside radius of the seal is usually slightly larger than the inside radius of the pipe and depends primarily on the flange design. The seal leg design is based on the above considerations.

The seal web is primarily a structural member, but it also has a direct effect on the sealing abilities of the seal. Radial motion between the seal lip and flange face will break a seal effected between the lip and flange and may cause leakage. Therefore, in the seal web design, consideration is given to the radial growth of the seal due to internal pressure and differential thermal growth of the flanges and seal. The seal is not as stiff as the flanges and will tend to grow more radially when pressurized. Relative motion between the seal and flange may result from different amounts of thermal expansion of the seal and flange, and it may occur due to a differential thermal growth of the flanges. If one flange grows more than the other, the seal will have to rotate about an axis normal to its cross-section, Figure 51.2, in order to follow the motion of the flanges. Otherwise the seal lip must slip on the flange face.

Making the seal and flange of the same material will tend to eliminate the problem of differential thermal expansion of the seal and flange. However, during thermal transients there is still the possibility of the seal and flange being at different temperatures. A stiffer seal web will decrease the differential radial growth of the seal and flange due to internal pressure, but will also make the seal cross-section more difficult to rotate about its own axis. Therefore, the web design is a balance between the need to limit the growth due to pressure and the ability to accommodate the flange motion. Also, consideration should be given to the design of the recess in the flange face. It is possible to limit the radial motion of the seal by using the flange recess as a backing to the seal web.

The depth of the flange recess where the seal sits, see Figure 51.1,

is one of the prime factors determining the sealing force. As shown in the figure, if the restrained height of the seal, H_R, is less than the free height of the seal, H_F, the seal is axially compressed. This axial compression is essential when installing the seal in order to insure seating the seal and preventing leakage at low pressures. As an axial tensile load is applied to the flanged joint, the flanges will separate and the restrained height of the seal increases. If this tensile load is applied prior to the pressurization of the joint, it is important that the restrained height remains less than the free height, otherwise the seal will separate from the flange. If the flanged joint is pressurized as the tensile load is applied, the pressure will force the seal leg to follow the flange separation. In this case, it is important to match the seal-leg deflection characteristics to those of the flanges so that the required sealing force is maintained. A decrease in the sealing force may cause leakage, and an increase may cause damage to the sealing material on the seal lip. In this section the restrained height of the seal is assumed known. The determination of the restrained height comes from the load-deflection analysis of the flanged joint. Each type of flanged joint may require a different analytical approach. Included in this report are analyses of some design examples illustrating different approaches, Section 13. Then the seal leg itself can be designed on the assumption that the flange face is flat. If the soft material coating were not used, it would be necessary to deform the seal lip plastically or to deform the seal leg to follow the contour of the asperity.

An analysis is included in Section 51.3.5 to determine the increase in internal pressure necessary to make the seal leg conform elastically to a sinusoidal edge restraint. A radial scratch in the flange face is simulated by making the peak-to-peak length of the sinusoid very small. Flange warpage can also be simulated by a long peak-to-peak length.

The seal leg cross-section shown in Figure 51.2 indicates that the seal leg is a circular flat plate. Also, in some seal designs the seal leg is a conical shell. However, in most seal leg designs the leg length is sufficiently smaller than the inside radius to analyze the leg as a beam. This procedure is used in this report, but not without justification. A set of curves are included in Section 51.5.8 showing the error incurred by applying beam theory to a particular seal leg. These errors are generally negligible for design purposes.

51.3.1 Seal with Straight Leg of Constant Width

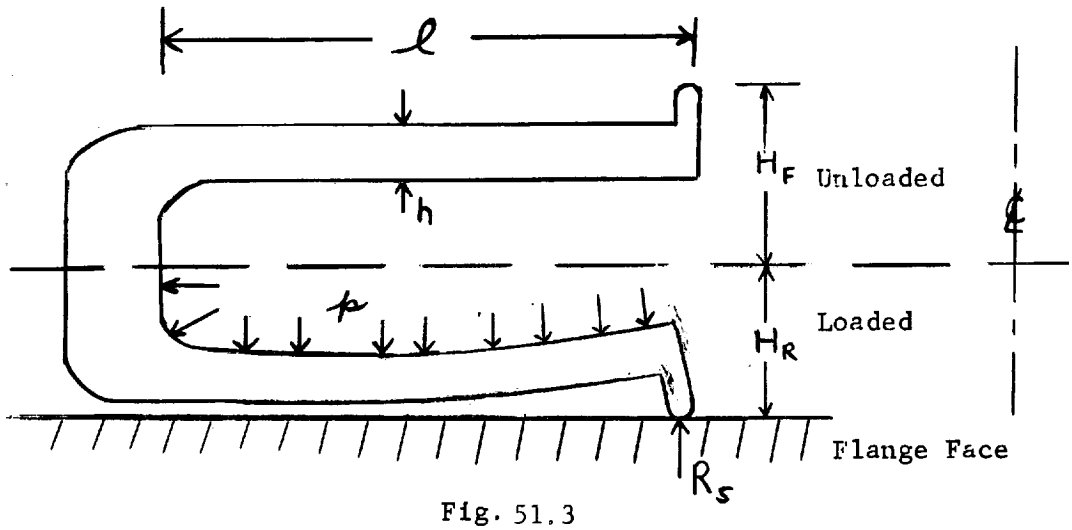

Fig. 51.3

SEAL CROSS-SECTION

The leg is analyzed as a built-in beam of length, ℓ, loaded by a uniform load p and deflected a distance y_ℓ by a simple support. The distance y_ℓ is the difference between the free height, H_F, and restrained height, H_R. The analysis determining the equations for the leg deflection and stresses, and the sealing force, R_s, is in the appendix, Section 51.5.1.

The dimensions for the cross-section are determined from the design equations of Section 51.5.1. Having determined the modulus of elasticity, Poisson's ratio, the minimum sealing force and maximum allowable stress, select one or more reasonable values of the length to thickness ratio, ℓ/h, and calculate y_ℓ from equation (5).

$$y_\ell = -\ (4R_s/E)\ (1-\nu^2)\ (\ell/h)^3 \qquad (5)$$

Calculate ℓ from equation (6)

$$\ell = \frac{6y_\ell E}{(1-\nu^2)\ (\ell/h)\left[4\sigma_m - 3p(\ell/h)^2\right]} \qquad (6)$$

Choose the most reasonable values of h and ℓ using design judgment.

If the seal leg is at an angle ϕ to the flange face, see Fig. 51.4, equation (5) changes to the following:

$$y_\ell = -\ (4R_s/E)\ (1-\nu^2)\ (\ell/h)^3 \cos\phi \qquad (9)$$

Equation (6) is the same as before, but the value of y_ℓ is changed to

$$y_\ell = -(H_F - H_R)/\cos\phi \qquad (1)$$

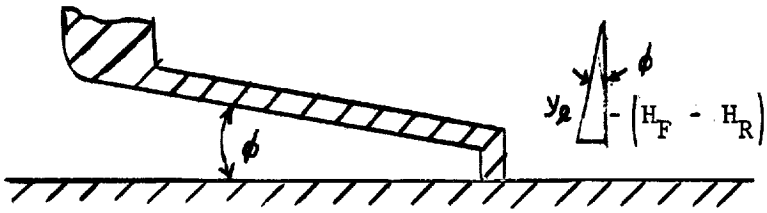

FIGURE 51.4 Seal Leg

The web design formulas are given in the appendix, Sec. 51.5.4. The web length is chosen as short as possible consistent with the overall structural requirements of the seal, see Section 51.3.4. The web thickness should be equal to or greater than the leg thickness at the web end of the leg. It must also be equal to or larger than the thickness calculated using equation (49). r_3 is the mean web radius.

$$t = p\, r_3/\sigma_m \qquad (49)$$

12

51.3.2 Seal With Straight Leg of Linearly Varying Thickness.

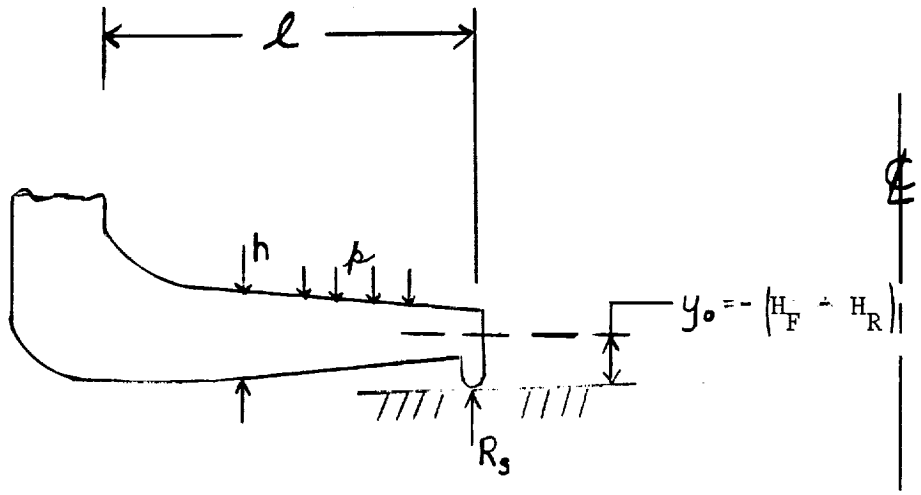

Fig. 51.5

TAPERED SEAL LEG

As in Section 51.3.1, the seal leg is analyzed as a built-in beam loaded by a uniform pressure load p and deflected a distance y_o by a simple support. The leg deflection and stress, sealing force and design equations are derived in the appendix, Section 51.5.2.

The design method begins with the specification of the modulus of elasticity, Poisson's ratio, minimum sealing force and maximum allowable stress. The initial deflection of the sealing end, y_o, required to give the minimum sealing force, R_s, is given by equation (21).

$$y_o = \frac{dR_s}{2b^3}\left[\frac{b\ell(2a + 3b\ell)}{(a + b\ell)^2} - 2\log(1 + b\ell/a)\right] \qquad (21)$$

Substituting equation (21) directly into the equation for the maximum bending stress (equation 20) results in a relationship relating a, b, and ℓ.

$$\sigma_m = \frac{3\ell}{(a + b\ell)^2}\left\{p\ell - 2R_s + \frac{p\left[\frac{b\ell}{(a + b\ell)^2}(6a^2 + 9ab\ell + 2b^2\ell^2) - 6a\log(1 + b\ell/a)\right]}{b\left[\frac{b\ell}{(a + b\ell)^2}(2a + 3b\ell) - 2\log(1 + b\ell/a)\right]}\right\} \qquad (22)$$

This is too complex to solve in general terms for either a, b or ℓ. To make the equation more tractable, assume a value for the leg thickness at both ends, a and h_ℓ.

$$h_\ell = a + b\ell$$

Another relation between b and ℓ is obtained from the above equation which may be solved for b.

$$b = (h_\ell - a)/\ell \qquad (23)$$

Substitution of values of a and h_ℓ reduces equation (22) by allowing numerical evaluation of the natural logarithm terms. Further substitution of equation (23) for b and all the other known parameters reduces equation (22) to a polynomial in ℓ. This equation can then be solved for ℓ and b can be determined from equation (23).

The calculated values may be unreasonable, in which case other values should be tried for a and h_ℓ. As an alternate procedure, σ_m may be unspecified and calculated for chosen values of a, b, and ℓ. Any calculated value of σ_m less than the maximum allowable is acceptable.

The web design is the same as that for the case described in Section 51.3.1. See also Section 51.3.4.

11

51.3.3 Seal with Straight Leg of Constant Width Without Lip

The seal is similar to the seal described in Section 51.3.1 except there is no lip at the end of the seal legs. The seal is effected between the seal leg and flange face. As the leg is usually at a small angle to the flange face, decreasing the restrained height, H_R, of the seal or increasing the internal pressure, p, causes the point of sealing to move closer to the seal web, see Figure 51.6.

As in Sections 51.3.1 and 51.3.2 the seal leg is analyzed as a built-in beam. The portion of the leg from $X = \ell_i$ to ℓ is in simple compression. A free-body diagram of this section shows that the end shears and moments must be zero. Therefore, the end moment on the other section of the leg ($x = 0$ to ℓ_i) must be zero and the end shear is only due to the reaction of the flange face, R_s. This means the sealing between the seal and flange is effected only along the line of contact (into the paper on Figure 53.6) at ℓ_i. For further information on the seal characteristics see Section 51.5.3 of the appendix.

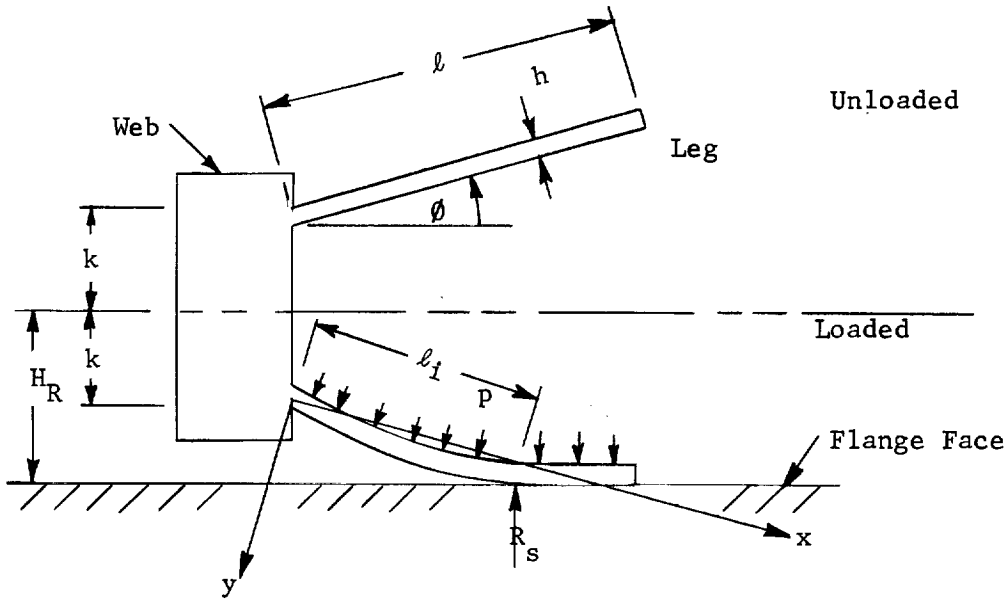

FIGURE 51.6

Cross-section of Seal with Straight Leg
of Constant Width Without Lip

The design of the seal begins with a choice of material and determination of the minimum sealing force, R_o, required. The web design is the same as that for the seal described in Section 51.3.1 and is discussed in Section 51.3.4. The leg design is an iterative procedure beginning with the selection of the lengths H_r, k, and y_ℓ. Then calculate the minimum leg length required using equation (47).

$$\ell_o = - \frac{3\, y_\ell\, (H_r - k)}{\sqrt{y_\ell^{\,2} - 4\,(H_r - k)^2}} \qquad (47)$$

This is the active leg length ℓ_i when the internal pressure is zero. Unless the leg length is greater than ℓ_o the seal leg will not effect a seal with the flange face at assembly.

Next calculate the seal leg thickness h.

$$h = \sqrt[3]{- \frac{216\,(1 - \nu^2)\, y_\ell\, R_o\, (H_R - k)^4}{E \left[y_\ell^{\,2} - 4\,(H_R - k)^2 \right]^{3/2}}} \qquad (45)$$

Then calculate the minimum active leg length ℓ_m.

$$\ell_m = \frac{(H_r - k) \sqrt[4]{216\, y_\ell^{\,2}\, R_o / P_m}}{\left[y_\ell^{\,2} - 4\,(H_r - k)^2 \right]^{3/8}} \qquad (46)$$

This is the active leg length when the internal pressure is a maximum (P_m). If the calculated dimensions do not constitute an acceptable design, choose other values of H_r, k and y_ℓ and repeat the calculations until an acceptable design is obtained. Where a number of iterations are required or a number of seals are to be designed, it is suggested that curves be plotted for equations (45), (46) and (47).

51.3.4 Radial Motion of the Seal Lip

As a separate design problem, the radial motion of the seal lip due to internal pressure and the rotation of the seal section is considered in this section. Both problems may be considered irrespective of the leg configuration and are, therefore, not included as part of the design consideration of a specific leg.

Each of the seals considered is loaded by a radial force proportional to the internal pressure and internal seal area. The radial growth of the seal is greater than that of the adjacent flanges because of its much lower stiffness. It is assumed that the flanges are rigid compared to the seal and therefore the seal radial growth may be taken as the radial growth of the seal relative to the flange face. This relative radial motion of the seal lip may prevent the forming of a good seal and cause leakage. It is probable that there is some minimum allowable value for which leakage will not occur.

The radial deflection of the seal due to internal pressure is determined in the appendix, Sec. 51.5.5. The analysis leads to an equation which sets an upper limit on the web length L. When the leg design has been completed, all of the parameters except the allowable radial deformation, δ_r, will have been determined. This parameter will be determined from tests and experience.

$$L = 2h\ell / \left[\left(p r_1^2 / E\delta_r \right) - t \right] \qquad (56)$$

Another cause of relative motion between the seal lip and flange face is any differential radial growth of the flange faces. A non-uniform temperature distribution or the use of dissimilar metals in the flange faces will result in a differential radial growth of the flange faces. The result is a moment applied to the seal by forces acting at the seal lips. These forces are equal to the coefficient of friction times the normal sealing force, R_s. Therefore, as the differential radial growth of the flange faces increases, the forces required to twist the seal increase and a point is reached where the frictional couple is unable to further twist the seal. At this point the seal lip must slip on the flange face and leakage may occur.

The sequence of design calculations assumes design of the seal leg prior to the web. Therefore, in designing the web the rotational rigidity of the seal is considered. Having calculated the differential radial growth of the flanges and determined the maximum allowable relative motion between the seal lip and flange face from tests and experience, the differential radial motion of the seal lips, $\Delta\delta_D$, may then be calculated. $\Delta\delta_D$ must be at least as large as the difference between the differential radial growth of the flanges and the maximum relative motion between the seal lip and flange face. Then the desired total area moment of the seal section may be calculated from equation (63)of the appendix, Section 51.5.6.

$$I_c = 4\mu R_s H_R^2 r_2^2 / E\delta_D \qquad (63)$$

This is the sum of the area moments of the seal legs and web. As I_c varies as the square of the web length, L, it may be possible to achieve the desired I_c by only verifying L.

The maximum bending stress due to the applied couple is a circumferential stress and the maximum is at the upper and lower seal surfaces, $\pm H_R$.

$$\sigma_m = E\delta_D / 2r_2 \qquad (62)$$

Other design approaches are possible using the equations in the appendix, Section 51.5.6.

51.3.5 Seal with Straight Leg of Constant Width Seating on Flange Face With Circumferential Waviness

In all of the seal leg analyses the flange face has been assumed perfectly flat. This is never the case, but may be closely enough approximated to be a reasonable assumption. In order to validate this assumption the effect of surface irregularities must be investigated. As an analysis of a general irregularity is difficult and may not be of greatest interest a simplified model was chosen.

The surface irregularity chosen is a groove running radially, whose cross-section in the circumferential direction is sinusoidal. The mean depth of the groove does not necessarily coincide with the flange face surface and the groove depth may be below the flange surface with a hill to either side, whose peak is above the flange surface.

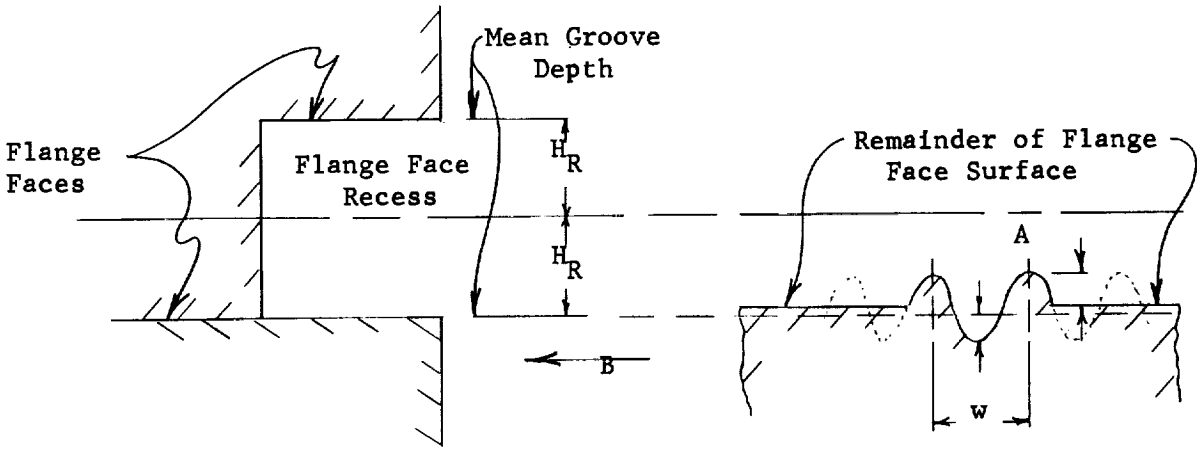

FIG. 51.7
Cross-section of Flange Recess

The groove is assumed part of a continuous sinusoidal wave (dotted line) with a cycle length of w. As shown above, the irregularity length is slightly more than w and blends in with the flat flange face to either side of w. The analysis of a seal leg of constant width seating on a flat surface is covered in Section 51.3.1. In this section only the analysis of the seal leg seating on the irregularity is considered. Whereas in the case of flat flange faces the restrained height of the seal, H_R, is one half the distance between the flange faces, in the case of an irregularity it is defined as the axial distance from the axial midpoint of the flange recess to the mean

groove depth. The initial deflection is then given by the same relation as for the flat flange face case.

$$y_\ell = -(H_F - H_R) \tag{64}$$

The coordinates, Fig.51.8 have their origin at the base of the seal leg. The half depth of the groove is A, Fig. 51.7. The groove shape is A $\cos(2\pi z/w)$.

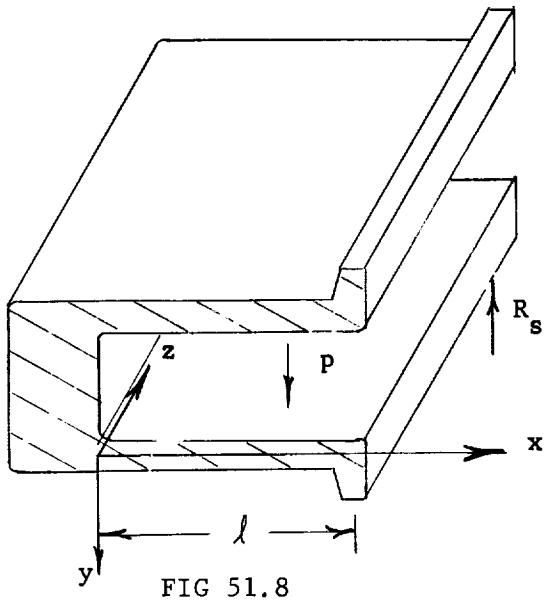

FIG 51.8
COORDINATES FOR SINUSOIDALLY RESTRAINED SEAL

The analysis of the seal leg and a further description of the flange surface irregularity are in the appendix, Section 51.5.7. The sealing force, R_s, and maximum stress at the base of the seal leg, σ_m, for the length w are:

$$R_s = (3p\ell/8) - (3y_\ell\, D/\ell^3) + \frac{AD\,(2\pi/w)^3 \cos(2\pi z/w)}{\sinh(4\pi\ell/w) - 2(2\pi\ell/w)} \left\{(1-\nu)^2(2\pi\ell/w)^2 + (1+\nu)^2 + (1-\nu)(3+\nu)\cosh^2(2\pi\ell/w)\right\} \tag{78}$$

$$\sigma_m = (3p\ell^2/4h^2) + (18y_\ell\, D/\ell^2 h^2) - \frac{EhA}{(1-\nu^2)}\left(\frac{2\pi}{w}\right)^2 \left\{\frac{(1+\nu)\sinh(2\pi\ell/w) + (1-\nu)(2\pi\ell/w)\cosh(2\pi\ell/w)}{\sinh(4\pi\ell/w) - 2(2\pi\ell/w)}\right\} \tag{79}$$

The first two terms in the above equations are identical to the equations for the sealing force, equation (4), and stress, equation (3) for the seal leg on a flat surface in Section 51.5.1.

Of particular interest in the above equations is the change in sealing force and stress due to the sinusoidal restraint. This change is given by the last term in each of the above equations and is a function of the half-depth of the groove, A, and peak-to-peak circumferential length of the groove, w. The change in sealing force for a unit half-depth of groove is:

$$\frac{\Delta R_s}{A} = \frac{D(2\pi/w)^3 \cos(2\pi z/w)}{\sinh(4\pi\ell/w) - 2(2\pi\ell/w)}$$

$$\left\{(1-\nu)^2(2\pi\ell/w)^2 + (1+\nu)^2 + (1-\nu)(3+\nu)\cosh^2(2\pi\ell/w)\right\}$$

This change in sealing force was calculated for a seal of constant width leg with a lip, Fig. 51.9. The peak of the groove is considered (z=0) and the dimensions are those of case 2. Note that in the curve the half-groove depth is given in mils. As w becomes larger the change in sealing force for a one mil deflection, from a zero mean deflection, is the same as the sealing force for a one mil end deflection for a constant width seal leg with a lip seating on a perfectly smooth surface.

If y_ℓ and p are zero in equation (78) the change in sealing force is the total sealing force. There is then a positive maximum value at x=0 and a negative maximum at x=w/2 , see Fig.51.16 in the appendix. It is physically impossible to have a negative R_s and this can only be interpreted qualitatively that the seal leg is not in full contact with the flange face. This means leakage will occur. To prevent leakage the sealing force must always be equal to or greater than some minimum value. Assuming that the initial deflection is just right to give the desired minimum sealing force it is then possible to use the internal pressure to force the seal leg into the groove. The pressure must be large enough to give a zero change in sealing force in the bottom of the groove.

$$p = 8\Delta R_s/3\ell$$

The curve in Fig. 51.9 is based on the dimensions for case 2 and if in addition w is taken equal to the leg length, ℓ (.15 inches) and A is taken as one tenth of y_ℓ, (.15 mils) the pressure may be calculated using the above equation. The pressure is 10,000 psi, which is more than the expected maximum value of the internal pressure (6000 psi). However, if w is ten times the leg length the pressure required is only 120 psi. The pressure increases linearly as A increases and exponentially as w decreases. It may be concluded that it is extremely difficult to make the seal leg comply with deep grooves with a small peak-to-peak length.

Fig. 51.9. Change in Sealing Force as a Function of Groove Circumferential Length Calculations Based on Case 2 Dimensions for a Seal Leg of Uniform Width with a Lip on the Sealing End.

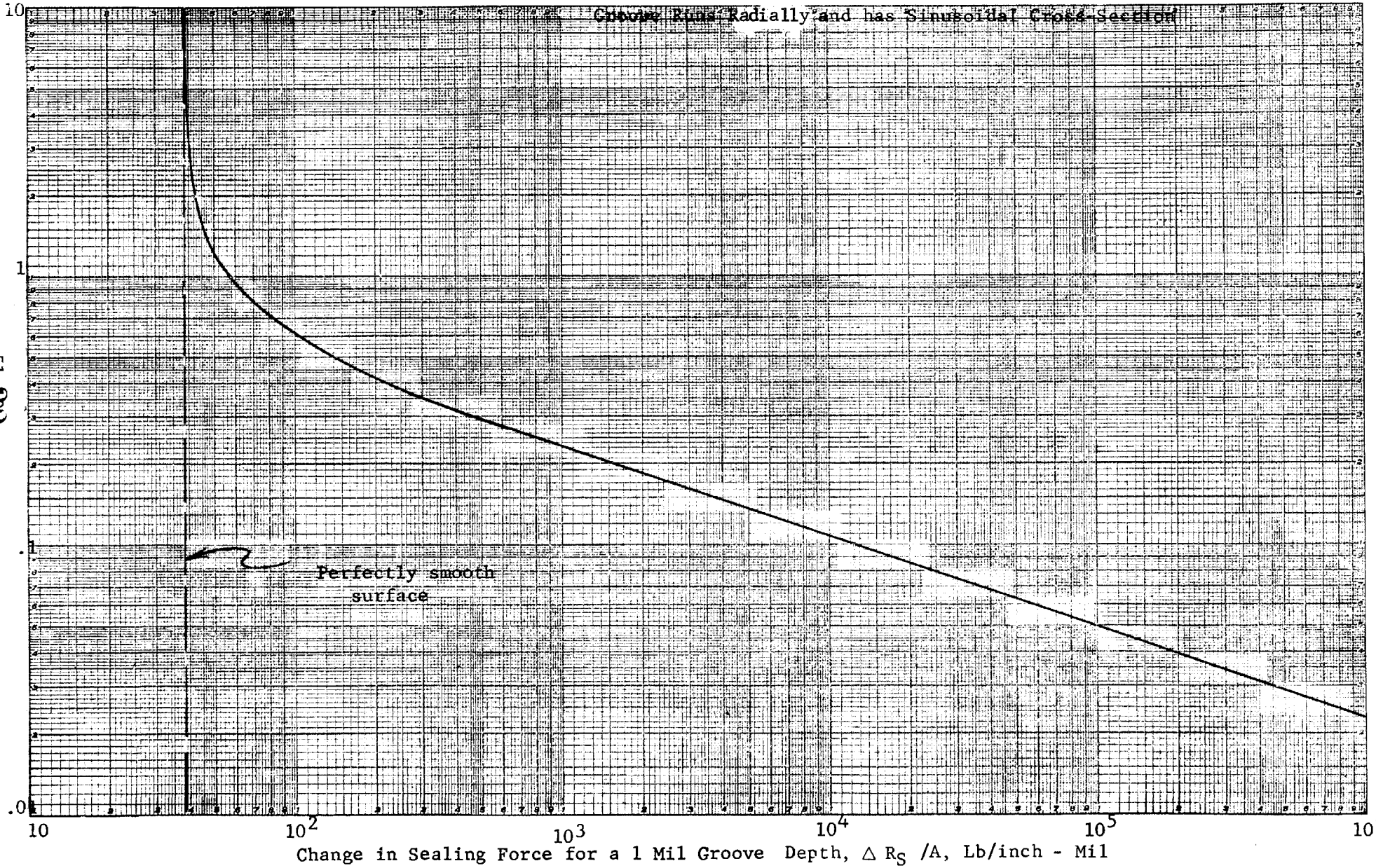

3.6 Summary of Seal Characteristics

Pressure energized seals may be grouped according to the shape of the seal leg. Three major types have been considered.

1. Seal with Straight Leg of Constant Width
   Section 51.3.1

2. Seal with Straight Leg of Linearly Varying Width
   Section 51.3.2

3. Seal with Straight Leg of Constant Width Without Lip
   Section 51.3.3

The seal web is usually a ring which is much stiffer than the seal leg. Therefore, the seal legs and the web have been considered separately.

Of particular importance in the design of pressure energized seals is the sealing force obtained as a function of the internal pressure. Also, the maximum stress in the seal leg is important. Both of these parameters have been calculated as a function of pressure for the three types of seal legs. The results are included in Sec. 51.5.9 in the form of curves for each type of seal leg and are summarized in this section. Typical seal dimensions were chosen. Most of the dimensions for the three types of seals considered are identical and the others are equivalent. This makes it possible to compare the seal leg characteristics directly.

The curves of sealing force versus pressure, Fig. 51.10 show that the slopes of the constant width seal legs are the same with or without the lip and are steeper than that for the tapered leg. Also, from Fig. 51.25 it is seen that the slope of the curve for a tapered leg is a function of the taper. The curves also show that the initial sealing force ($p = 0$ psi) is higher for the tapered leg and a function of the taper. The ability to vary the initial sealing force and slope of the curve in the case of a seal with a tapered leg is a desirable factor in seal design. Another factor in favor of the tapered leg is that the stresses are lower, Fig. 51.10.

The seal web is primarily a structural member and does not directly affect the sealing properties of the seal. However, the sealing properties are indirectly affected. The web must be sufficiently rigid to limit the radial displacement of the seal lip when pressure is applied. Excessive radial motion of the seal lip relative to the flange face may cause leakage. Also, the web must not be too rigid so that the seal may rotate and allow for differential radial motion of the flange faces without slippage. If the seal is stiff in rotation of its cross-section the frictional couple from the flange faces will not be large enough to rotate the seal and the seal lip must slide on the flange face. This slippage may cause leakage.

The radial growth of a pressure energized seal as a function of internal pressure and inside radius is given in Fig. 51.12. The seal leg configuration and dimensions of case 2 were used. The web axial length was taken as one-half the leg length, and the web thickness was calculated based

Fig. 51.10 SEALING FORCE VERSUS PRESSURE FOR SEAL LEG DESIGNS

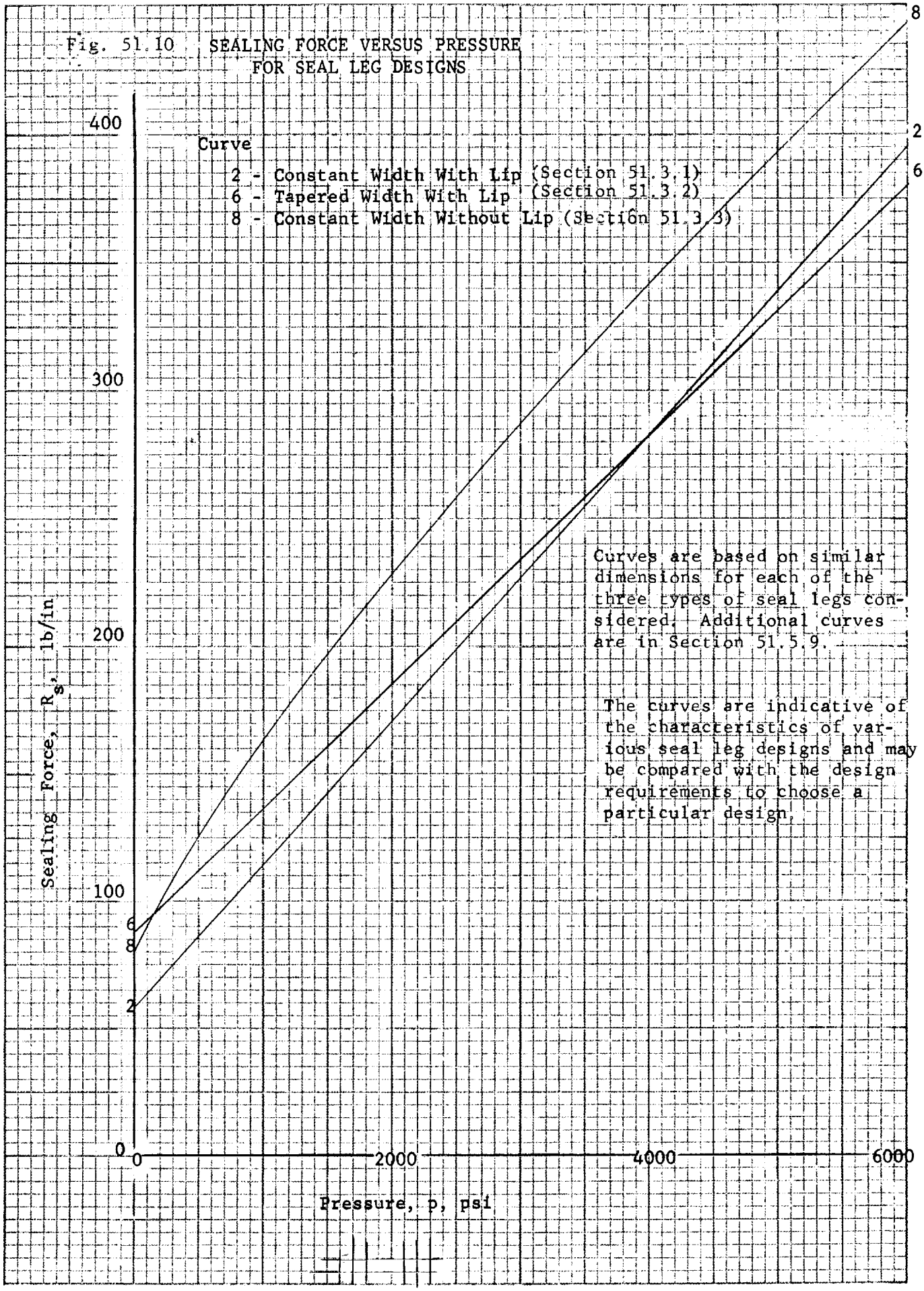

Fig. 51.11 MAXIMUM STRESS AT BASE OF SEAL LEG VERSUS PRESSURE

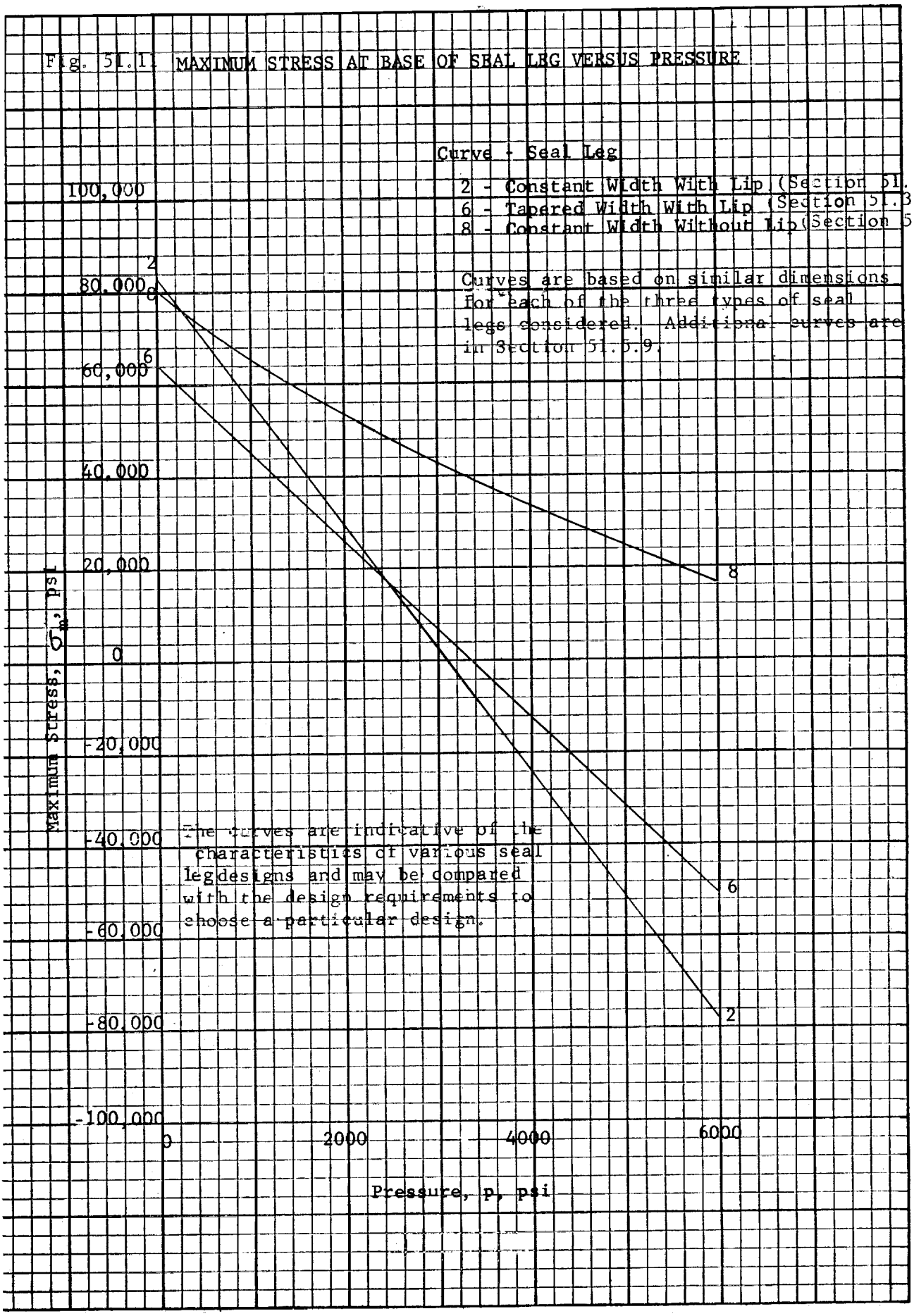

FIG. 51.12 RADIAL GROWTH VERSUS PRESSURE AND INTERNAL RADIUS

CALCULATIONS FOR CASE 2

Pressure-Energized Seal with Uniform Width Leg and Lip. Flange Faces Remain Rigid.

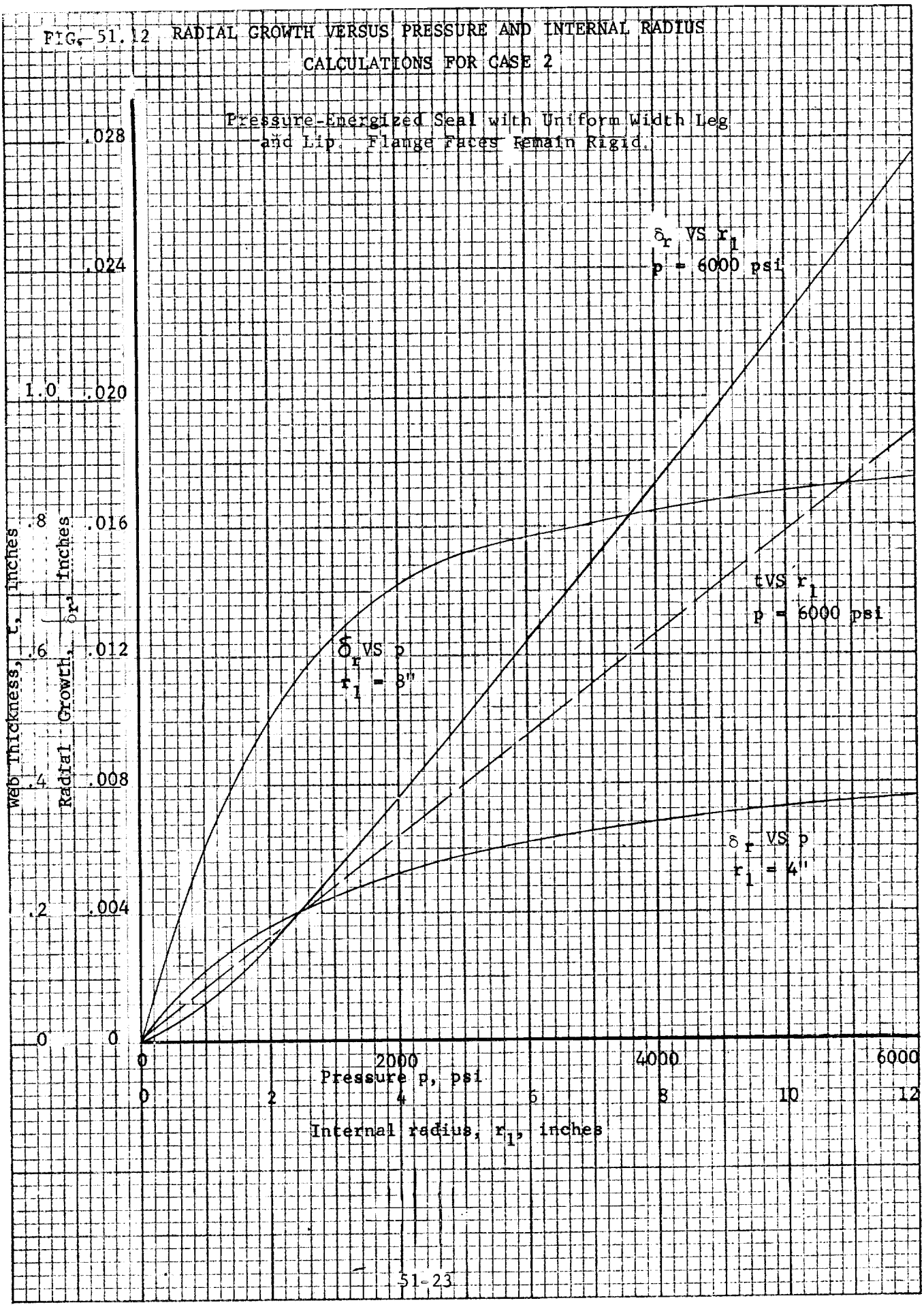

on an allowable hoop stress of 80,000 psi. For an internal pressure of 6000 psi the web thickness becomes very large for larger radii. At these pressures and radii a better design may be to use a small web thickness and have the flange recess support the seal radially. A very wide seal web could also be used with flat flange faces so that the web is a spacer between the flange faces and the bolts pass through the web.

51.4 Conclusions

A pressure-energized static seal may be chosen and designed using the formulas and procedures in this section. The desired sealing-force characteristics and gross flange deformation must be known. These are determined from a consideration of the flange face surface and seal lip coating, and an analysis of the complete flanged joint and pipe. The type of seal leg is chosen by making a comparison of the seal leg characteristics with the required characteristics. Then the seal leg and web are detailed using the design formulas given in this section.

The seal leg with a linearly varying thickness and a lip on the sealing end is the best design of those considered. This is due to the ability to change the slope of the sealing-force-versus-pressure curve by changing the leg taper. The uniform-thickness seal leg with a lip on the end is a special case of the tapered leg. The other case considered, uniform-thickness leg without a lip on the sealing end, has no advantages in its sealing-force characteristics and has less advantageous stress characteristics.

The radial motion of the seal lip may be a cause of leakage. From a consideration of the flange face and seal coating material, an allowable maximum radial motion of the seal lip relative to the flange face is determined. The seal web dimensions may then be chosen to limit the radial seal growth due to internal pressure. If the web dimensions become too large, it may be necessary to limit the radial growth with a back-up ring or the flange recess. Stiffening the seal web to limit the radial motion due to internal pressure will limit the seal's ability to comply with differential radial growth of the flange faces. In order to prevent relative motion of the seal lip with respect to the flange face when there is differential radial growth of the flange faces, the seal cross-section must rotate about its centroid. If the seal is too stiff in rotation, the frictional couple applied by the flange faces will be too small to rotate the seal, and slippage will occur. Either type of slippage of the seal lip on the flange face is a possible cause of leakage.

The ability of a seal to comply with a small radial scratch in the flange surface will depend on the seal lip coating. The increase in internal pressure needed to maintain the minimum sealing force in the bottom of the scratch by deforming the seal leg is extremely large even for a scratch whose width is equal to the length of the seal leg. It is possible to make the seal leg comply with gradual flange face irregularities such as flange warpage, but small sharp irregularities require the use of a soft coating on the seal lip.

The use of beam theory to analyze the seal components that are more closely approximated by a circular plate or conical shell was justified in the appendix, Section 51.5.8. Calculations of the sealing force were made using beam theory, plate theory and shell theory. Curves of the error using beam theory instead of plate theory show that the error is less than ten percent for a ratio of outside radius to inside radius of 1.2 or less. The curves of the error using beam theory instead of shell theory show that the error is less than ten percent for a radius ratio of 1.15 or less and an angle of 15 degrees or less. The error increases more rapidly as the angle increases than as the radius ratio increases.

51.5 Appendix, Analysis of Various Types of Beams Which are Typical of Seal Cross-sections.

51.5.1 . Straight Uniform Beam Loaded by Internal Pressure and End Restraint

The beam is built-in at one end and has a small leg on the free end which is supported on the flange face. The internal pressure acts as a uniformly distributed transverse load. However, even without any internal pressure the beam is loaded, as the axial recess between flange faces is less than the axial length of the seal.

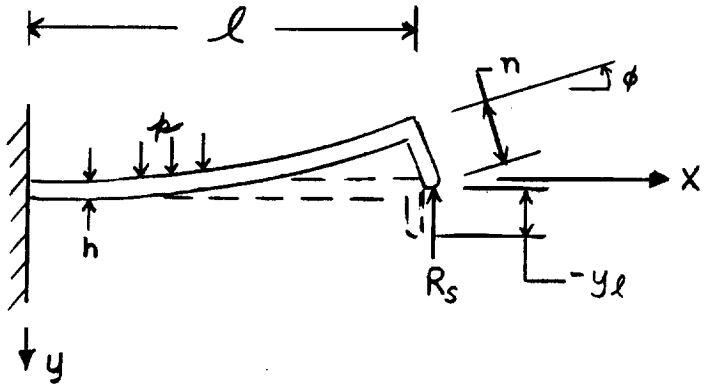

The leg (n) is assumed rigid. The rotation of this leg results in a moment being applied equal to m R_s sin ϕ. However, this moment is only two hundredths of the moment due to the force R_s at the built-in end and results in a deflection at the free end equal to three hundredths of that due to the force R_s. Therefore, the moment arm is neglected. The deflection curve is found by combining formulas 1 and 23 from table III of Ref. 3.

$$y = p(2x^4+3\ell^2x^2-5\ell x^3)/48D + y_\ell (3\ell x^2 - x^3)/2\ell^3 \quad (1)$$

The moment is flexural rigidity, D, times d^2y/dx^2.

$$M = p(4x^2 + \ell^2 - 5\ell x)/8 + 3y_\ell D (\ell-x)/\ell^3 \quad (2)$$

The maximum stress is the bending stress at the built-in end.

$$\sigma_m = 3p\ell^2/4h^2 + 18y_\ell D/\ell^2h^2 \quad (3)$$

The sealing force is the reactive force R_s.

$$R_s = 3p\ell/8 - 3y_\ell D/\ell^3. \quad (4)$$

Setting p=o and substituting for D in equation (4), the initial deflection, y_ℓ, required for a specified sealing force may be found as a function of the length-to-thickness ratio.

$$y_\ell = - (4R_s/E) (1-\nu^2) (\ell/h)^3 \tag{5}$$

Then specifying the maximum stress, the length, ℓ, may be determined as a function of the length to thickness ratio from equation (3).

$$\ell = \frac{6 y_\ell E}{(1-\nu^2) (\ell/h) \left[4\sigma_m - 3p(\ell/h)^2 \right]} \tag{6}$$

If the beam (seal leg) in the unstressed state is at an angle ϕ to the flange face, only the sealing force is changed.

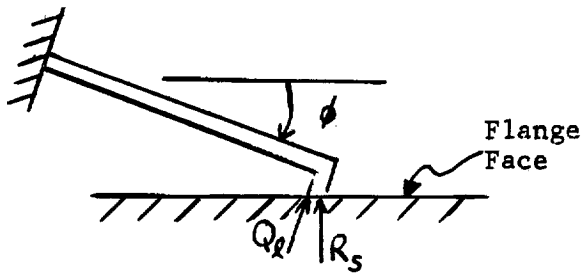

The end shear, Q_ℓ, is given by equation (4).

$$R_s = Q_\ell / \cos \phi \tag{7}$$

$$R_s = (3/\cos \phi) (p\ell/8 - y_\ell D/\ell^3) \tag{8}$$

Note that y_ℓ is still measured normal to the beam and is positive in the positive y direction.

Equation (5) changes slightly to:

$$y_\ell = - (4R_s/E) (1-\nu^2) (\ell/h)^3 \cos \phi \tag{9}$$

The moment at the built-in end is found from equation (2):

$$M_o = p\ell^2/8 + 3 y_\ell D/\ell^2 \tag{10}$$

51.5.2 Linearly Tapered Beam Loaded by Internal Pressure and End Restraint.

This case is identical to the previous case except that h varies linearly.

$$h = a + bx \tag{11}$$

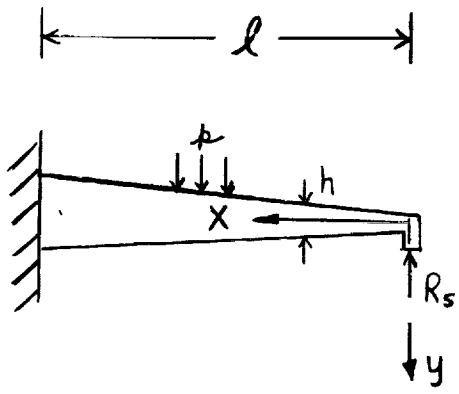

To find the deflection equation for the above beam requires the integration of the differential equation of the elastic curve.

$$D \frac{d^2y}{dx^2} = M \tag{12}$$

where

$$D = \frac{E\,(a + bx)^3}{12\,(1 - \nu^2)} = (a + bx)^3/d \tag{13}$$

After integration the deflection equation contains three constants.

$$y = (d/2b^4)\left[(3ap + bpx - 2bK_1)\log(a + bx) + (a/2)(ap - 2bK_1)/(a + bx) - bpx\right] + K_2 x + K_3 \tag{14}$$

The constants are determined by applying boundary conditions.

$$K_1 = \frac{2b^4 y_o/d + 3ap\log(1+b\ell/a) - (b\ell p/2)(6a^2 + 9ab\ell + 2b^2\ell^2)/(a+b\ell)^2}{2b\log(1+b\ell/a) - b^2\ell(3b\ell+2a)/(a+b\ell)^2} \tag{15}$$

$$K_2 = -(d/2b^3)\left[p\log(a+b\ell) + \frac{ap(3a + 4b\ell) - 2b(a+2b\ell)K_1}{2(a+b\ell)^2}\right] \tag{16}$$

$$K_3 = -(d/2b^4)\left\{(3ap - 2bK_1)\log(a + b\ell) + \frac{1}{2(a+b\ell)^2}\left[(2b^2\ell^2 - a^2)\,2bK_1 + p(a^3 - 4a^2b\ell - 8ab^2\ell^2 - 2b^3\ell^3)\right]\right\} \quad (17)$$

The sealing force, R_s, must equal the shear force at x=0.

$$R_s = -K_1 \quad (18)$$

Of particular interest is the sealing force when the internal pressure is zero.

$$R_s = \frac{2b^3 y_o}{bd\ell\,(3b\ell + 2a)/(a+b\ell)^2 - 2d\log(1+b\ell/a)} \quad (19)$$

The bending stress at the built-in end is usually the maximum stress. However, this is not necessarily true for a tapered beam.

$$\sigma_m = 3\ell\,(p\ell + 2K_1)/(a+b\ell)^2 \quad (20)$$

The above equations are too complex to arrive at simple design formulas. The end defection, y_ℓ, required to give the minimum sealing force when the pressure is zero is found from equation (19).

$$y_o = \frac{d\,R_s}{2b^3}\left[\frac{b\ell\,(2a + 3b\ell)}{(a + b\ell)^2} - 2\log(1 + b\ell/a)\right] \quad (21)$$

Substituting y_o in equation (15) for K_1 and substituting K_1 in equation (20) for σ_m gives one equation relating a, b and ℓ. Known are p, E, γ, R_s and σ_m. However, the relationship for a, b and ℓ is complex and nonlinear.

$$\sigma_m = \frac{3\ell}{(a + b\ell)^2}\left\{p\ell - 2R_s + \frac{p\left[\frac{b\ell}{(a+b\ell)^2}(6a^2 + 9ab\ell + 2b^2\ell^2) - 6a\log(1 + b\ell/a)\right]}{b\left[\frac{b\ell}{(a+b\ell)^2}(2a + 3b\ell) - 2\log(1 + b\ell/a)\right]}\right\} \quad (22)$$

By choosing two of the three variables, it is possible to solve for the third. The leg thickness at the sealing end may be chosen smaller than that at the web end, and just large enough to prevent local overstressing and maintain manufacturability. Choosing the leg thickness at the web, h_ℓ, end eliminates the natural logarithm terms from the terms involving the dependent variable and results in an equation relating b and ℓ that is more tractable. Also, a second simple relationship between b and ℓ is obtained.

$$b = (h_\ell - a)/\ell \tag{23}$$

The two equations for b and ℓ may be solved simultaneously. If the values of b and ℓ so obtained are unreasonable, other values of a and h_ℓ should be chosen.

If the seal leg is at an angle $\emptyset$ to the flange face, R_s in equations (21) and (23) is replaced by $R_s \cos \emptyset$. This means R_s is still an axial force with a component normal to the beam equal to $R_s \cos \emptyset$. The end deflection y_o is still defined as normal to the beam.

51.5.3 Straight Uniform Beam Loaded by Internal Pressure and Moving End Restraint

This case is similar to the case discussed in Section 51.5.1 except that there is no lip at the sealing end of the seal leg. The seal section consists of a thick web with two constant thickness seal legs. The

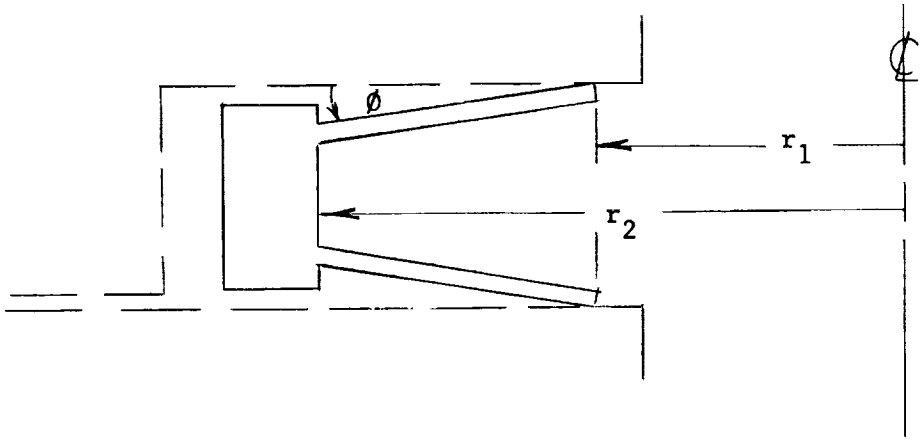

FIGURE 51.13 Cross-section of Seal and Flange Recess

flange faces may clamp directly on the web or be recessed and clamp only on the seal legs. All of the seal designs considered have this option. If the web is clamped by the flanges, the web load can only be determined by an analysis of the total flange joint. This case will not be covered in this section and it is here assumed that the seal sits in a recess. Therefore, the web analyses of the following sections are applicable.

The seal leg is analyzed as a built in beam at a small angle ø to the flange face. The leg is loaded by the internal pressure, p, and an initial deflection normal to the leg, y_1. As shown in the diagram below, the seal leg length, $(\ell - \ell_i)$ is in simple compression due to the internal pressure load and does not affect the leg length ℓ_i. An equilibrium diagram of the ℓ to ℓ_i length shows that the end shears and moments must be zero. Therefore, there is no end moment on the seal leg, ℓ_i, and the end shear is only the sealing force R_s acting at the distance ℓ_i. This point of contact moves toward the seal web as the restrained height, H_R, is decreased or the pressure increased.

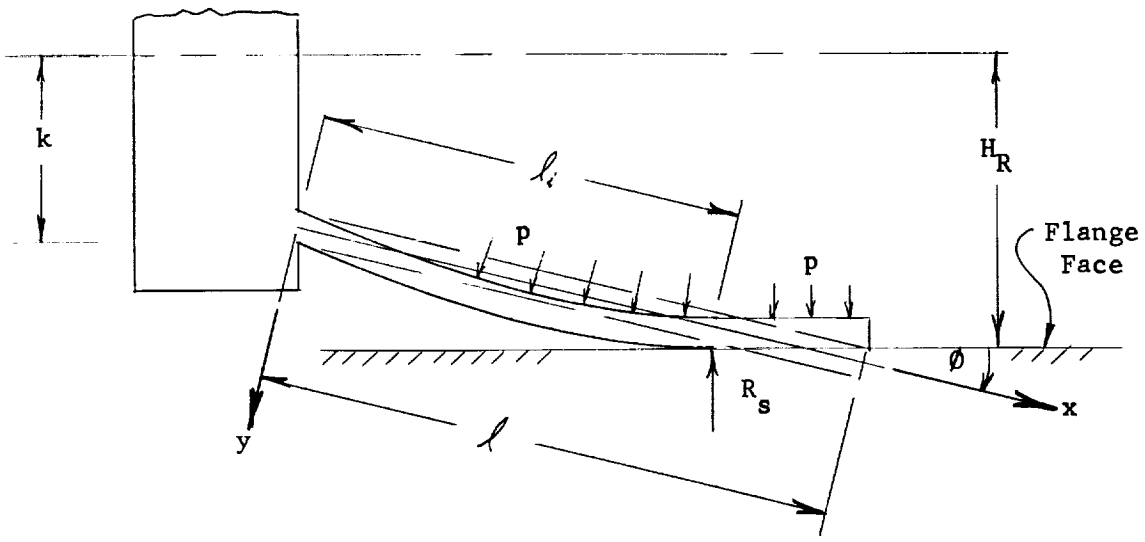

FIG. 51.14

Cross-section of Seal Showing Loaded Seal Leg

The initial deflection, y_{ℓ}, is the deflection normal to the beam when the pressure is zero. The corresponding active beam length is designated ℓ_o. Defining the distance k as the distance from the midpoint of the axial web length to the flange side of the seal leg, the leg deflection at ℓ_o is:

$$y_{\ell} = (H_R - k - \ell_o \sin \phi) \; / \; \cos \phi \qquad (24)$$

Likewise the deflection of the instantaneous end point of the active beam length is:

$$y_i = (H_R - k - \ell_i \sin \phi) \; / \; \cos \phi$$

Differentiating the equation for the elastic curve of a uniform beam gives a relation between the fourth derivative and uniform pressure load.

$$D \frac{d^4 y}{dx^4} = p \qquad (25)$$

Integration of this equation gives four constants which are evaluated from the following boundary conditions:

$$y = 0 \quad \text{at} \quad x = 0$$

$$\frac{dy}{dx} = 0 \quad \text{at} \quad x = 0$$

$$y = y_i \quad \text{at} \quad x = \ell_i \tag{26}$$

$$\frac{dy}{dx} = -\tan \phi \quad \text{at} \quad x = \ell_i$$

Note: ϕ is a small angle and the small angle approximations for the trigonometric functions are made later in the analysis. If ϕ is large the effective length of the seal leg, ℓ_i, will not vary much as the end deflection or internal pressure are changed and the analyses of sections 51.5.1 and 51.5.2 are applicable.

The deflection equation for the seal leg is:

$$y = \left[p(1-\nu^2)/(2Eh^3)\right] x^4 - \left[p\ell_i(1-\nu^2) / (Eh^3)\right.$$
$$\left. + 2(H_R-k)/(\ell_i^3 \cos \phi) - (\tan \phi)/\ell_i^2\right] x^3 \tag{27}$$
$$+ \left[p\ell_i^2(1-\nu^2)/(2Eh^3) + 3(H_R-k)/(\ell_i^2 \cos \phi) - (2 \tan \phi)/\ell_i\right] x^2$$

As mentioned above, the section of leg ℓ to ℓ_i has no end moment, and the end moment at ℓ_i on the remainder of the leg is zero. This additional boundary condition is:

$$M = D \frac{d^2y}{dx^2} = 0 \quad \text{at} \quad x = \ell_i \tag{28}$$

Using this condition on equation (27) gives the following equation in ℓ_i:

$$\ell_i^4 + \frac{2Eh^3 \tan \phi}{p(1-\nu^2)} \ell_i - \frac{6Eh^3(H_R-k)}{p(1-\nu^2)\cos \phi} = 0 \tag{29}$$

When p = 0 in equation (29) it may be solved directly for ℓ_o.

$$\ell_o = 3(H_R-k)/\sin \phi \tag{30}$$

Substituting for ℓ_o in equation (24) allows solving explicitly for cos ϕ.

$$\cos \phi = -2(H_R-k)/y_\ell \tag{31}$$

Note this puts a restriction on H_R, k and y_ℓ.

$$\left| 2(H_R-k)/y_\ell \right| \leq 1 \tag{32}$$

The equation for the maximum bending stress at the built in end is:

$$\sigma_i = \frac{p\ell_i^2}{2h^2} + \frac{3Eh(H_R-k)}{\ell_i^2(1-\nu^2)\cos \phi} - \frac{2Eh \tan \phi}{\ell_i(1-\nu^2)} \tag{33}$$

The subscript 'i' is used to denote the stress for any pressure p, not necessarily the maximum pressure. The corresponding active leg length is ℓ_i. When reference is made to the maximum stress corresponding to the maximum pressure, the subscript m is used. As this latter stress, σ_m, is the largest, it is the stress for which an allowable maximum is specified.

By using equation (29), the pressure term may be eliminated from equation (33).

$$\sigma_i = -\frac{3Eh \tan \phi}{\ell_i(1-\nu^2)} + \frac{6Eh(H_R-k)}{\ell_i^2(1-\nu^2)\cos \phi} \tag{34}$$

From equation (31) the sine and tangent of ϕ may be determined

$$\begin{aligned} \sin \phi &= -\sqrt{y_\ell^2 - 4(H_R-k)^2}\,/\,y_\ell \\ \tan \phi &= \sqrt{y_\ell^2 - 4(H_R-k)^2}\,/\,2(H_R-k) \end{aligned} \tag{35}$$

Substituting these in equation (34) gives:

$$\sigma_i = -\frac{3Eh\sqrt{y_\ell^2 - 4(H_R-k)^2}}{2\ell_i(1-\nu^2)(H_R-k)} - \frac{3Eh\, y_\ell}{\ell_i^2(1-\nu^2)} \tag{36}$$

Returning to equation (29) and combining it with equation (33) a quadratic equation in ℓ_i^2 is obtained.

$$\ell_i^4 - \frac{2\sigma_i h^2}{3p}\ \ell_i^2 - \frac{2Eh^3(H_R-k)}{p(1-\nu^2)\cos\phi} = 0 \qquad (37)$$

Using the quadratic formula gives the solution for ℓ_i^2. The minus sign is dropped because the radical is larger than the first term and a negative value of ℓ_i^2 gives imaginary values for ℓ_i.

$$\ell_i^2 = \frac{\sigma_i h^2}{3p} + \sqrt{\frac{\sigma_i^2 h^4}{9p^2} + \frac{2Eh^3(H_R-k)}{p(1-\nu^2)\cos\phi}}$$

Then the solution for ℓ_i must be plus so the negative root is again discarded.

$$\ell_i = \left\{h\sqrt{\frac{\sigma_i}{3p}}\right\}\sqrt{1+\sqrt{1+\frac{18pE(H_R-k)}{h\,\sigma_i^2(1-\nu^2)\cos\phi}}} \qquad (38)$$

In equation (A-15) the following quantitative relations are noted when the maximum value of pressure, p_m, is used.

$$\frac{18p_m E(H_R-k)}{h\,\sigma_m^2(1-\nu^2)\cos\phi} \gg 1 \qquad (39)$$

and

$$\sqrt{\frac{18p_m E(H_R-k)}{h\,\sigma_m^2(1-\nu^2)\cos\phi}} > 1$$

For example, if the following typical values are used for the parameters,

E	=	30×10^6	psi	- for steel
H_R	=	.05	inch	
h	=	.01	inch	
k	=	.04	inch	
p_m	=	6000	psi	- this is maximum pressure
σ_m	=	60,000	psi	- this is maximum allowable strees
ν	=	.3		- for steel
ϕ	=	18^o		

then $$\sqrt{\frac{18p_m E(H_R - k)}{h\,\sigma_m^2(1-\nu^2)\cos\phi}} = 33.1$$

Therefore, equation (38) reduces to the following:

$$\ell_m = h \sqrt[4]{\frac{2E(H_R - k)}{hp_m(1-\nu^2)\cos\phi}} \tag{40}$$

Substituting for $\cos\phi$ from equation (31) gives:

$$\ell_m = h \sqrt[4]{\frac{-E\,y_\ell}{hp_m(1-\nu^2)}} \tag{41}$$

The value of ℓ_m given by equation (41) corresponds to the maximum pressure and is the minimum active leg length.

The sealing force, R_s, at length ℓ_i is:

$$R_s = \frac{p\ell_i}{2\cos\phi} - \frac{Eh^3(H_R - k)}{\ell_i^3(1-\nu^2)\cos^2\phi} + \frac{Eh^3\tan\phi}{2\ell_i^2(1-\nu^2)\cos\phi} \tag{42}$$

Solving equation (29) for p and substituting in the above equation, and also substituting for the trigonometric functions of ϕ give the following equation for R_s.

$$R_s = \frac{Eh^3 y_\ell \left[4y_\ell (H_R - k) + \ell_i \sqrt{y_\ell^2 - 4(H_R - k)^2} \right]}{8 \ell_i^3 (H_R - k)^2 (1 - \nu^2)} \tag{43}$$

For p = 0, equation (30) is used to reduce equation (43).

$$R_o = - \frac{Eh^3 \left[y_\ell^2 - 4(H_R - k)^2 \right]^{3/2}}{216\, y_\ell (1 - \nu^2) (H_R - k)^4} \tag{44}$$

R_o is the sealing force due to the clamping action of the flange faces.

Equation (44) may be solved for h explicitly assuming a value of R_o is specified for the particular application.

$$h^3 = - \frac{216(1 - \nu^2)\, y_\ell R_o (H_R - k)^4}{E \left[y_\ell^2 - 4(H_R - k)^2 \right]^{3/2}} \tag{45}$$

Substituting in equation (41) for h^3:

$$\ell_m = \frac{(H_R - k) \sqrt[4]{216\, y_\ell^2 R_o / p_m}}{\left[y_\ell^2 - 4(H_R - k)^2 \right]^{3/8}} \tag{46}$$

The seal leg design assumes prior knowledge of the material properties, E and γ, the minimum sealing force, R_o, and allowable stress, σ_m. The value of σ_m is not explicitly used, but the derivation of equation (41) does depend on the value of σ_m being in a certain range. With these parameters known, the equations in this section may be used to determine the leg geometry.

Assume values for H_R, k and y_ℓ and calculate the active leg length for zero pressure (see equation below) and for maximum pressure (equation 46). Calculate the seal leg thickness (equation 45). Revise the values

$$\ell_o = - \frac{3\, y_\ell (H_R - k)}{\sqrt{y_\ell^2 - 4(H_R - k)^2}} \tag{47}$$

of H_R, k and y_ℓ until reasonable design values of ℓ_o, ℓ_m and h are obtained. If this method does not converge sufficiently well it may be necessary to select all the geometric parameters and just make check calculations to determine whether the sealing force (equation 44) and allowable stress (equation 36) are within the required limits.

51.5.4 Web Design Formulas.

The loads on the seal web are the internal pressure and shears and moments from the seal legs.

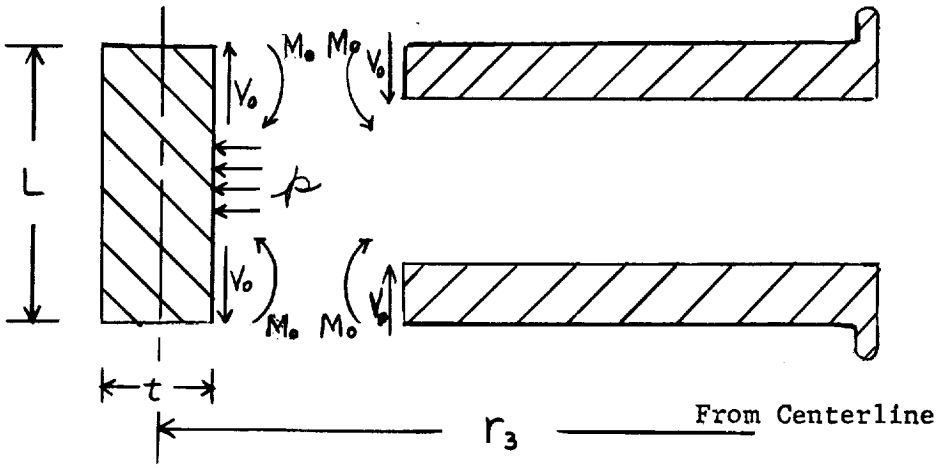

The shears will not result in high enough compressive stresses to be concerned about. The ratio of web thickness t to the mean radius r_3 is very small. Therefore, the web section may be analyzed as a beam of length L with equal and opposite moments on each end and a plane of symmetry at L/2. The bending stresses at the plane of symmetry are found from beam theory.

$$\sigma = 6\ M_o\ /\ t^2 \qquad (48)$$

The maximum stress in the leg is given by an equivalent formula where t is h. Therefore, the first requirement is that $t \geq h_o$, the leg thickness at the built-in end.

The second requirement for the web design is that the membrane stress is within the allowable. The minimum value of t may be calculated.

$$t = p\ r_3\ /\sigma_m \qquad (49)$$

The larger value of t is chosen. This is a conservative value, as the whole radial pressure load is assumed to be taken by the web. For a more detailed analysis, see Section 51.5.5. The determination of L is also described in that section.

51.5.5 Radial Deflection of Seal Due to Internal Pressure.

The radial deflection of the seal is important as any radial movement of the sealing lip relative to the flange face may disturb the seal and cause leakage. Relative radial motion of the sealing lip is always present. However, there may be a tolerable amount for which it is possible to design.

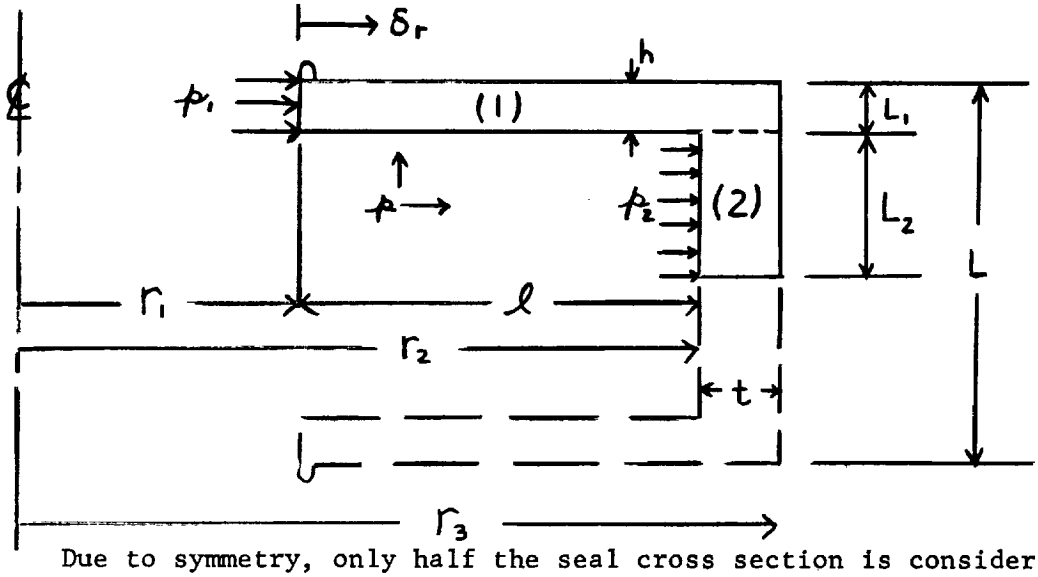

Due to symmetry, only half the seal cross section is considered. Rings (1) and (2) are assumed simple rings. Because ring (1) is radially stiffer than ring (2) it will carry some of the pressure load on ring (2). The redistributed pressure loads are represented as p_1 and p_2 and are related to p by the equation.

$$p_1 r_1 L_1 + p_2 r_2 L_2 = p(r_1 L_1 + r_2 L_2) \qquad (50)$$

The strains in both rings must be equal:

$$p_1 /(r_3 - r_1) = p_2 /(r_3 - r_2) \qquad (51)$$

Equations (50) and (51) are solved for p_1 and p_2. Using the value of p_1 so found, the radial deflection of the seal lip, δ_r, is found.

$$\delta_r = (p r_1^2/E)(r_1 L_1 + r_2 L_2)/\left[r_1 L_1 (r_3 - r_1) + r_2 L_2 (r_3 - r_2)\right] \qquad (52)$$

The following relations are noted on the diagram.

$$L_1 = h \text{ (of the leg at the web)}$$

$$r_2 = \ell + r_1$$

$$r_3 = r_2 + t \qquad (53)$$

$$L = 2(L_1 + L_2)$$

Substituting these relations in equation (52):

$$\delta_r = \frac{pr_1^2}{E\left[t + r_1 h\ell/(Lr_1/2 + L_2\ell)\right]} \qquad (54)$$

In equation (54) $Lr_1/2 \gg L_2\ell$ and the equation may be reduced:

$$\delta_r = \frac{pr_1^2}{E\ (t + 2h\ell/L)} \qquad (55)$$

Equation (55) may be used to determine the web length, L. Once the seal leg has been designed it remains only to specify δ_r. Allowable values for δ_r will be determined from tests and experience.

$$L = 2h\ell/(pr_1^2/E\ \delta_r - t) \qquad (56)$$

51.5.6 Rotation of Seal Section Due to an Applied Moment.

Differential radial expansion of the flange faces as the result of non-uniform temperature or dissimilar metals results in a moment being applied to the seal in the plane of the seal section. The larger the differential expansion the larger will be the moment and the more likely is sliding to occur between the seal lip and flange face. A small amount of sliding is probably tolerable, but a point may be reached where leakage occurs. It seems desirable to design the seal to allow a small amount of differential radial growth of the flange faces without sliding of the seal lip.

Consider a seal of arbitrary section to which a couple is applied. The forces are radial in direction, tangent to the flange face and applied at the seal lip.

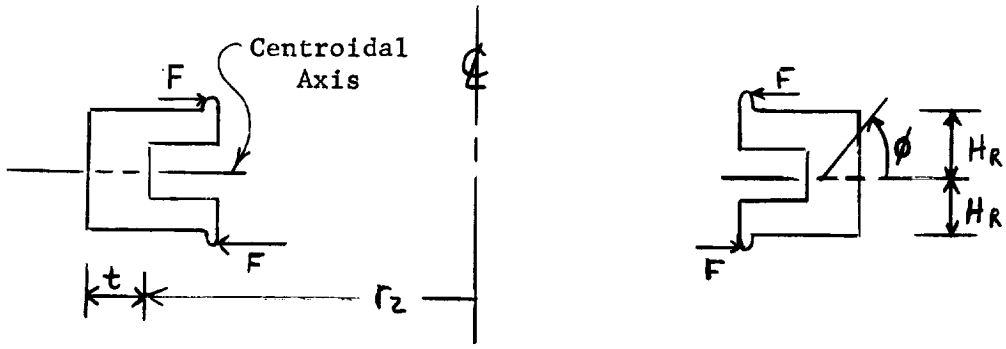

The applied moment is $2H_RF$ where F is the friction force between the seal lip and flange face. The friction force is equal to the sealing force times the coefficient of friction.

$$F = \mu R_s \tag{57}$$

The problem of a ring subjected to an applied moment is solved in section 138 of Ref. 1 . The angle of rotation of the seal section and the maximum bending stress are given.

$$\phi = 2\mu R_s H_R r_2^2 / E I_c \tag{58}$$

$$\sigma_m = 2\mu R_s H_R^2 r_2 / I_c \tag{59}$$

The differential radial motions of the sealing lips is given for small angles of rotation.

$$\delta_D = 2 H_R \phi \tag{60}$$

Substituting for ϕ gives.

$$\delta_D = 4\mu R_s H_R^2 r_2^2 / E I_c \qquad (61)$$

Combining equations (59) and (61),

$$\sigma_m = E \delta_D / 2 r_2 \qquad (62)$$

Equation (62) allows quick checking of the maximum bending stress based on the value of δ_D chosen. The desired value of I_c may be calculated from equation (61)

$$I_c = 4\mu R_s H_R^2 r_2^2 / E\delta_D \qquad (63)$$

I_c is the sum of the area moment for the legs and the web. It is assumed in equation (63) that the leg has been designed. Therefore, the value of I_c calculated will effect only the web design.

51.5.7 Straight Uniform Beam Loaded by Internal Pressure and Sinusoidal End Restraint.

All of the previous analyses have assumed a perfectly smooth flange face surface. This idealization is never met in practice. There are always irregularities in the surface. Although there is nothing regular about the surface imperfections a simplified model is chosen for the analysis. The choice of model is based on the fact that a radial scratch offers the best leakage path. A circular scratch may not offer any leakage path.

The leakage path chosen is a radial groove in the flange face with a sinusoidal cross-section. Part of the metal is assumed raised above the flange face. As shown below the cross-section is a deep valley between two

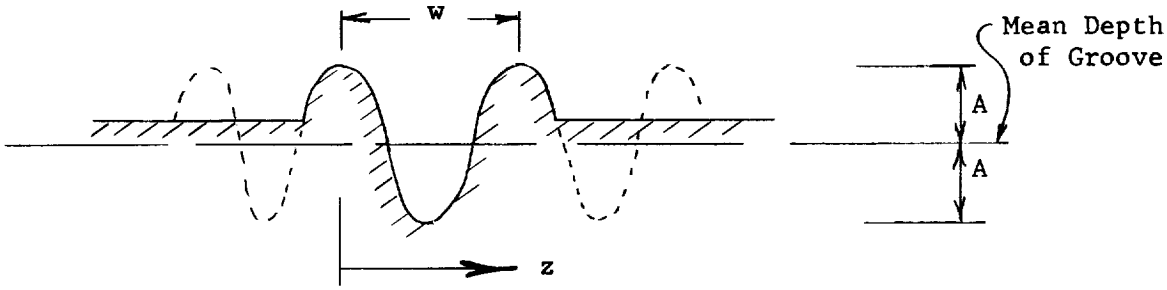

FIG. 51.15
Circumferential Cut Through a Radial Groove

hills. The shape is assumed sinusoidal, $A \cos \frac{2\pi z}{w}$. It is further assumed that the single groove is part of a sinusoidal surface waviness as shown by the dotted lines.

The pressure-energized seal considered has a "U" shaped cross-section and straight legs of uniform thickness. Just as the seal leg analyzed in Section 51.5.1, the sealing edge is a small lip which is assumed rigid. The web is also assumed rigid and therefore, the seal leg acts as if built in at the web end and simply supported at the lip end. The loading of the leg is due to the restraint of the flanges and internal pressure.

Of particular interest in this case is the relationship between the pressure load and the sealing force in the bottom of the groove. Compared to a perfectly flat surface how much more pressure is needed to maintain an adequate sealing force? Also, how much more preloading by the flanges is necessary and what is the increase in the seal leg stress?

The ratio of the outside seal diameter to inside diameter is assumed close enough to one so that the seal leg, which is a flat ring plate, may be analyzed as a continuous rectangular plate. Then as the pressure loading

is uniform and the groove in the flange face is assumed part of a continuous sinusoidal surface waviness, it is possible to select a length w of the plate for analysis. In the hypothetical case of a continuous wavy surface this length w is one cycle of the wave and in the physical model the length w is the one groove of particular interest. The analysis for the seal leg contacting a flat surface is in Section 51.5.1. In this analysis only the sinusoidal length w is considered.

The length w is a rectangular plate built in at one end and simply supported on a cosine-wave shaped support on the other end. This is one cycle of a cosine-wave which is assumed to repeat to either side of the plate. Therefore, the boundary conditions may be determined from symmetry.

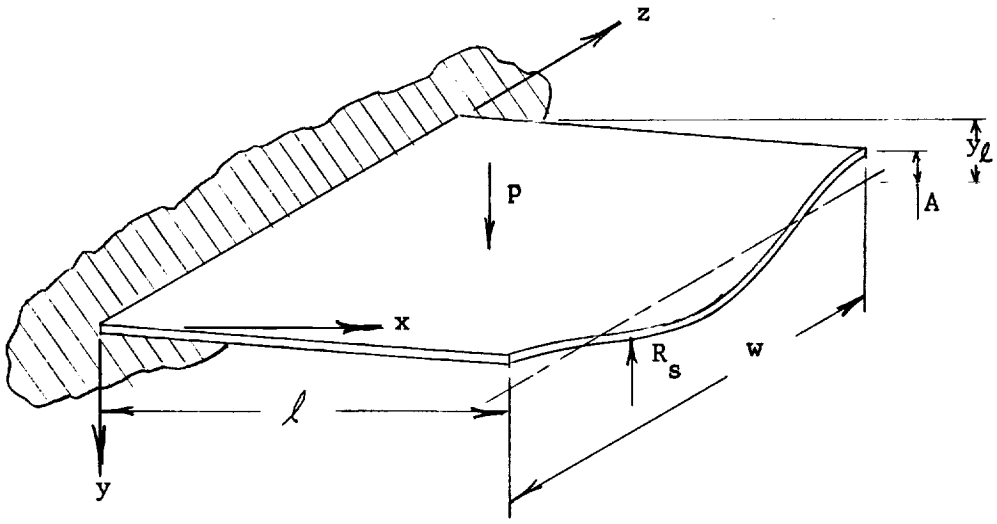

FIG. 51.16

SINUSOIDALLY RESTRAINED PLATE

The boundary conditions along the z = constant edges are:

$$z = 0 \text{ or } w$$

$$\frac{\partial y}{\partial z} = 0$$

$$V_z = -D\left[\frac{\partial^3 y}{\partial z^3} + (2-\nu)\frac{\partial^3 y}{\partial z \partial x^2}\right] = 0$$

The boundary conditions along the x = constant edges are:

$$x = 0$$

$$y = \frac{\partial y}{\partial x} = 0$$

$$x = \ell$$

$$y = y_\ell - A \cos(2\pi z/w)$$

$$M_x = - D\left[\frac{\partial^2 y}{\partial x^2} + \nu \frac{\partial^2 y}{\partial z^2}\right] = 0$$

Note the mean edge deflection, y_ℓ, is shown in a positive sense. Actually the seal leg is given an initial deflection in the negative y direction so that an initial sealing force, R_s, is obtained. The initial deflection is calculated from the following relation:

$$y_\ell = - (H_F - H_R) \tag{64}$$

H_F is the unrestrained axial half-length of the seal and H_R is the restrained half-length. For a perfectly flat flange face, H_R was measured from the axial mid-point of the seal to the flange face. However, in the case of a grooved flange surface H_R is measured from the axial mid-point of the seal to the mean groove depth. The mean groove depth is not necessarily at the same level as the flange face.

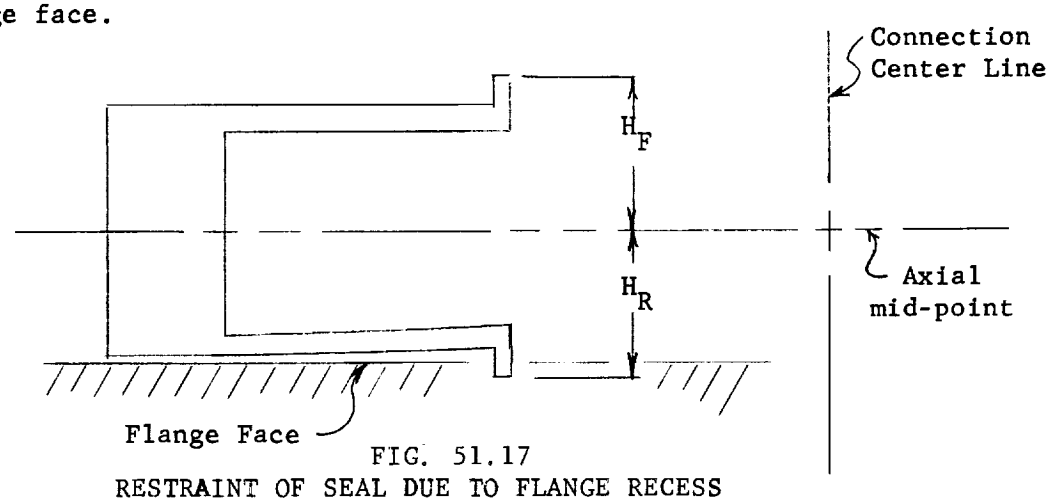

FIG. 51.17
RESTRAINT OF SEAL DUE TO FLANGE RECESS

The deflection equation for the plate is determined in two parts. It is assumed that the deflections are small and the principle of superposition applies. First the deflection equation for a built-in, simply supported, and uniformly loaded continuous plate is determined. Then the deflection for a built-in, sinusoidally restrained and continuous beam is determined. The two solutions are added to give the total deflection equation.

Neglecting the sinusoidal edge restraint reduces the plate problem to that of a wide beam (in the z direction) loaded transversely.

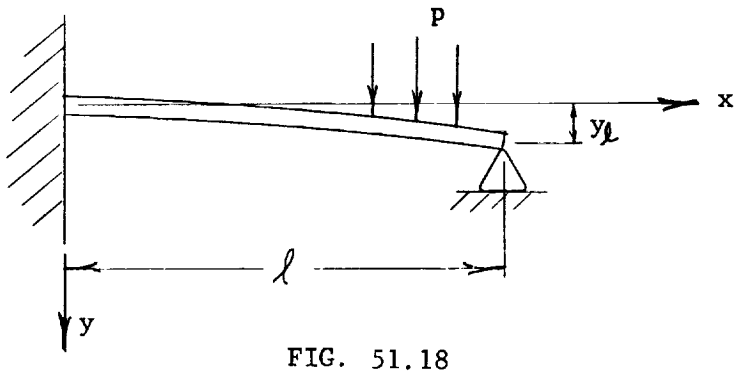

FIG. 51.18

Uniformly Loaded Plate with Constant Edge Restraint

The deflection equation for this configuration is equation (1).

$$y_1 = p(2x^4 - 5\ell x^3 + 3\ell^2 x^2)/48D + y_\ell (3\ell x^2 - x^3)/2\ell^3 \tag{65}$$

This solution satisfies the Lagrange plate equation

$$\Delta^4 y = p/D \tag{66}$$

and the boundary conditions at z = 0 and w and x = 0. At $x = \ell$ the moment boundary condition is met, but the deflection boundary condition is only partially met. That is, at $x = \ell$, $y_1 = y_\ell$.

To complete the solution a deflection equation is determined that satisfies the homogeneous Lagrange plate equation, $\Delta^4 y = 0$, and all the boundary conditions except the deflection at $x = \ell$. In order that the sum of the two deflection equations satisfy the boundary conditions the boundary condition for the second solution at $x = \ell$ must be $y_2 = -A \cos(2\pi z/w)$.

A solution is assumed of the form:

$$y_2 = -A \cos(2\pi z/w) Y(x) \tag{67}$$

where Y(x) is a function of x only. This function satisfies the boundary conditions at z = 0 and w. The boundary conditions at x = 0 and ℓ are met by y_2 by making Y(x) meet the following conditions:

$x = 0$

$$Y'(x) = \frac{\partial Y(x)}{\partial x} = 0 \tag{68}$$

$x = \ell$

$$Y'(x) = 1 \tag{69}$$

$$M_x = -D\left[\frac{\partial^2 y_2}{\partial x^2} + \nu\,\frac{\partial^2 y}{\partial z^2}\right] = 0$$

which is upon substitution:

$$\frac{\partial^2 Y}{\partial x^2} - \nu(2\pi/w)^2 Y = 0 \tag{70}$$

Substituting y_2 (equation 67) in the Lagrange equation results in a fourth order differential equation for Y.

$$\frac{\partial^4 Y}{\partial x^4} - 2\left(\frac{2\pi}{w}\right)^2 \frac{\partial^2 Y}{\partial x^2} + \left(\frac{2\pi}{w}\right)^4 Y = 0 \tag{71}$$

The general solution to this equation is given on page 114 of Ref. 2.

$$\begin{aligned} Y = {} & K_4 \sinh(2\pi x/w) + K_5(2\pi x/w)\sinh(2\pi x/w) \\ & + K_6 \cosh(2\pi x/w) + K_7(2\pi x/w)\cosh(2\pi x/w) \end{aligned} \tag{72}$$

Applying boundary conditions the constants are evaluated.

$$K_6 = 0$$

$$K_7 = -K_4$$

$$K_4 = \frac{2\cosh(2\pi\ell/w) + (1-\nu)(2\pi\ell/w)\sinh(2\pi\ell/w)}{\sinh(4\pi\ell/w) - 2(2\pi\ell/w)} \tag{73}$$

$$K_5 = \frac{(1+\nu)\sinh(2\pi\ell/w) + (1-\nu)(2\pi\ell/w)\cosh(2\pi\ell/w)}{\sinh(4\pi\ell/w) - 2(2\pi\ell/w)} \tag{74}$$

Substituting in equation (72) for Y and (67) for y_2:

$$y_2 = -A\cos(2\pi z/w)\left\{K_5(2\pi x/w)\sinh(2\pi x/w) + K_4\left[\sinh(2\pi x/w) - (2\pi x/w)\cosh(2\pi x/w)\right]\right\} \tag{75}$$

The complete solution for y is:

$$y = y_1 + y_2 \tag{76}$$

where y_1 is given by equation (65) and y_2 by equation (75). The edge load, R_s, is equal to, but opposite in sign, to the total edge shear at $x=\ell$.

$$R_s = -\left(V_x\right)_{x=\ell} = D\left[\frac{\partial^3 y}{\partial x^3} + (2-\nu)\frac{\partial^3 y}{\partial x \partial z^2}\right] \tag{77}$$

Substituting for y from equation (76).

$$R_s = (3p\ell/8) - (3y_\ell D/\ell^3) + \frac{AD(2\pi/w)^3 \cos(2\pi z/w)}{\sinh(4\pi\ell/w) - 2(2\pi\ell/w)} \tag{78}$$

$$\left\{(1-\nu)^2(2\pi\ell/w)^2 + (1+\nu)^2 + (1-\nu)(3+\nu)\cosh^2(2\pi\ell/w)\right\}$$

The maximum stress at the built in end (x=0) is given by:

$$\sigma_m = -6\left(M_x\right)_{x=0}/h^2$$

Upon substituting for M_x this is:

$$\sigma_m = \frac{3p\ell^2}{4h^2} + \frac{18y_\ell D}{\ell^2 h^2} - \frac{EhA}{(1-\gamma^2)}\left(\frac{2\pi}{w}\right)^2 K_5 \tag{79}$$

51.5.8 Justification of Beam Analogy

Consideration of the typical dimensions of commonly used static seals leads to the conclusion that the sealing leg of the seal can be analyzed as a beam. This simplifies the analysis and makes possible the investigation of changes in certain parameters, such as leg thickness, which are difficult to treat in a plate or shell analysis. The accuracy of the beam analysis is sufficient for design purposes and for analytical studies of seal performance.

To verify the fact that the beam analogy is adequate, the error resulting from the use of beam theory to calculate the sealing force for a seal leg of the flat plate and conical shell type was calculated. The sealing force was chosen because it is the most important parameter in the seal design. A seal leg of uniform width, with the point of sealing fixed, was used in the calculations.

51.5.8.1 Beam-Plate Analogy

The sealing force is the sum of two terms in both beam and plate theory. One term is the force due to the initial restraint and the other is due to the internal pressure. The error resulting from the use of beam theory is defined as the absolute difference between the force calculated using plate theory and beam theory divided by the force calculated using plate theory.

$$\epsilon = \frac{\left| R_s(\text{Plate}) - R_s(\text{Beam}) \right|}{R_s(\text{Plate})} \times 100 \tag{80}$$

This error is a function of the radius ratio and ratio of initial deflection to internal pressure. As the initial deflection and internal pressure are difficult to predict, the error was calculated separately for the case of initial deflection only and internal pressure only. In this way the error is a function of radius ratio only.

The sealing force using beam theory is found from the formulas in Ref. 3. Equation (81) is the term

$$R_s(\text{Beam}) = 3pr_1(r_2/r_1 - 1)/8 \tag{81}$$

$$R_s(\text{Beam}) = -y_\ell m^2 E h^3 / \left[4r_1^3 (m^2-1)(r_2/r_1-1)^3 \right] \tag{82}$$

due to internal pressure and equation (82) is the term due to initial deflection.

The sealing force due to the initial deflection is also found in Ref. 3 for a flat circular plate.

$$R_s(\text{Plate}) = -2m^2 E h^3 y_\ell \Bigg/ \Bigg\{ 2r_1^3 (m^2-1) \left[\left(\frac{r_2}{r_1} \right)^2 - 1 + \frac{2m(r_2^2 - r_1^2) - 8mr_2^2 \log(r_2/r_1) + 4r_2^2 (m+1) \left[\log(r_2/r_1) \right]^2}{r_2^2 (m-1) + r_1^2 (m+1)} \right] \Bigg\} \tag{83}$$

The sealing force due to the internal pressure is found from the general solution for the Lagrange plate equation. The solution for a circular symmetric plate is:

$$y = pr^4/64D + K_1 r^2 \log r + K_2 r^2 + K_3 \log r + K_4 \tag{84}$$

The boundary conditions are:

$$r = r_1$$

$$y = 0$$

$$\frac{d^2y}{dr^2} + \frac{1}{mr}\frac{dy}{dr} = 0 \qquad (85)$$

$$r = r_2$$

$$y = 0$$

$$\frac{dy}{dr} = 0$$

The sealing force is the edge shear at $r = r_1$. This is a function only of

$$R_s = -D\left\{\frac{d^3y}{dr^3} + \frac{1}{r}\frac{d^2y}{dr^2} - \frac{1}{r^2}\frac{dy}{dr}\right\}_{r=r_1} \qquad (86)$$

one of the constants of integration, K_1. This constant is determined by applying the boundary conditions to equation (84).

$$R_s(\text{Plate}) = (pr_1/8)\left\{(m-1)(r_2/r_1)^6 - (7m-5)(r_2/r_1)^4 - (m+7)(r_2/r_1)^2 + (7m+3) + 4\left[(m+1)(r_2/r_1)^2 + (5m-1)\right](r_2/r_1)^2 \log(r_2/r_1) - 16(m+1)(r_2/r_1)^2\left[\log(r_2/r_1)\right]^2\right\} \Big/ \left\{(m-1)(r_2/r_1)^4 + 2(m+1)(r_2/r_1)^2 - (3m+1) - 8m(r_2/r_1)^2\log(r_2/r_1) + 4(m+1)(r_2/r_1)^2\left[\log(r_2/r_1)\right]^2\right\} \qquad (87)$$

The error in the calculated sealing force due to the initial deflection resulting from the use of beam theory is found by using equations (82) and (83) in (80).

$$\epsilon_y = 100 - \left[37.5/(r_2/r_1-1)^3\right]\left\{(r_2/r_1)^2 - 1 + \frac{2m\left[(r_2/r_1)^2-1\right] - 8m(r_2/r_1)^2\log(r_2/r_1)+4(r_2/r_1)^2(m+1)\left[\log(r_2/r_1)\right]^2}{(r_2/r_1)^2(m-1)+m+1}\right\} \quad (88)$$

The error in the calculated sealing force due to the internal pressure resulting from the use of beam theory is found by using equations (81) and (87) in (80).

$$\epsilon_p = 100-300(r_2/r_1-1)\left\{(m-1)(r_2/r_1)^4+2(m+1)(r_2/r_1)^2 - (3m+1) - 8m(r_2/r_1)^2\log(r_2/r_1) + 4(m+1)(r_2/r_1)^2\left[\log(r_2/r_1)\right]^2\right\} \Big/ \left\{(m-1)(r_2/r_1)^6 - (7m-5)(r_2/r_1)^4-(m+7)(r_2/r_1)^2 + (7m+3) + 4\left[(m+1)(r_2/r_1)^2+(5m-1)\right](r_2/r_1)^2\log(r_2/r_1) - 16(m+1)(r_2/r_1)^2\left[\log(r_2/r_1)\right]^2\right\} \quad (89)$$

ϵ_y and ϵ_p were calculated for values of the radius ratio from 1.0 to 1.4. These results were plotted, Fig. 51.19 and are very closely approximated by the straight line equations:

$$\epsilon_y = 51.62\ (1-r_2/r_1)$$
$$\epsilon_p = 18.66\ (1-r_2/r_1) \quad (90)$$

Note the error in the calculated sealing force due to the initial deflection is nearly three times that in the calculated sealing force due to internal pressure. This does not mean that the error in calculating the sealing force is the sum of these two errors, but it will be somewhere between the two curves. From the curves for sealing force versus internal pressure it is seen that the sealing force at 6000 psi is approximately six times that at

Fig. 51.19 PERCENT ERROR IN CALCULATED SEALING FORCE, R_s, AS A FUNCTION OF RADIUS RATIO. BEAM THEORY COMPARED TO PLATE THEORY. SEALING FORCE DUE TO END RESTRAINT AND PRESSURE LOAD CALCULATED SEPARATELY. CALCULATIONS BASED ON UNIFORM WIDTH BEAM AND FLAT CIRCULAR PLATE.

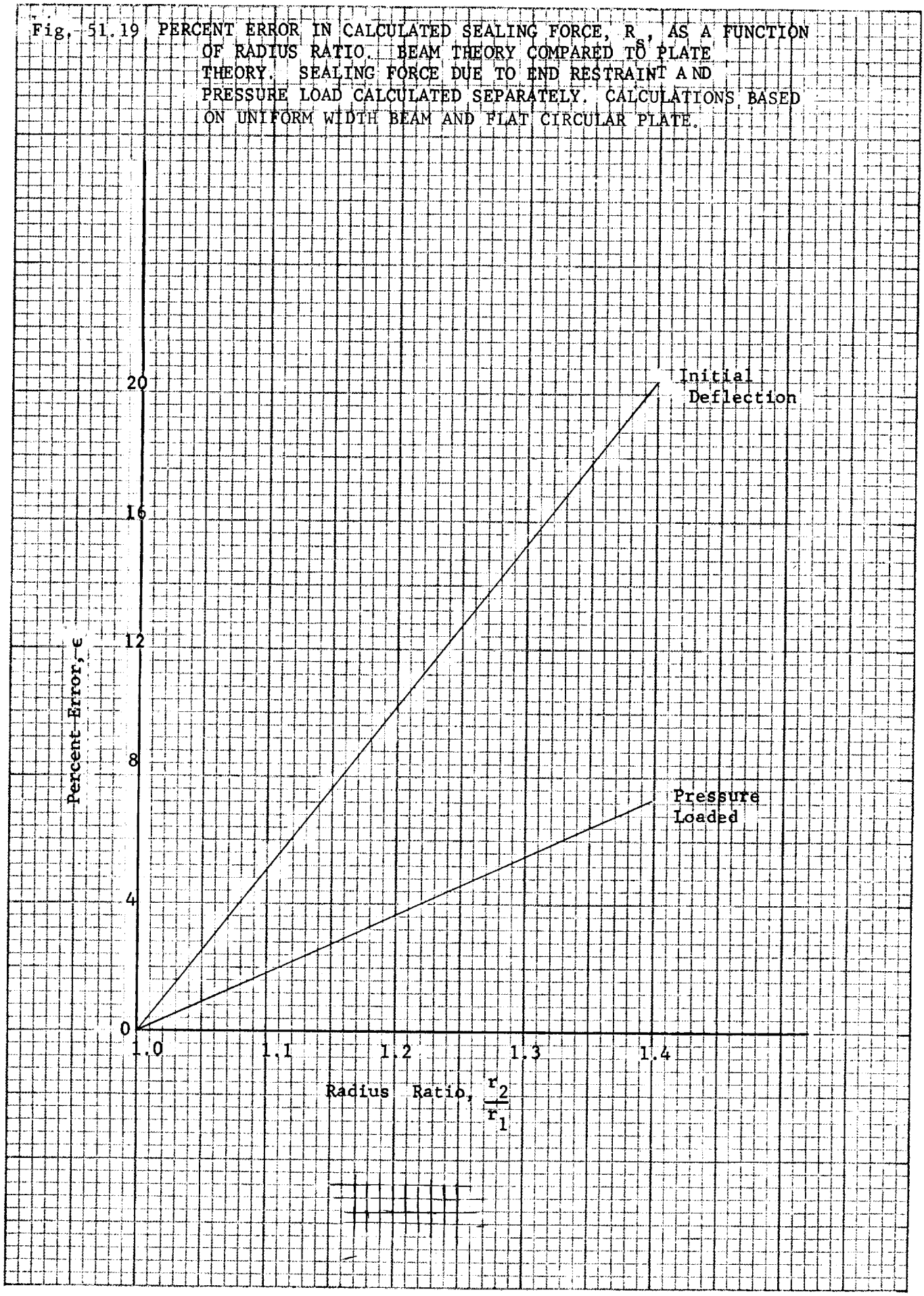

FIG. 51.20 TOTAL ERROR IN SEALING CALCULATION USING BEAM THEORY, BASED ON CALCULATIONS FOR "SEAL WITH STRAIGHT LEG OF CONSTANT WIDTH". A RATIO OF SEALING FORCE AT 6000 PSI TO 0 PSI OF 6 WAS USED. SEE FIG. 51.23.

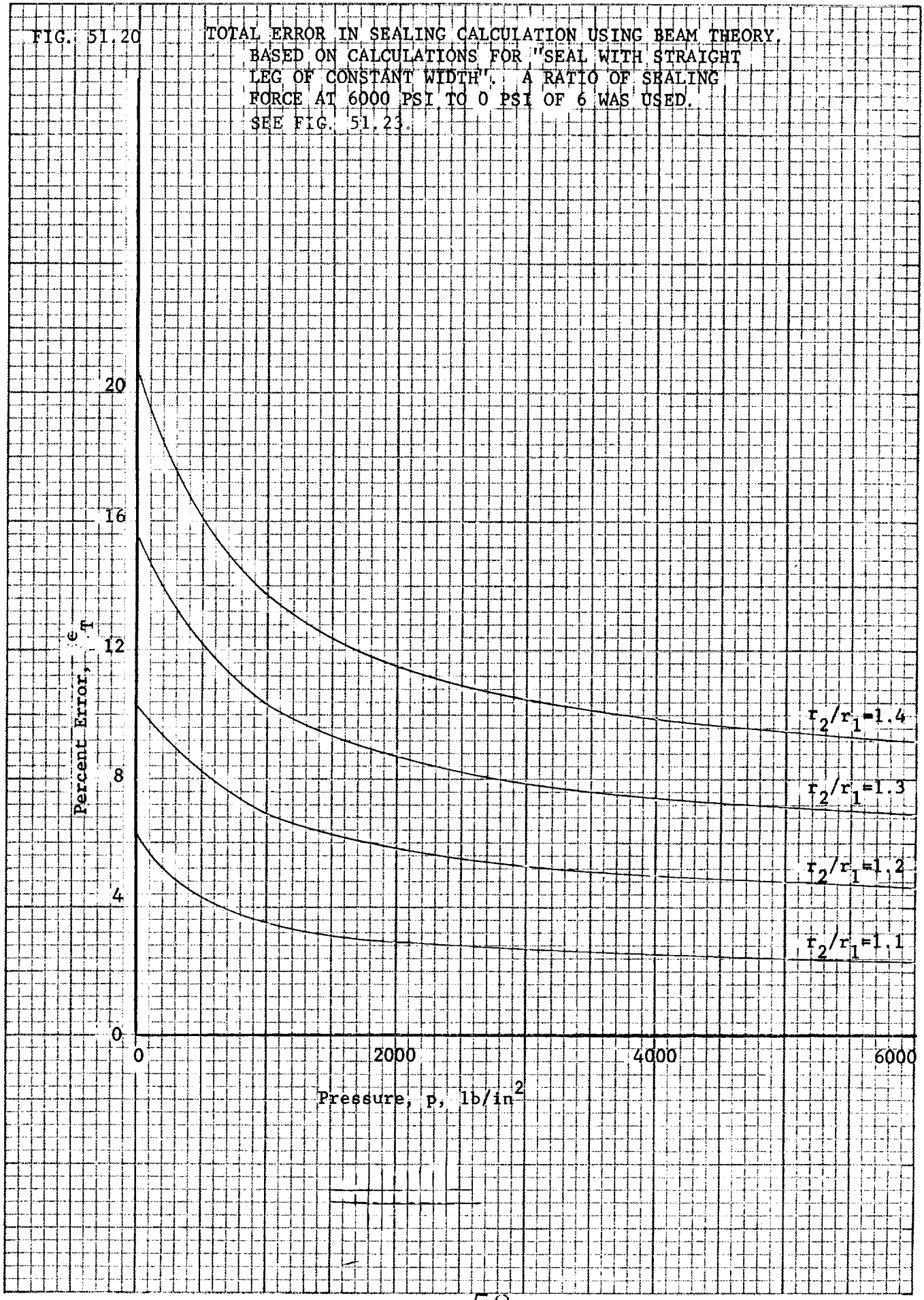

zero psi. An expression for the total error may be found from the two errors previously calculated and the sealing force ratio.

$$\epsilon_T = \frac{\epsilon_y(100+\epsilon_p) + 6\,\epsilon_p(100+\epsilon_y)}{(100+\epsilon_p) + 6(100+\epsilon_y)} \tag{91}$$

Using this formula a set of curves of total error versus pressure for constant radii ratios were calculated, Fig. 51.20. These curves show a marked decrease in the error as the pressure increases. Above 4000 psi the error in the sealing force is less than ten percent even for a radius ratio as large as 1.4. For a seal with a seal leg length of .2 inches this means that beam theory will give answers accurate to within ten percent for internal radii as small as .5 inches.

51.5.8.2 Beam-Shell Analogy

The sealing force using beam theory was readily found using the formulas of Ref. 3, where $\emptyset$ is the cone angle.

$$R_s(\text{Beam}) = 3\ell p \cos^2 \emptyset/8 + Eh^3(H_F - H_R) \cos \emptyset / \left\langle 4(1 - \nu^2)\ell^3 \right\rangle \quad (92)$$

The sealing force using shell theory is not readily found, and it is not possible to determine an expression for the error which is a function only of radius ratio and cone angle. The error is defined like the error in the beam-plate analogy.

$$\epsilon = \frac{R_s(\text{Shell}) - R_s(\text{Beam})}{R_s(\text{Shell})} \times 100 \quad (93)$$

The sealing force was calculated, using the following for the parameters:

$E = 30 \times 10^6$ psi

$h = .015$ inches

$H_F - H_R = .01$

$\ell = .15$ inches

$p = 6000$ psi

$\nu = .3$

The beam-theory results were easily calculated by hand, using equation (92). The shell-theory calculations were done on a digital computer, using an existing computer program. The results were combined and the error calculated as a function of radius ratio, Fig. 51.21 and cone angle, Fig. 51.22. Note that the error increases very rapidly as the cone angle increases, particularly for angles larger than twenty degrees.

FIG. 51.21.

BEAM-SHELL ANALOGY

ERROR IN CALCULATED SEALING FORCE USING BEAM THEORY INSTEAD OF CONICAL SHELL THEORY. BEAM AND SHELL OF UNIFORM WIDTH. TYPICAL DIMENSIONS IN TEXT.

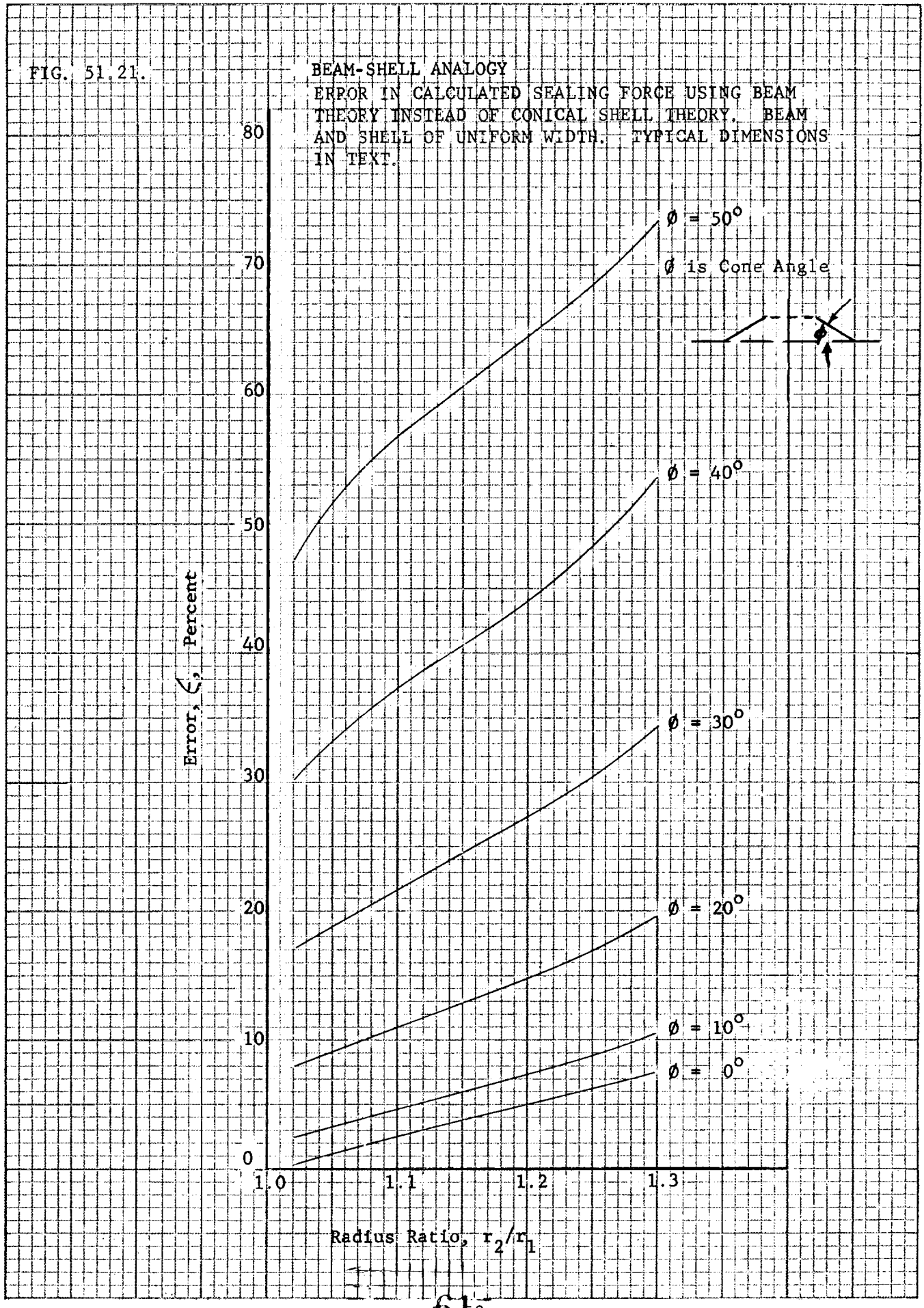

FIG. 51.22 BEAM - SHELL ANALOGY :

ERROR IN CALCULATED SEALING FORCE USING BEAM THEORY INSTEAD OF CONICAL SHELL THEORY. BEAM AND SHELL OF UNIFORM WIDTH. TYPICAL DIMENSIONS IN TEXT.

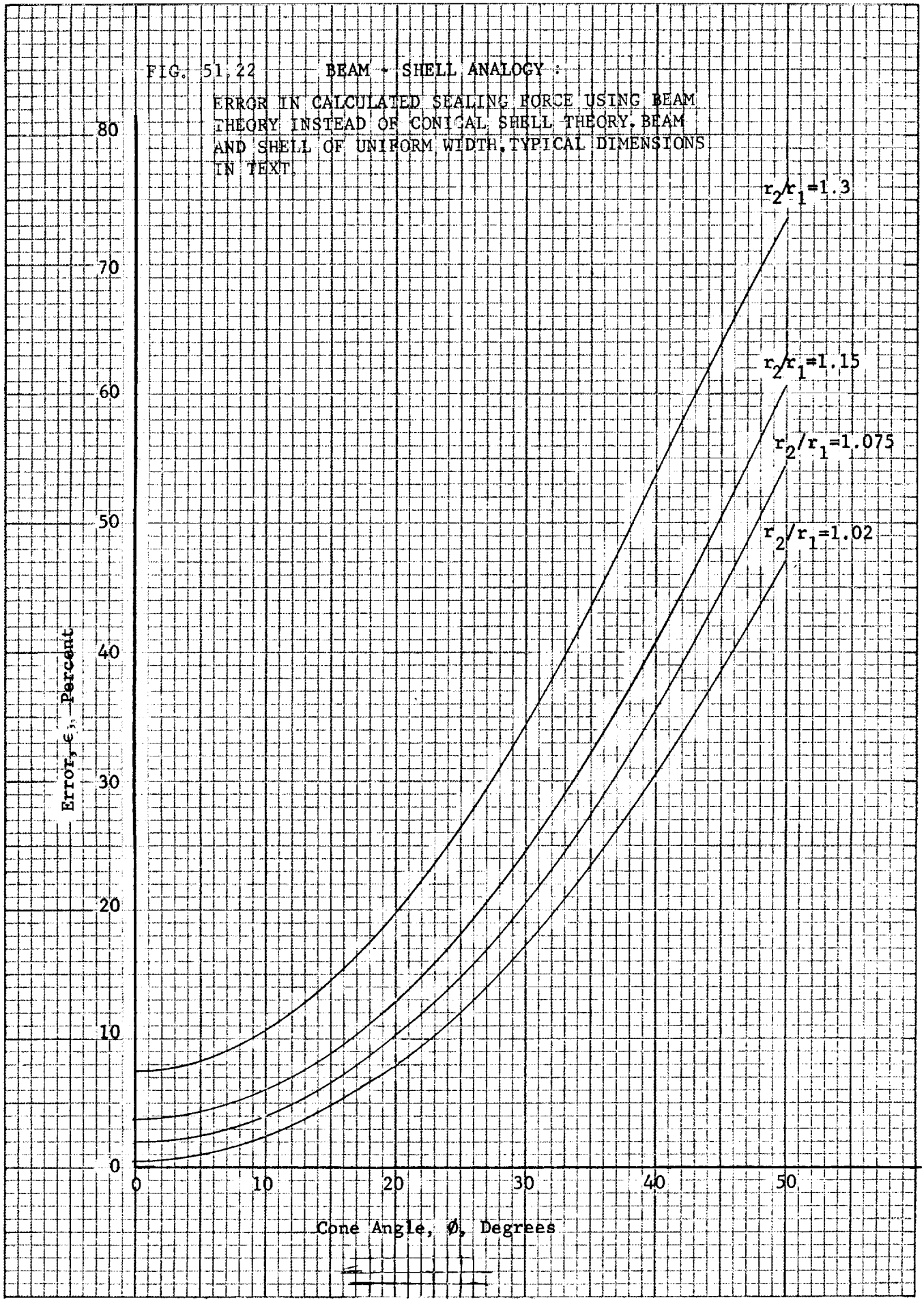

51.5.9 Calculation of Seal Characteristics

A number of different seals were analyzed in this report. In order to illustrate the characteristics of these seals and obtain a comparison of these characteristics, typical dimensions were chosen and numerical values calculated. The action of both seal legs and webs was calculated. These calculations should be an aid to the designer in selecting a type of seal and in determing the seal dimensions.

51.5.9.1 Seal with Constant-Width Leg

Of the various seal legs, this is the simplest. It is analyzed using beam theory in Section 51.5.1. As for all seal legs, the sealing force is of primary importance and the maximum stress of secondary importance. The sealing force was calculated using equation (4). The following parameters were used:

Curve	1	2	3
E psi	30×10^6	30×10^6	30×10^6
h inches	.029	.0251	.0224
ℓ inches	.15	.15	.15
y_ℓ inches	- .001	-.0015	-.002
ν	.3	.3	.3

The sealing-force-versus-pressure curves are straight lines, Fig. 51.23. Note that slopes of all three lines are alike and that there is a greater than six-fold increase in sealing force from zero to 6000 psi pressure. From equation (4), it is seen that the slope is proportional to the length of the seal leg. Cutting the leg length in half will decrease the ratio of sealing force at 6000 psi to that at zero psi to slightly over three. Adjustment of the slope of the curve is possible within reasonable limits. To achieve a desired slop(may necessitate an impractically long or short seal leg. For this reason the other seal designs should be considered.

The curves for maximum stress as a function of internal pressure were calculated from equation (3). Note that seal-leg dimensions were chosen to give a complete stress reversal as the pressure increases from zero to 6000 psi and to give specified end stresses. This design method optimizes the use of the material for a particular maximum allowable stress.

FIG. 51.23 SEALING FORCE AS A FUNCTION OF INTERNAL PRESSURE

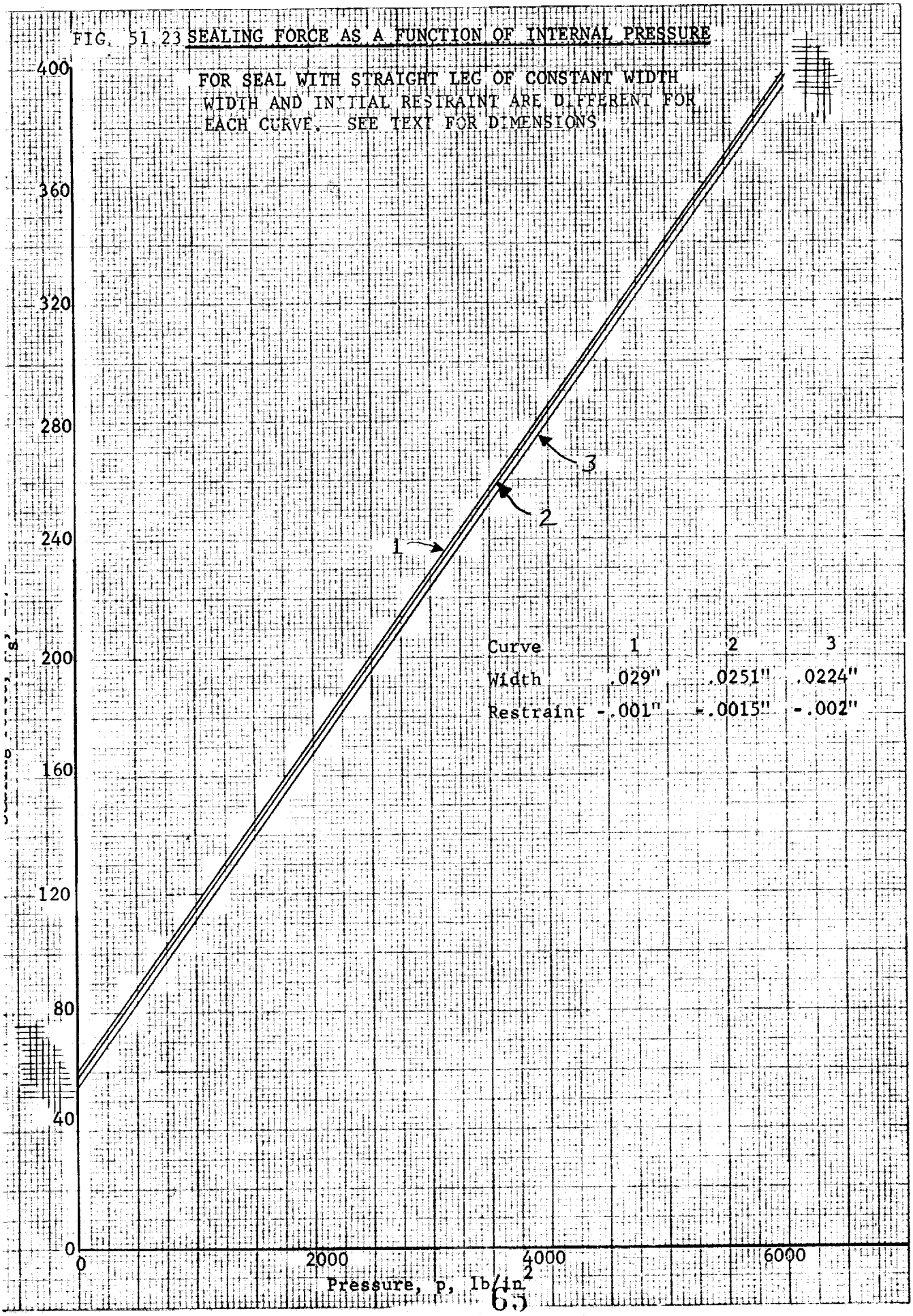

FIG. 51.24 MAXIMUM STRESS AS A FUNCTION OF INTERNAL PRESSURE FOR A SEAL WITH CONSTANT WIDTH LEG WIDTH AND INITIAL RESTRAINT ARE DIFFERENT FOR EACH CURVE. SEE TEXT FOR DIMENSIONS.

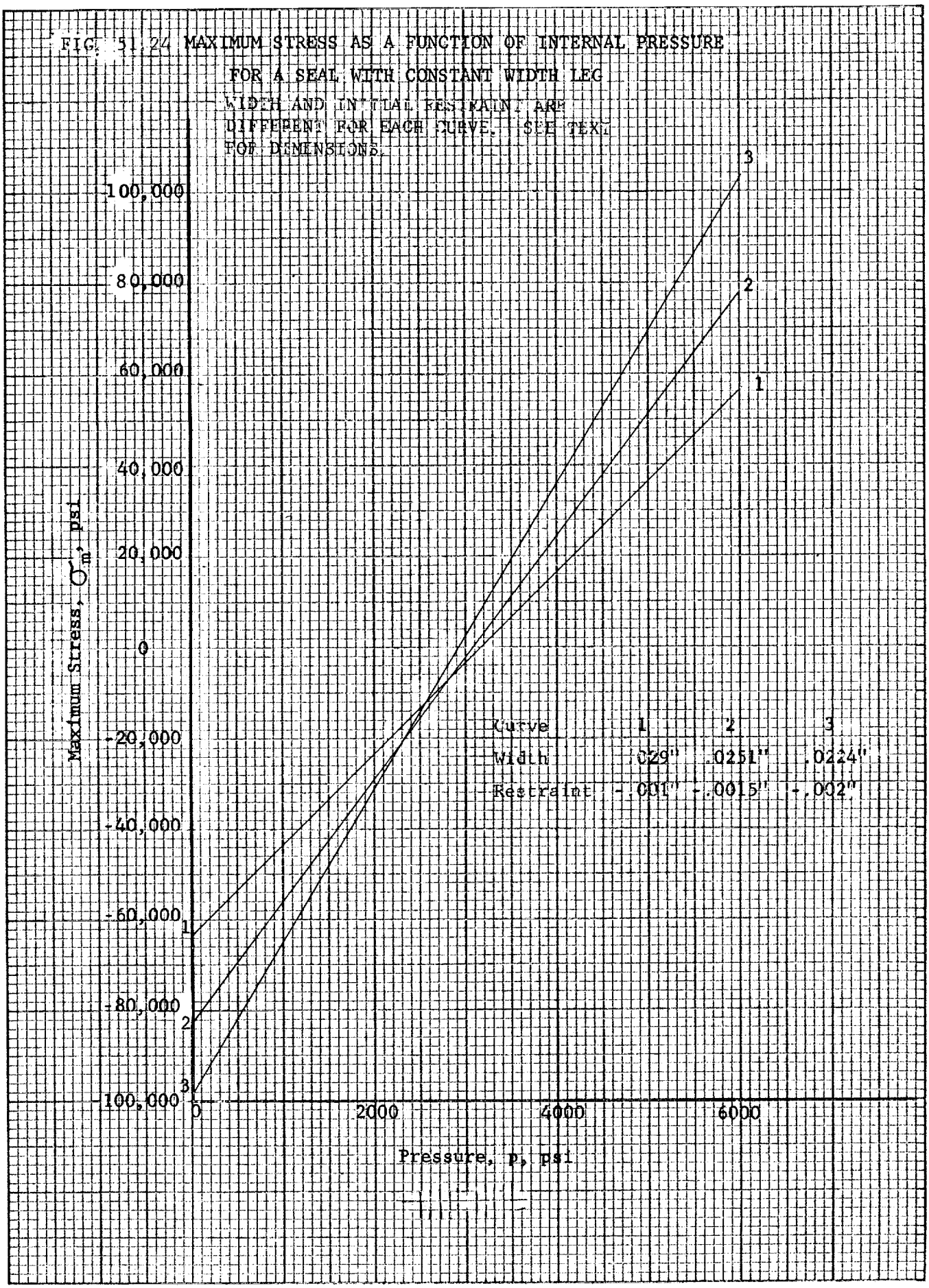

51.5.9.2 Seal with Leg of Linearly Varying Thickness

The linearly tapered seal leg was analyzed in Section 51.5.2. The equations, although more complex than the previous case, are amenable to hand calculations. Note that once the geometric parameters have been substituted in the equations, they are linear functions of the end restraint and internal pressure.

Four cases were chosen, each with a different taper but all with the same mean width. The case with zero taper is case 2 of the previous section. Only the amount of taper was varied in order to highlight this effect. One of the cases has a reverse taper.

Curve	2	4	5	6
a inch	.0251	.0301	.0201	.0151
b inch	0	-.0667	.0667	.1333
E psi	$30x10^6$	$30x10^6$	$30x10^6$	$30x10^6$
ℓ inch	.15	.15	.15	.15
y_ℓ inch	-.0015	-.0015	-.0015	-.0015
ν	.3	.3	.3	.3

The beam is given by equation (11).

$$h = a + bx \tag{11}$$

The sealing force as a function of initial deflection and internal pressure is given by equation (18) of Section 51.5.2. Note that as the amount of taper is increased, with the web end of the leg becoming thicker, the sealing-force curve becomes more flat. The ratio of sealing force at 6000 psi to the sealing force at 0 psi is 4.3 for curve 6, with maximum taper, compared to a ratio of 6.8 for curve 2, without taper.

The slope of the curve is determined by the coefficient of the pressure term. By setting $y_o=0$ in equation (18) and grouping the parameters, the following equation is obtained:

$$\frac{R_s}{p\ell} = \frac{2\left(\frac{b\ell}{a}\right)^3 + 9\left(\frac{b\ell}{a}\right)^2 + 6\left(\frac{b\ell}{a}\right) - 6\left(1+\frac{b\ell}{a}\right)^2 \log\left(1+\frac{b\ell}{a}\right)}{4\left(\frac{b\ell}{a}\right)\left(1+\frac{b\ell}{a}\right)^2 \log\left(1+\frac{b\ell}{a}\right) - 6\left(\frac{b\ell}{a}\right)^3 - 4\left(\frac{b\ell}{a}\right)^2} \tag{94}$$

Note that $b\ell/a$ is the change in leg width divided by the leg width at the lip end. This is related to the ratio of the leg width at the web end to that at the lip end by the relation:

$$\frac{h(web)}{h(lip)} = \frac{b\ell+a}{a} = \frac{b\ell}{a} + 1 \tag{95}$$

FIG. 51.25 SEALING FORCE AS A FUNCTION OF INTERNAL PRESSURE

SEAL WITH LEG OF LINEARLY VARYING THICKNESS

MEAN WIDTH OF SEAL LEG HELD CONSTANT

TAPER FOR EACH CURVE IS DIFFERENT

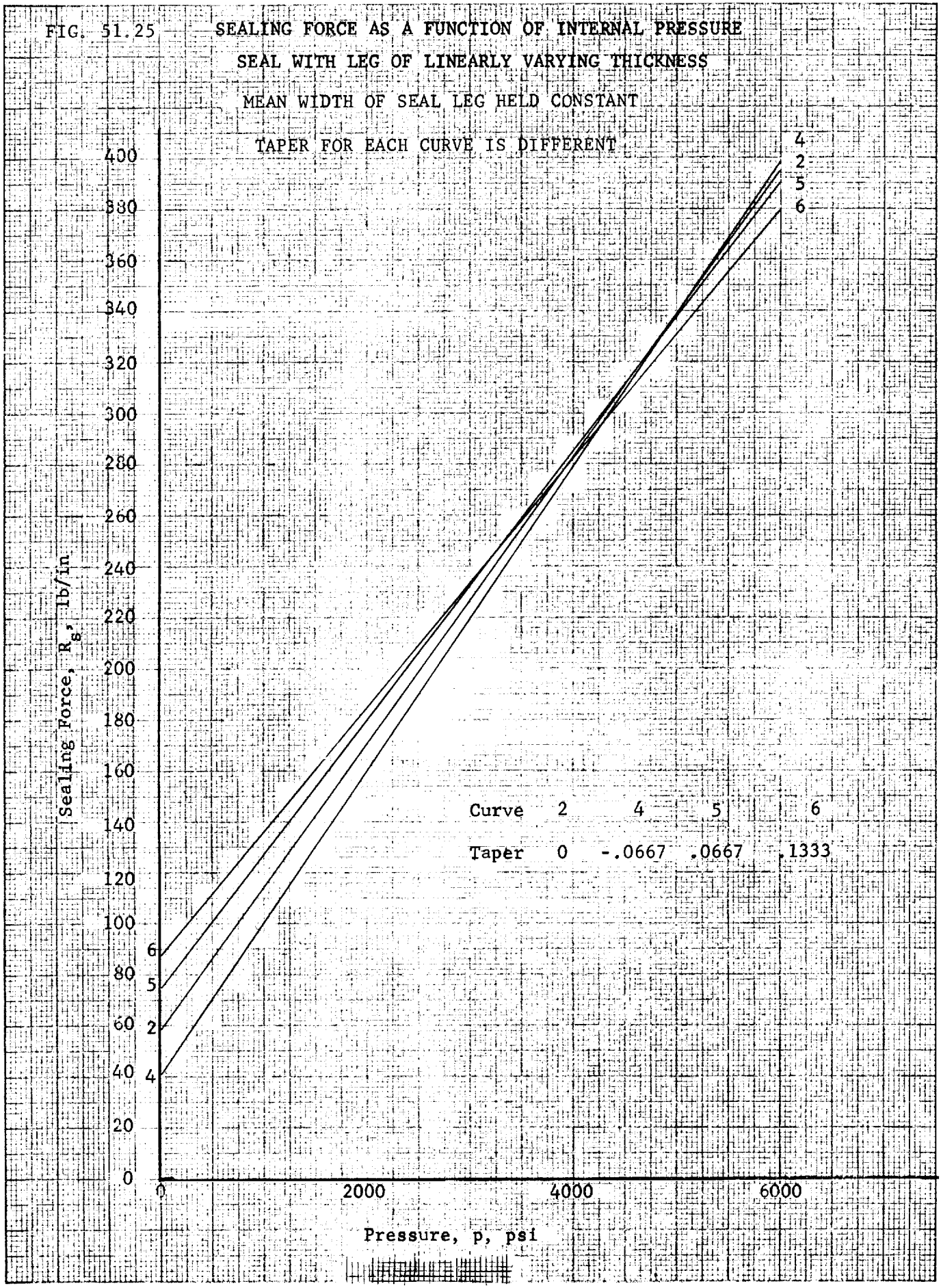

Therefore, the slope of the line R_s versus p is a function of the leg width ratio and leg length. $R_s/p\ell$ is plotted as a function of leg width ratio on Fig. 51.26. This curve shows that the slope of the R_s versus p curve decreases as the leg width ratio is increased and the leg length is decreased.

The curve of maximum stress as a function of internal pressure, Fig. 51.27, shows that the maximum stress decreases as the web end width is increased relative to the lip end width. This adds another reason for having a tapered seal leg whose width gets smaller toward the lip end.

FIG. 51.26 SEALING-FORCE RATIO AS A FUNCTION OF LEG WIDTH RATIO.
SEAL WITH LEG OF LINEARLY VARYING THICKNESS
NO INITIAL RESTRAINT OF SEAL LEG

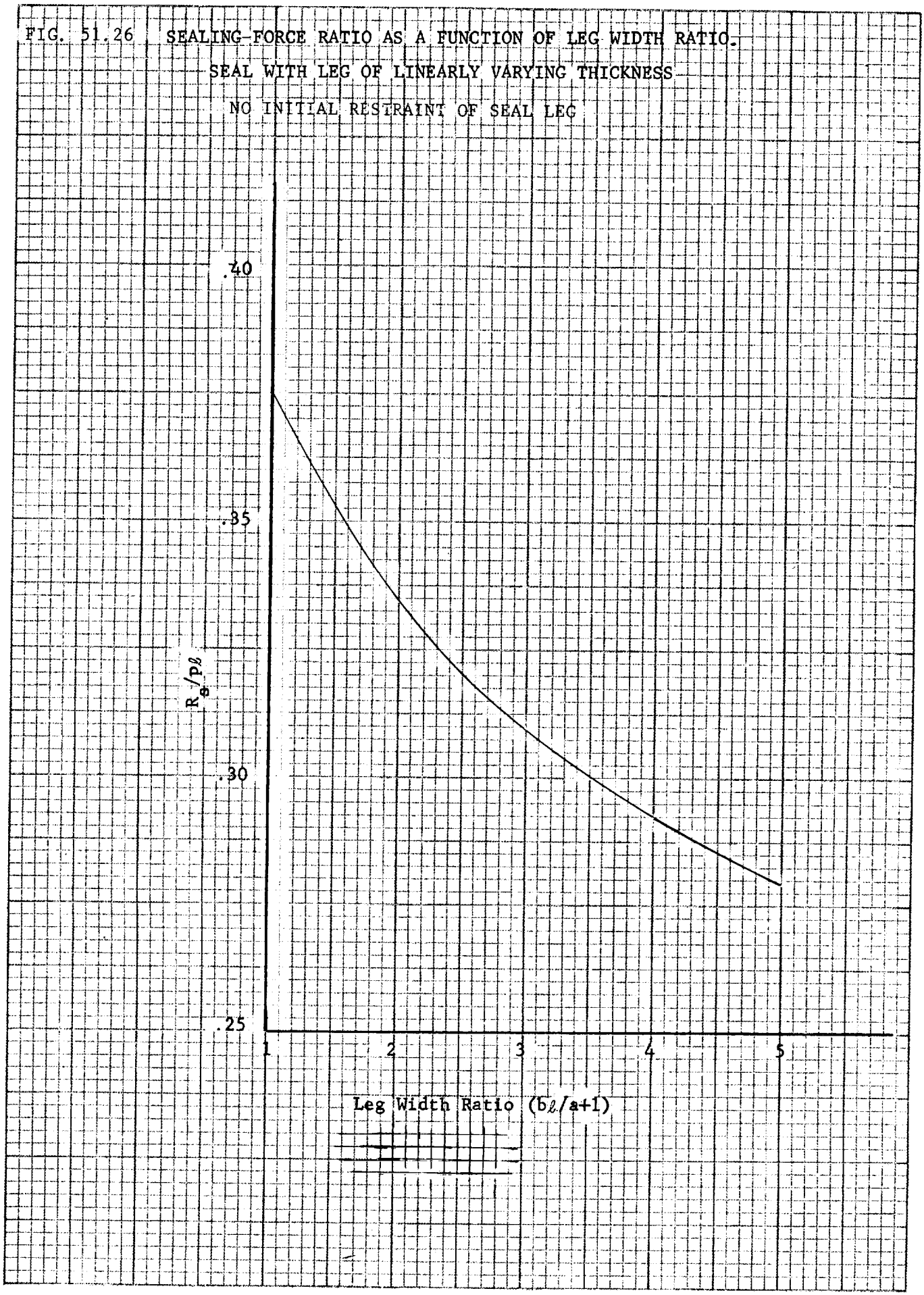

FIG. 51.27 MAXIMUM STRESS AS A FUNCTION OF INTERNAL PRESSURE.
SEAL WITH LEG OF LINEARLY VARYING THICKNESS.
MEAN WIDTH OF SEAL LEG HELD CONSTANT.
TAPER FOR EACH CURVE IS DIFFERENT.

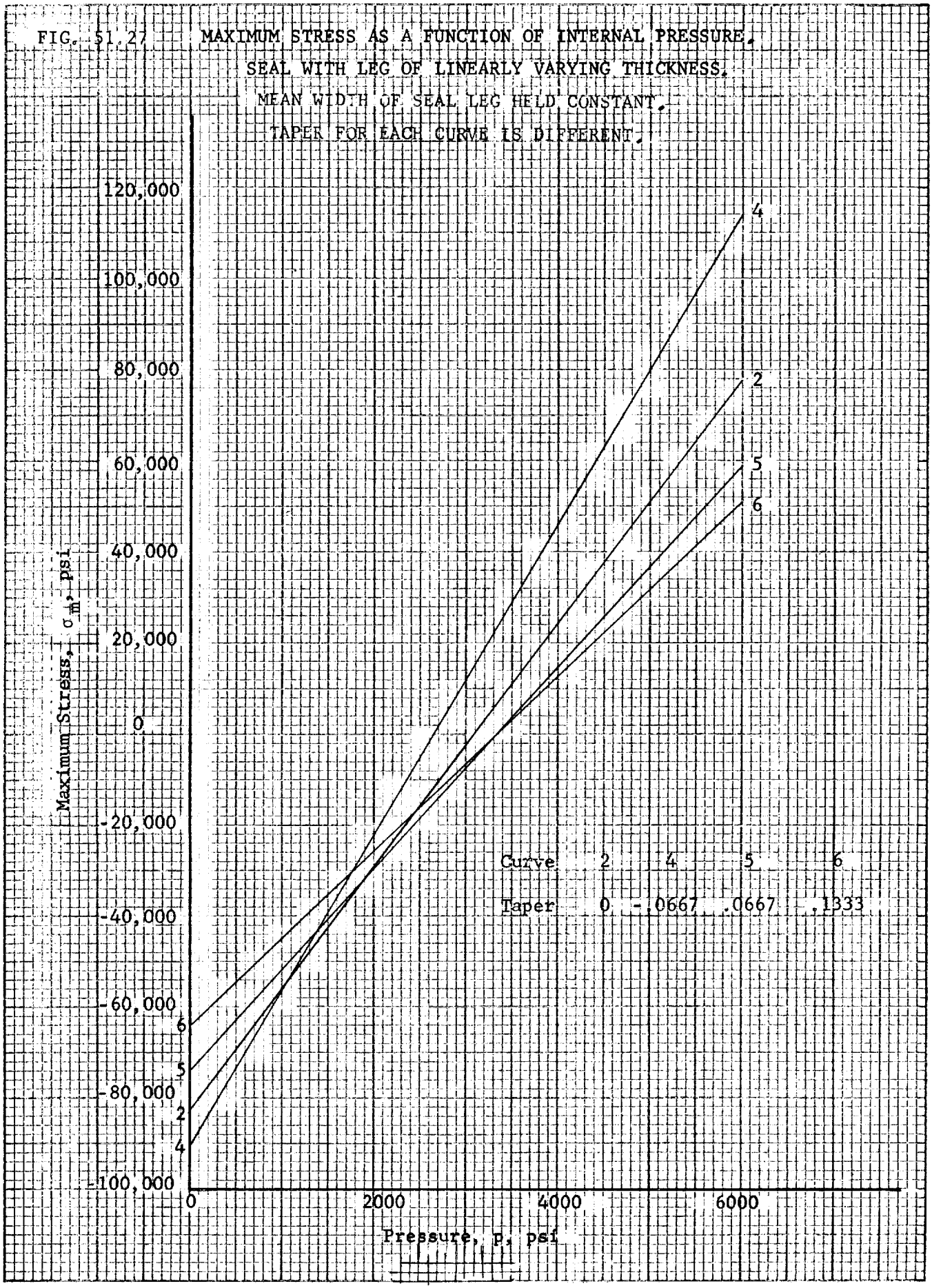

51.5.9.3 Seal Without Lip

The seal description and analysis are covered in Sections 51.3.3 and 51.5.3 of this report. This seal behaves differently from the two seals already discussed in that the point of sealing moves as the internal pressure and initial deflection are increased. The seal is at a very small angle to the flange face and as it is forced against the flange face part of the leg at the free end lays flat along the flange face. This part is in simple compression and has no effect on the remaining length of leg which is referred to as the active leg length.

This extra variable complicates the computations and makes it difficult to choose the parameters so as to obtain an exact comparison with the seal geometries for the previous two cases. Because the leg length decreases with increasing pressure a length slightly larger than that used for the previous cases was chosen. The material properties chosen are the same. The maximum allowable stresses are the same, but unlike the case of a uniform width leg with a lip, only the stresses on one end of the pressure scale approach these values.

Curve		7	8	9
E	psi	30×10^6	30×10^6	30×10^6
ℓ_o	inch	.2	.2	.2
R_o	lb/in	60	80	100
ν		.3	.3	.3
σ_o	psi	60,000	80,000	100,000

The calculated seal leg width for all three cases is .0346 inches and the end restraint is:

Case	y_ℓ inches
7	.0014
8	.0019
9	.0023

The calculated value of the active leg length as a function of internal pressure is given by Fig. 51.28. Note that the change in active leg length decreases as the initial deflection increases.

The sealing force versus internal pressure curves, Fig. 51.29 are similar to those for a leg of uniform width with a lip. Curve 2 has been added to show the similarity. The curves are nearly linear and of approximately the same slope as curve 2.

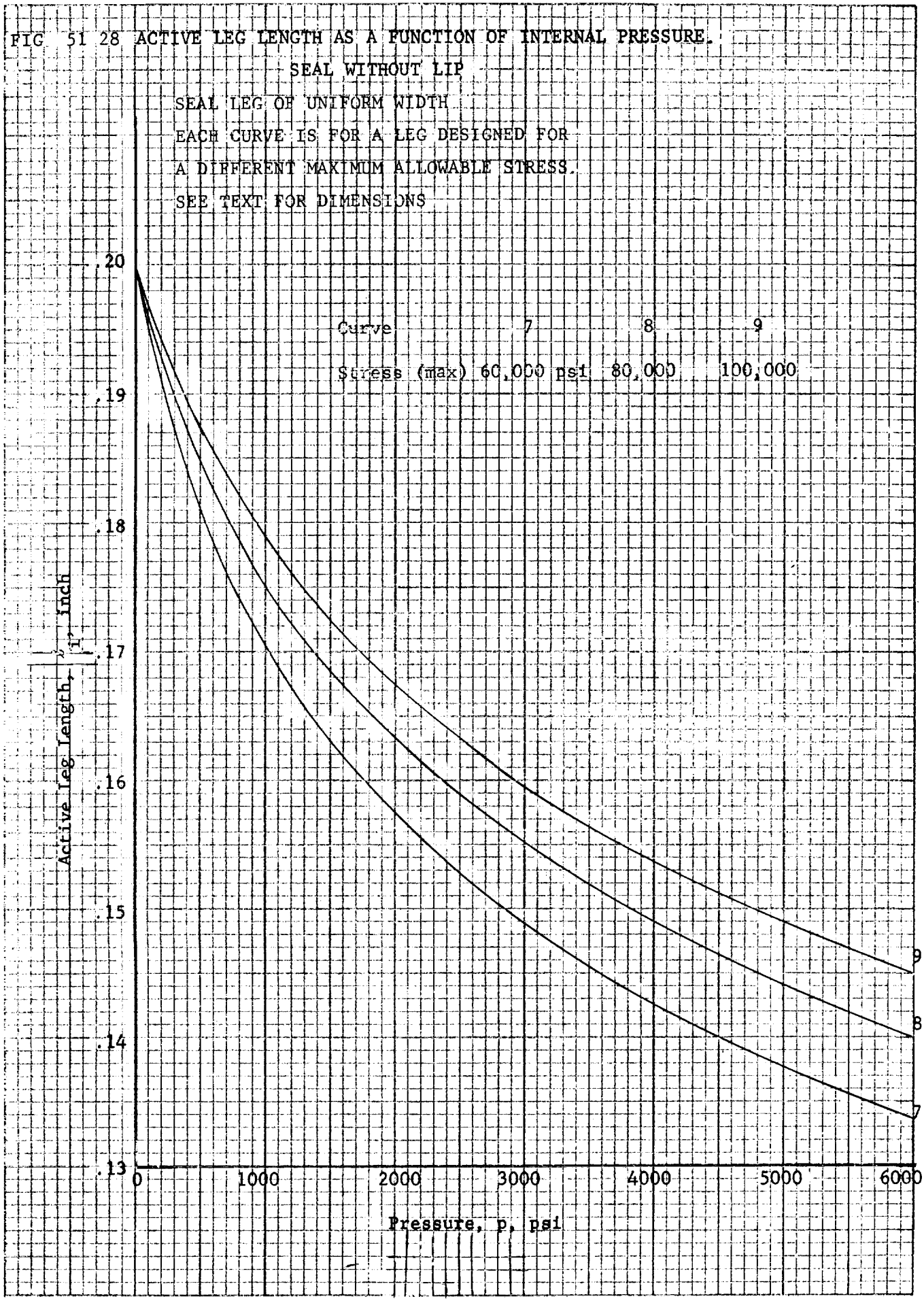
FIG 51 28 ACTIVE LEG LENGTH AS A FUNCTION OF INTERNAL PRESSURE.
SEAL WITHOUT LIP
SEAL LEG OF UNIFORM WIDTH
EACH CURVE IS FOR A LEG DESIGNED FOR
A DIFFERENT MAXIMUM ALLOWABLE STRESS.
SEE TEXT FOR DIMENSIONS
Curve 7 8 9
Stress (max) 60,000 psi 80,000 100,000
.20
.19
.18
.17
.16
.15
.14
.13
Active Leg Length, l, inch
0
1000
2000
3000
4000
5000
6000
Pressure, p, psi
9
8
7

FIG. 51.29 SEALING FORCE AS A FUNCTION OF INTERNAL PRESSURE.
SEAL WITHOUT LIP.
SEAL LEG OF UNIFORM WIDTH.
EACH CURVE IS FOR A LEG DESIGNED FOR
A DIFFERENT MAXIMUM ALLOWABLE STRESS.
SEE TEXT FOR DIMENSIONS

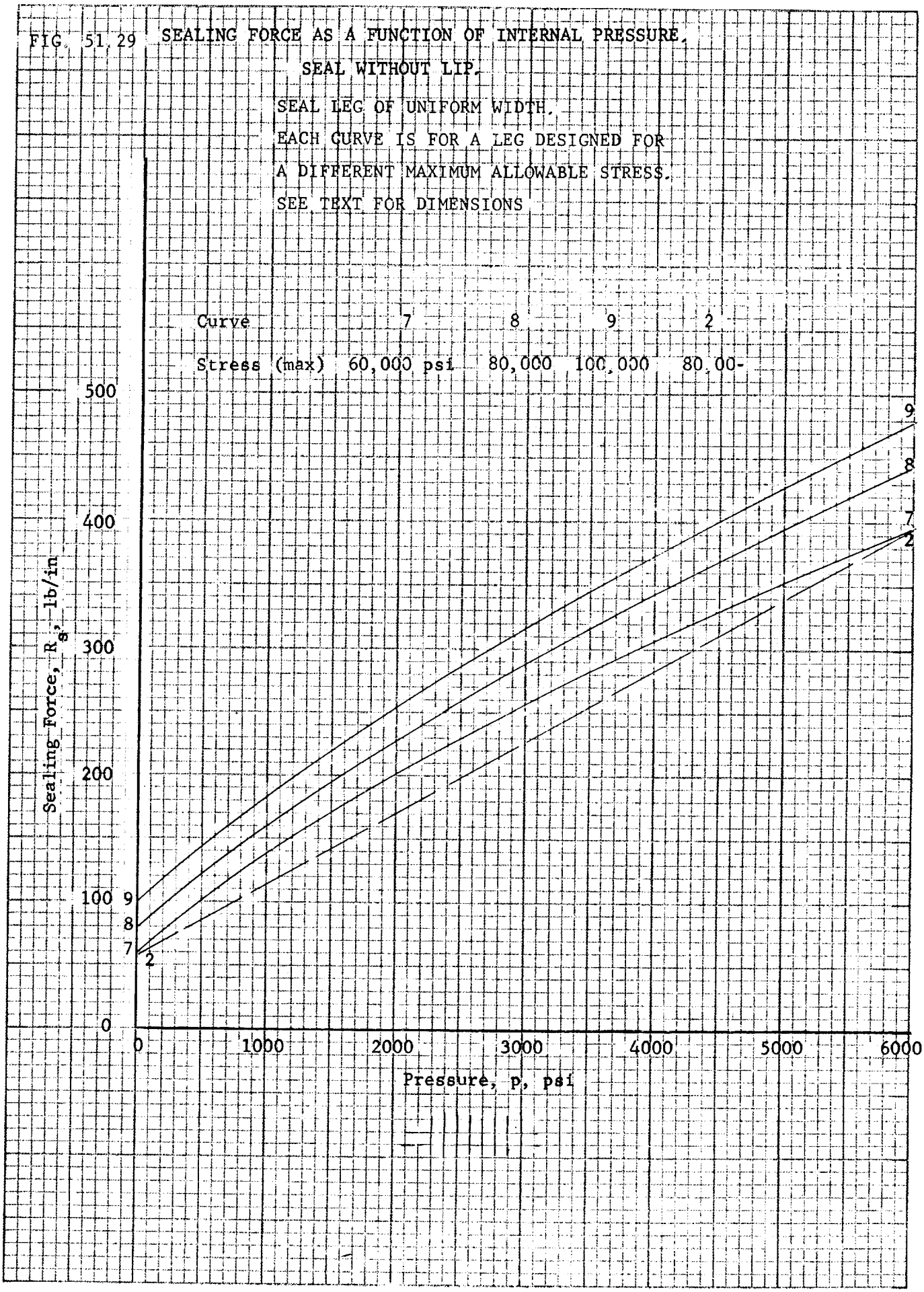

The stress-versus-pressure curves, Fig. 51.30, show that the maximum stress is equal to the allowable for the respective curve at zero pressure. As in the case of the other seal legs, the stress decreases as the pressure increases. However, unlike the other seal legs, the stress does not reverse itself.

The calculations are based on the equations derived in Section 51.5.3 of this report. Starting with equation (34) and substituting ℓ_o and cos ϕ from equations (30) and (31) respectively gives:

$$\sigma_o = 2Eh \tan^2\phi \Big/ \left[3y_\ell \, (1-\nu^2) \right] \tag{96}$$

Combining equations (30) and (31)

$$\tan \phi = - \, 3y_\ell / 2\ell_o \tag{97}$$

Substituting in equation (96)

$$y_\ell = 2(1-\nu^2)\ell_o^{\,2}\sigma_{\,o}/3Eh \tag{98}$$

The sealing force, R_o, for zero internal pressure is obtained by setting p = 0 in equation (42). Then using equations (31) and (97) the equation for R_o is:

$$R_o = - \, Eh^3 y\ell \Big/ \left[4 \, \ell_o^{\,3}(1-\nu^2)\cos \phi \right] \tag{99}$$

From equation (97) the cos ϕ is:

$$\cos \phi = 2\ell_o \Big/ \sqrt{9 \, y_\ell^{\,2} + 4 \, \ell_o^{\,2}} \tag{100}$$

Substituting for cos ϕ and y_ℓ in equation (99) from equations (100) and (98) respectively gives the following equation for h.

$$h^4 + \left\{ (1-\nu^2)^2 \, \ell_o^{\,2} \, \sigma_o^{\,2} / E^2 \right\} h^2 - \left\{ 36 \, R_o^{\,2} \, \ell_o^{\,2} / \sigma_o^{\,2} \right\} = 0 \tag{101}$$

Values of ν, ℓ_o, σ_o, E, and R_o were chosen and h was calculated from equation (101). Then y_ℓ was calculated from equation (98).

Substituting for cos ϕ and tan ϕ in equation (29) from equations (31) and (97) respectively gives;

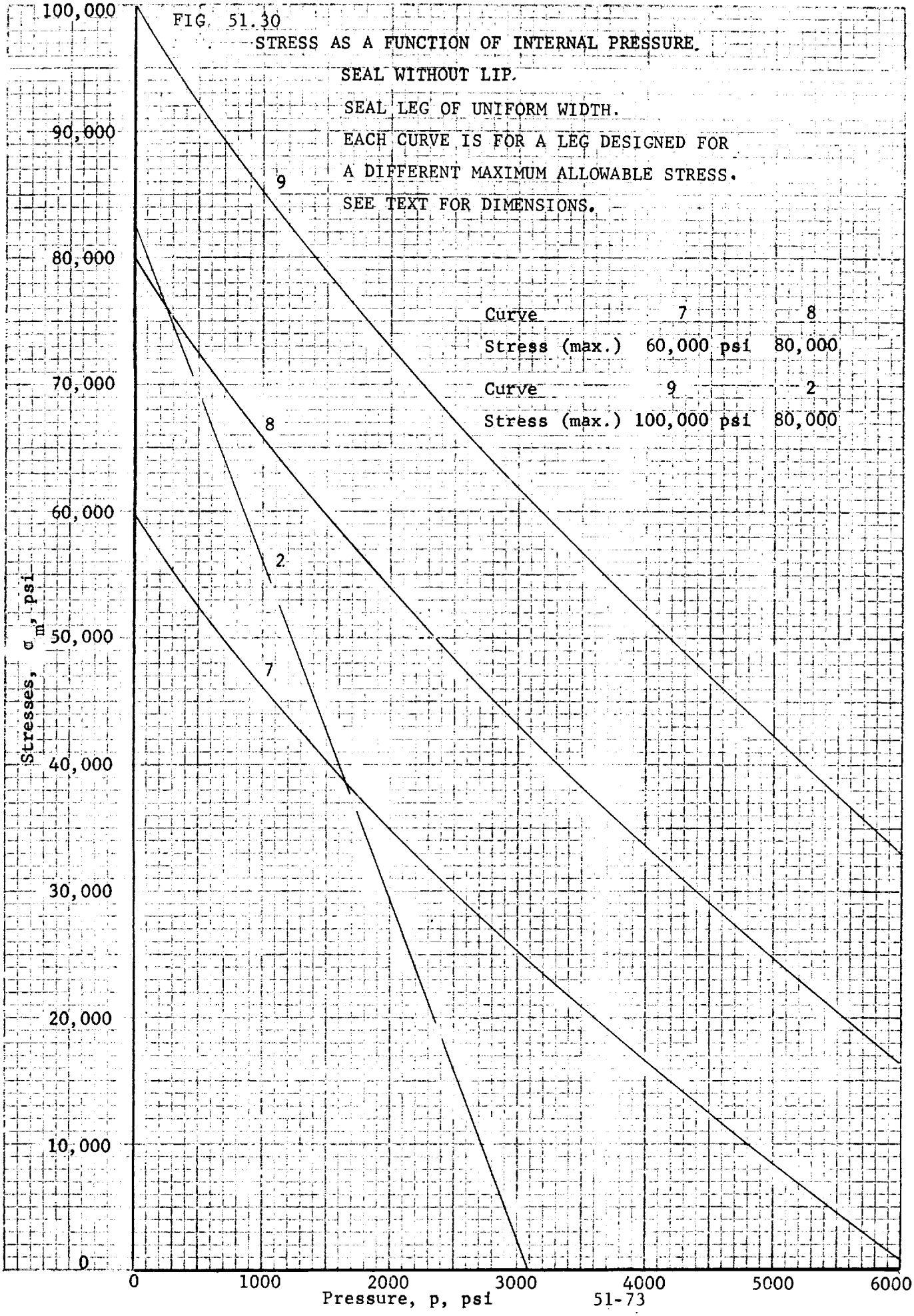
FIG. 51.30
STRESS AS A FUNCTION OF INTERNAL PRESSURE.
SEAL WITHOUT LIP.
SEAL LEG OF UNIFORM WIDTH.
EACH CURVE IS FOR A LEG DESIGNED FOR
A DIFFERENT MAXIMUM ALLOWABLE STRESS.
SEE TEXT FOR DIMENSIONS.
Curve 7 8
Stress (max.) 60,000 psi 80,000
Curve 9 2
Stress (max.) 100,000 psi 80,000
9
8
2
7
100,000
90,000
80,000
70,000
60,000
50,000
40,000
30,000
20,000
10,000
0
Stresses, σ_m, psi
0
1000
2000
3000
4000
5000
6000
Pressure, p, psi
51-73

$$p = 3Eh^3 y_\ell \left\{ 1/\ell_o - 1/\ell_i \right\} \Big/ \left[\ell_i^3 (1-\nu^2) \right] \qquad (102)$$

The curve of active leg length versus pressure was calculated from this equation.

Using equations (35) and (97) in equation (43) gives:

$$R_s = Eh^3 \sin \phi \left\{ 4\ell_o/3 - \ell_i \right\} \Big/ \left[2(1-\nu^2)\, \ell_i^3 \right] \qquad (103)$$

From equation (97):

$$\sin \phi = -3y_\ell \Big/ \sqrt{9y_\ell^2 + 4\ell_o^2} \qquad (104)$$

and the equation for R_s is:

$$R_s = -3Eh^3 y_\ell \left\{ 4\ell_o/3 - \ell_i \right\} \Big/ \left[2(1-\nu^2)\ell_i^3 \sqrt{9y_\ell^2 + 4\ell_o^2} \right] \qquad (105)$$

This equation was used to calculate the sealing force as a function of active leg length. The results were related to the pressure by the use of the calculations based on equation (102).

The stress equation was found by using equations (31) and (97) in equation (34).

$$\sigma_i = 3Ehy_\ell \left\{ 3/2\ell_o - 1/\ell_i \right\} \Big/ \left[\ell_i (1-\nu^2) \right]$$

The stress calculations were made using this equation and related to the pressure by equation (102).

For all three cases the angle between the seal leg and flange face is very small ($.6^o$, $.8^o$ and 1.0^o respectively for cases 7, 8 and 9). This was true for all the combinations of parameters tried unless ϕ was specifically set larger.

The mean active length for the three cases is slightly higher than the leg length for the previous cases. Another calculation was made specifying the mean length equal to the length of the seal leg of uniform width with a lip, case 2. The parameters used were:

$E = 30 \times 10^6$ psi

$h = .0251$ inch

$\ell(\text{mean}) = .15$ inch

$y_\ell = .0015$ inch

$\nu = .3$

51-74

The equations for the calculations were also derived from those in Section 51.5.3 of this report in a similar manner as those derived for the preceding calculations. The results have been combined in one figure, Fig. 51.31.

Another set of equations were derived in which the stress at 6000 psi internal pressure was made of equal magnitude to that at zero psi. Calculations were made specifying E (30×10^6 psi), ν (.3), R_o ($\sigma_o \times 10^{-3}$), and ϕ_o. The resulting values of the active leg length at zero pressure, ℓ_o, were too large, and the calculations were not carried further.

σ_o psi	ℓ_o inch	h, inch
60,000	.529	.0563
80,000	.7054	.0651
100,000	.8818	.0727

78

FIG. 51.31 ACTIVE LEG LENGTH, SEALING FORCE AND STRESS AS A FUNCTION OF PRESSURE.
SEAL OF UNIFORM WIDTH WITHOUT LIP.
MEAN LEG LENGTH EQUAL TO LEG LENGTH OF UNIFORM WIDTH SEAL LEG WITH A LIP (CASE 2).
SEE TEXT FOR DIMENSIONS.

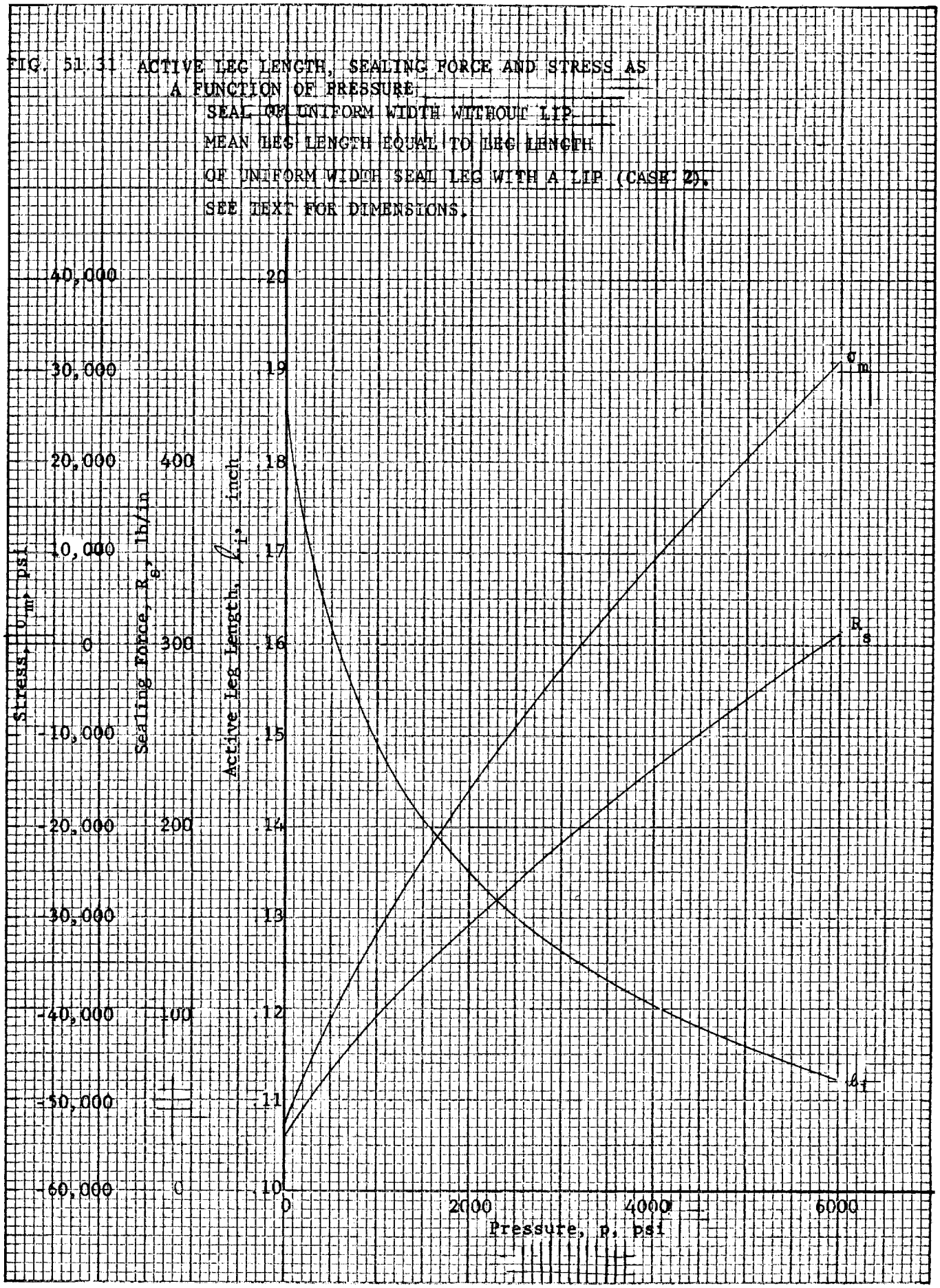

51.5.9.4 Radial Motion of Seal Lip

The radial motion of the seal lip due to internal pressure and differential radial growth of the flange faces was analyzed in Sections 51.5.5 and 51.5.6. Equation (55) of Section 51.5.5 gives the radial growth as a function of internal pressure. Using this equation, calculations based on the seal-leg dimensions used in case 2 were made. The web dimensions used were determined from equation (49) of Section 51.5.4, and L was chosen as 1/2 of ℓ. This gave an expression for δ_r as follows:

$$\delta_r = \frac{pr_1^2}{E\left(\frac{r_1 + \ell}{\frac{\sigma_m}{p} - \frac{1}{2}} + 4h\right)}$$

The calculations based on this equation are given in Fig. 51.12. Included is a curve of web thickness, t, as a function of inside radius, r_1, for a constant pressure of 6000 psi. Note that the other curves in the figures are based on the value of t calculated from equation (49) of Section 51.5.4.

The differential radial motion of the seal is the maximum displacement the seal can accommodate without having slippage between the seal lip and flange face. That is, for a differential radial growth of the flange faces less than δ_D, the seal will rotate and the seal lips will move with the flange face without slippage. If the differential radial motion of the flanges is greater than δ_D, the seal lips will slide on the flange face and leakage may result.

Calculations were made using equation (61) of Section 51.5.6 and equation (49) of Section 51.5.4. I_c in equation (61) was calculated using equation (49). The seal-leg dimensions and material properties of case 2 were used. The coefficient of friction used is a mean value for Teflon taken from the curves in Chapter 12 of Ref. 4. In accordance with the discussion of Section 51.5.4, the web thickness was not allowed to become less than the seal-leg thickness. For this reason the curves, Fig. 51.32, were begun at an inside radius of one inch and the lowest pressure used is 2000 psi. Smaller radii and lower pressures could be considered if necessary. It is noted that there is a finite δ_D versus r_1 curve at zero pressure as the initial deflection of the seal legs results in a normal force between the seal lip and flange face which makes it possible to apply a frictional moment on the seal.

The curves were not continued past a differential radial motion of .025 inches because the assumption of a small angle of rotation of the seal does not continue to be valid, and in the case of no internal pressure the seal lips rotate away from the flange faces when δ_D is greater than .0247 inches. The small-angle approximation made in the analysis is that the sine of the angle is equal to the angle in radian measure. The seal lips will break contact with the flange faces when the angle of rotation becomes so large that the seal lip-to-lip distance times the cosine of the angle is

FIG. 51.32

DIFFERENTIAL RADIAL MOTION VERSUS INSIDE RADIUS.
DIMENSIONS BASED ON CASE 2.
DIFFERENTIAL RADIAL MOTION OF FLANGE FACES
ALLOWABLE WITHOUT CAUSING THE SEAL LIP
TO SLIDE ON THE FLANGE FACE.
CALCULATIONS FOR SEAL WITH UNIFORM WIDTH
LEG WITH LIP. SEE TEXT FOR DIMENSIONS.

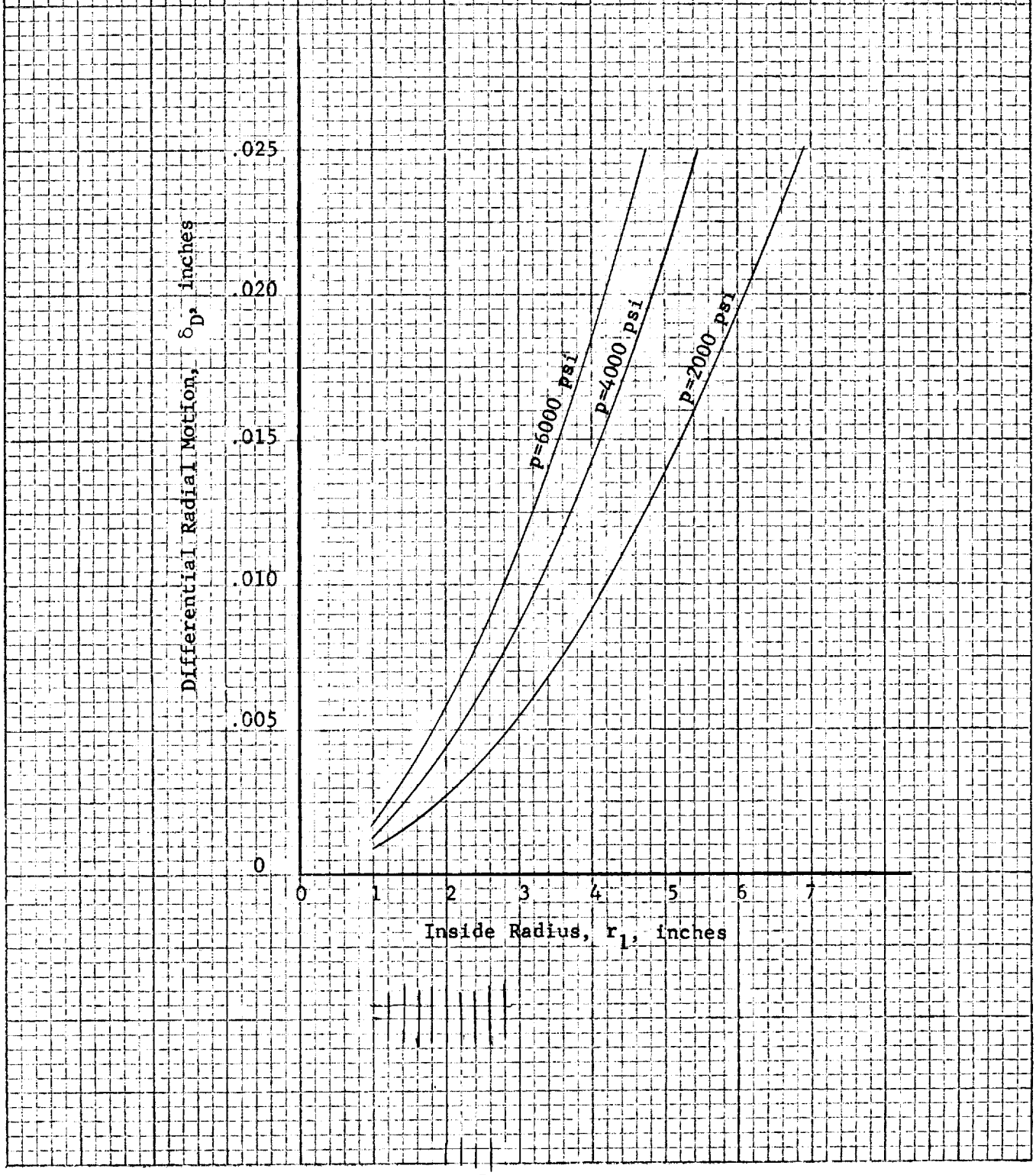

less than the height of the flange-face recess. When the pressure is zero, $y = 0$.

and the angle ϕ is readily determined. For finite pressures y is a function of the pressure, and the value of ϕ when $(H_F+y)\cos\phi=H_R$, increases with p.

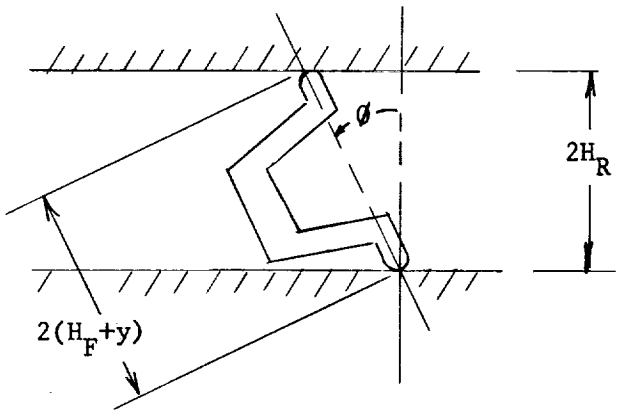

$$2\,(H_F+y)\,\cos\,\phi\,<\,2\,H_R$$

FIG. 51.33

ROTATION OF SEAL CROSS-SECTION

However, the relationship becomes non-linear and more difficult to solve. For a seal with a 10 inch inside radius, the results of linear theory are that for 6000 psi δ_D is .087 inches and for zero psi δ_D is .014 inches. The larger number is not accurate. δ_D for 6000 psi should be lower. However, the curves do show that not only because of slippage between the seal lip and flange face, but also because of seal and flange separation leakage may occur.

The seal rotation also causes additional hoop stresses and may overstress the seal. A 4.7 inch inside radius seal when subjected to an internal pressure is stressed in hoop tension to its allowable maximum of 80,000 psi (using dimensions for case 2). If in addition the seal is subjected to a differential radial motion of .025 inches the additional hoop stress is 76,800 psi. This is calculated using equation (62) of Section 51.5.6.

51.6 References

1. S. Timoshenko, Strength of Materials, Part II, Third Edition, D. Van Nostrand, 1959.

2. S. Timoshenko and S. Woinowsky-Kreger, Theory of Plates and Shells, Second Edition, McGraw-Hill, 1959.

3. R. J. Roark, Formulas for Stress and Strain, McGraw-Hill, 1954.

4. Machine Design Plastics Book, September 20, 1962.

83

52. HOLLOW METALLIC O-RINGS

by

B.T. Fang

52.0 Summary

Metallic O-rings have been used extensively as static seals under extreme temperature and pressure conditions. They are made of metal tubing formed into rings by welding the two ends together. A spacer or recessed flange must be used to limit the compression of the O-ring. When the connector is assembled, the O-ring is squeezed to the desired thickness and also expands radially so that it is tight against the back-up material provided by the spacer or the flange. The O-ring is often coated with a material such as Teflon or silver that can flow into the asperities of the flange and make a leak-tight joint.

There are three basic types of O-rings; the difference in their construction is evident from the following figure.

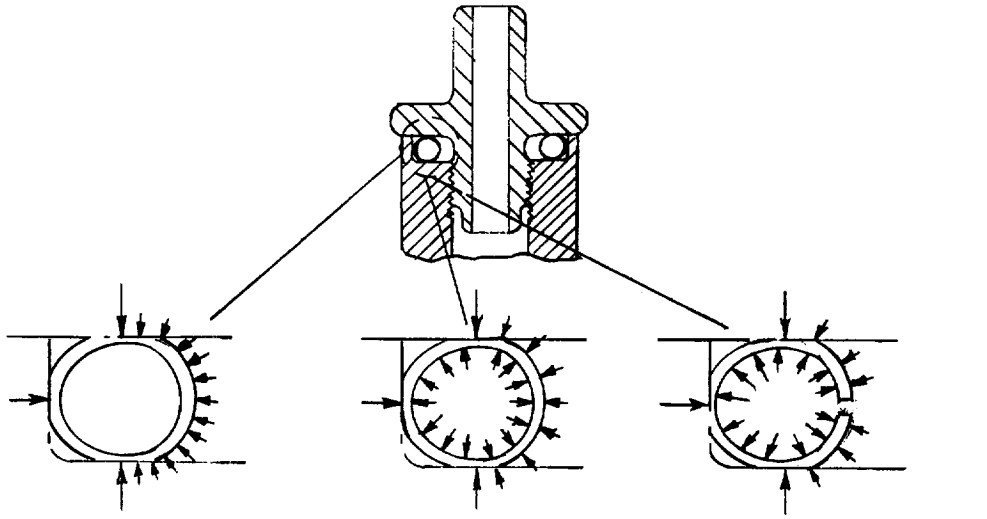

FIGURE 52.1 Three Common Types of Metallic O-ring

The standard O-ring is the most common of the three. The sealing force is derived from the initial compression and maintained by the resiliency of the O-ring. At high pressures there is the danger that the internal pressure may become larger than the sealing stress. Furthermore, the high pressure may cause the O-ring to buckle. The pressure-filled O-ring is filled with an inert gas at usually about 600 psi. At high temperature this gas expands and tightens the seal, while at low temperature it has the reverse effect. Because of the enclosed gas, the pressure-filled O-ring can withstand higher pressure before buckling would occur. The pressure-energized O-ring has holes drilled in the tube wall, and the pressure inside the ring is the same as the pressure in the system; therefore, the higher the pressure in the system, the greater is the sealing force.

A general elastic analysis of O-rings is given in Section 52.4. This is not only a prerequisite to a more general elastic-plastic analysis but also yields some useful information which is applicable despite the presence of plastic deformation in the practical application of O-rings. Among the conclusions are:

(1) Within the elastic theory, all three types of O-rings behave similarly. In particular, they all may have the same pressure-energizing effect.

(2) The use of a retaining ring or other mechanical back-up is desirable because it increases the pressure-energizing effect considerably.

O-rings currently in use are compressed to such an extent that large permanent deformation occurs. Because of the plasticity and large deformation effect, a theoretical analysis of the O-ring behavior becomes extremely difficult. Based on very much simplified assumptions, some considerations of the plastic behavior of O-rings are given in Section 52.3. The results obtained include

(1) A conservative estimate of the sealing force.

(2) An estimate of the decrease of the sealing force when the flanges tend to separate as a result of differential thermal expansion, external loads, etc.

(3) An estimate of the area of contact between the O-ring and the flange.

52.1 Summary of the Results of Elastic Analysis of O-rings

One of the primary requirements of face seals such as metallic O-rings is to maintain sufficient sealing pressure between the O-ring and the flange surfaces. In order to find out the variation of sealing pressure with the bolt load, the internal and external pressure, and so forth, we need to know the load-deflection relations. The deflection parameters of importance are the shortening of vertical diameter of the tube δ_V and the increase of the outside diameter of the O-ring δ_H. The elastic load-deflection relations for the four basic types of loading are obtained in Section 52.4 and are summarized as follows:

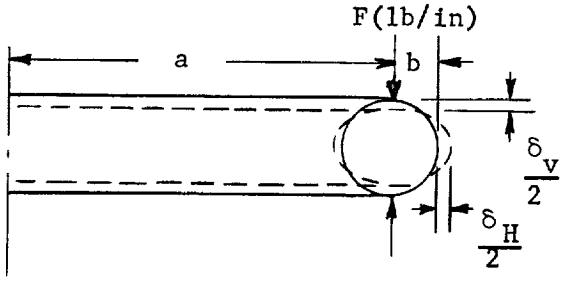

FIGURE 52.2 Axial Load

$$\frac{F}{\delta_v} = \frac{D}{b^3\left[0.149 - \dfrac{0.141}{1 + 14.4/\mu^2}\right]} = \text{Spring constant of the 0-ring} \quad (11a)$$

$$\frac{F}{\delta_H} = \frac{D}{b^3\left[0.137 - \dfrac{0.141}{1 + 14.4/\mu^2}\right]} \quad (11b)$$

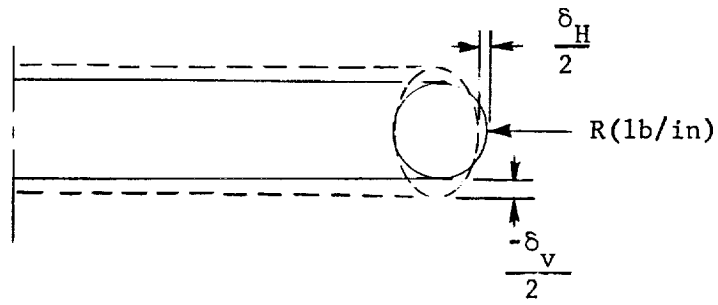

FIGURE 52.3 Radial Load

$$\frac{R}{\delta_v} = -\frac{D}{b^3\left[0.193 - \dfrac{0.199}{1 + 14/\mu^2} + \left(\dfrac{\nu}{\pi\mu m}\right)\left(\dfrac{h}{b}\right)\right]} \quad (27a)$$

$$\frac{R}{\delta_H} = -\left(\frac{b}{a}\right)\frac{Eh/a}{0.318 + 2/(1 + 14/\mu^2)} \quad (27b)$$

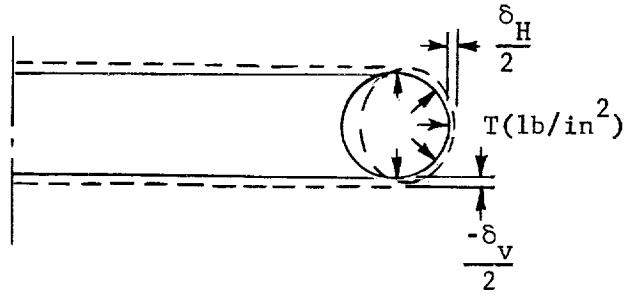

FIGURE 52.4 Pressure Load on Half of Cross-Section

$$\frac{T}{\delta_v} = -\frac{D}{b^4\left[0.25 - \dfrac{0.232}{1 + 14/\mu^2} - 0.636\left(\dfrac{h}{b}\right)\left(\dfrac{\nu}{\mu m}\right)\right]} \quad (37a)$$

$$\frac{T}{\delta_H} = \frac{Eh}{a^2\left[0.636 - \dfrac{1.18}{1 + 14/\mu^2}\right]} \quad (37b)$$

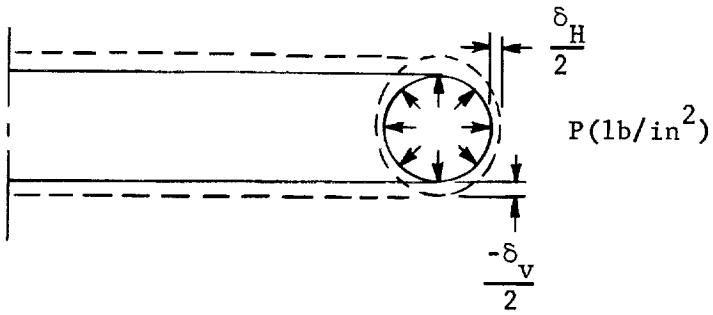

FIGURE 52.5 Pressure Load on Entire Cross-Section

$$\frac{P}{\delta_v} = \frac{-Eh}{2b^2(1 - \nu/2)} \tag{39a}$$

$$\frac{P}{\delta_H} = \frac{Eh}{ab(1 - 2\nu)} \tag{39b}$$

where $D = \dfrac{Eh^3}{12(1 - \nu^2)}$ = bending rigidity

$\mu^2 = 12(1 - \nu^2)b^2/ah$

h = wall thickness

E = Young's modulus

ν = Poisson's ratio

$m = \sqrt{12(1 - \nu^2)}$

The way in which these four types of loading can be combined to represent the total load for each type of O-ring is illustrated by the examples of Section 52.2.

In the above load-deflection relations μ appears as an important parameter. The physical significance of μ is discussed in Section 52.4. For most O-rings, μ is small. Our results are restricted to $\mu^2<10$. Among these load-deflection relations, Eq. (1) is of primary importance since it gives the spring constant of the O-ring.

In addition to the load-deflection relations, we would also like to know the stresses in the ring under load so that overstressing does not occur. The stress and moment resultants under the four basic loadings are given in Eqs. (10), (26), (36), and (38) of Section 52.4. When these resultants are known, the stresses are given by

$$(\sigma_\theta)_{max} = \frac{N_\theta}{h} + \frac{6M_\theta}{h^2}$$

$$(\sigma_\phi)_{max} = \frac{N_\phi}{h} + \frac{6M_\phi}{h^2}$$

It is in general not possible to ascertain by inspection at what angle ϕ the right-hand side of these equations becomes a maximum under the particular loading. However, this can be found out by using a computer program, since the work involved is straightforward.

88

52.2 Illustrative Examples

We shall illustrate the application of the results of the preceding section by considering 0-rings of the following sizes:

(1) 5 O.D. x 1/4 x 0.012 wall, type 321 stainless steel

(2)20 O.D. x 1/4 x 0.012 wall, type 321 stainless steel

The parameter

$$\mu^2 = 12(1 - \nu^2)(b^2/ah)^2$$
$$= \begin{cases} 2.96 \text{ (5" O-ring)} \\ 0.185 \text{ (20" O-ring)} \end{cases}$$

The bending rigidity

$$D = Eh^3/12(1 - \nu^2) = 4.75 \text{ lb-in}$$

From Eq. (11a), the spring constants of the 0-rings are

$$\frac{F}{\delta_v} = \frac{D}{\left(0.149 - \dfrac{0.141}{1 + 14.4/\mu^2}\right) b^3}$$
$$= \begin{cases} 18800 \text{ lb/in}^2 \text{ (5" O-ring)} \\ 16400 \text{ lb/in}^2 \text{ (20" O-ring)} \end{cases}$$

If a unit compression load of F = 90 lb/in is required to seat the 0-rings, the groove depth should be smaller than the O.D. of the 0-rings by the amount

$$\frac{90}{18800} \text{ in (5" O-ring)}$$

$$\frac{90}{16400} \text{ in (20" O-ring)}$$

For this loadings, the bending stress is predominant (see Eqs. (10)). The maximum stress occurs at the top and bottom of the 0-ring.

$$(\sigma_\phi)_{max} = \frac{6M_\phi}{h^2} = \frac{6Fb}{h^2}\left[\frac{1}{\pi} - \frac{2}{3\pi(1 + 14.4/\mu^2)}\right]$$
$$= \begin{cases} 1.32 \times 10^5 \text{ psi (5" O-ring)} \\ 1.47 \times 10^5 \text{ psi (20" O-ring)} \end{cases}$$
$$(\sigma_\theta)_{max} = 0.3\,(\sigma_\theta)_{max}$$

These are indeed very high stresses and outer fibres of the 0-ring would have yielded locally. But plastic flow will be contained by the neighboring elastic regions so that the load-deflection relations obtained previously will still hold approximately.

Suppose that after the O-rings are installed, fluid under a pressure of 300 psig passes through the connector. We would like to know the O-ring compression F for

(1) Standard O-rings

(2) Pressure-energized O-rings

The load on the standard O-ring is now a combination of the basic loadings as shown when friction is neglected.

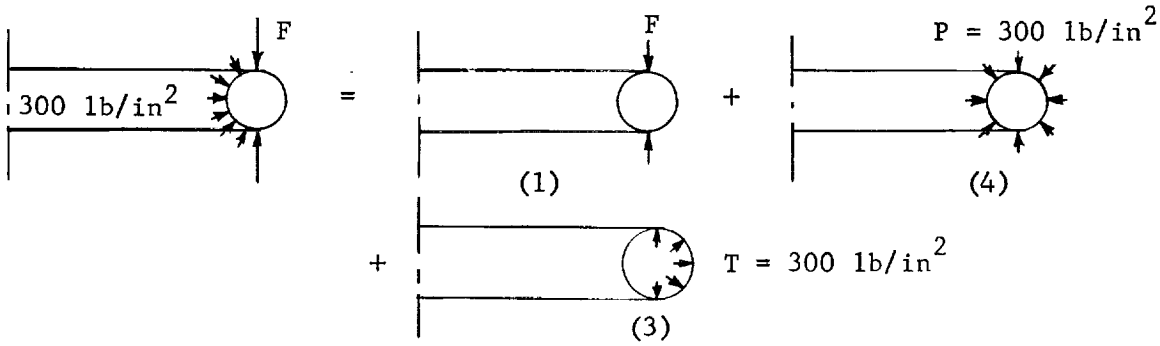

From Eq. (39a) we obtain the shortening of the vertical tube diameter under loading (4) as

$$\delta_v = \frac{-2Pb^2(1 - 0.3/2)}{Eh}$$

$$= 2.22 \times 10^{-5} \text{ in.}$$

The extension of the vertical tube diameter under loading (3) is, from Eq. (37a),

$$-\delta_v = \frac{Tb^4\left[0.25 - \dfrac{0.232}{1 + 14/\mu^2} - 0.636\left(\dfrac{h}{b}\right)\dfrac{\nu}{\mu m}\right]}{D}$$

$$= \begin{cases} 1.52 \times 10^{-2} \text{ in. (5" O-ring)} \\ 1.72 \times 10^{-2} \text{ in. (20" O-ring)} \end{cases}$$

The combined effect of loading (3) and (4) is that the vertical diameter of the tube would extend by the amount

$$1.52 \times 10^{-2} - 2.22 \times 10^{-5} = 1.52 \times 10^{-2} \text{ in. (5" O-ring)}$$
$$1.72 \times 10^{-2} - 2.22 \times 10^{-5} = 1.72 \times 10^{-2} \text{ in. (20" O-ring)}$$

Since the bolts clamping together the flanges are much more rigid than the O-ring, these would-be extensions of the vertical tube diameter are almost completely restrained. The corresponding increase in O-ring compression is equal to

(spring constant) x (extension restrained)

$$= \begin{cases} 0.0152 \times 18800 = 296 \text{ lb/in} & (5'' \text{ O-ring}) \\ 0.0172 \times 16400 = 323 \text{ lb/in} & (20'' \text{ O-ring}) \end{cases}$$

The maximum stress due to loading (4) is small compared with that due to loading (3). For loading (3) it can be seen from Eqs. (36) in Section 52.4 that the ratio between the bending stress and the membrane stress is

$$\frac{6M_{\phi}/h^2}{N_{\phi}/h} = 0(\mu) = 0(1) \text{ for both O-rings}$$

Therefore, the bending stress and the membrane stress are of equal importance. It can also be seen from Eqs. (10) and (36) that the ratio of bending stress for loading (1) and (3) is of the order of

$$0\left(\frac{F}{Tb}\right) = 0(1/b)$$

Therefore, an internal pressure of 300 psig adds a great deal to the stresses in the O-ring. This is all the more important, since considerable addition of the stress is in the form of membrane stress. This indicatesthat an O-ring of much thicker wall should be used. Notice that doubling the wall thickness would reduce the membrane strsss approximately by half and the bending stress by three quarters. The spring constant of the O-ring, however, becomes eight times as large.

In considering the effect of internal pressure in the above, we have not considered the relief of O-ring compression due to bolt and spacer extension. Given the bolt and spacer dimensions, this can be calculated readily. However, the spring constant of most O-rings is so small compared with that of the bolts and spacer, that the relief of O-ring compression is usually negligible.

For a pressure-energized O-ring the load is a combination of the basic loading (1) and (3)

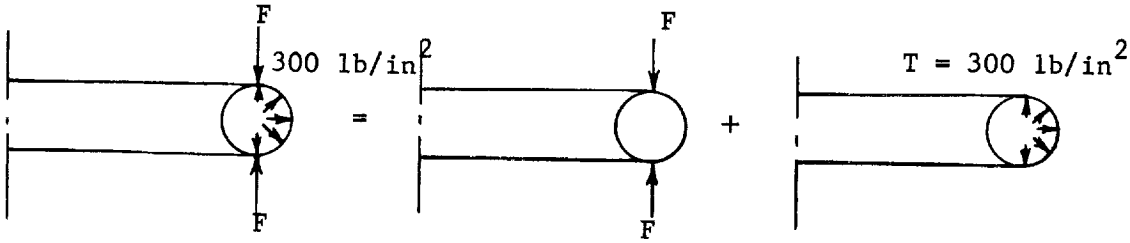

This differs from the load on a standard O-ring shown on Page 52-7 only in the absence of the basic loading (4). Since it is seen in the preceding case that the basic loading (4) does not add much to either the deflection or stresses of the O-ring, the conclusions reached for the standard O-rings apply also to the pressure-energized O-rings. This is a very surprising conclusion, since it shows that within the small-deflection elastic theory the standard O-ring has self-energizing action just as the vented "pressure-energized O-rings."

Another important conclusion can be obtained by reversing the direction of pressure in loadings (3) and (4) for the standard 0-rings. It can be seen that in this case the 0-ring compression decreases with the increase of external pressure. In other words, the pressure-energized 0-ring is entirely ineffective against external pressure unless a back-up ring is used.

We shall consider next that in addition to initial seating compression and internal pressure, the ring is backed up by the flange (or a back-up ring) which exerts a reaction force on the 0-ring. Suppose that the inside diameter of the flange is to be equal to the outside diameter of the compressed 0-ring so that during initial seating the flange (or back-up ring) will not react on the 0-ring. What should be the inside diameter of the flange? If the 0-ring is then subjected to 300 psig internal pressure, what is the reactive force between the 0-ring and the flange (or back-up ring), and what is the change in 0-ring compression? From Eq. (11b) we see that during initial seating the outside diameter of the 0-ring increases by the amount

$$\delta_H = \frac{b^3 F\left[0.137 - \dfrac{0.141}{1 + 14.4/\mu^2}\right]}{D}$$

$$= \begin{cases} 0.00418 \text{ in. (5" 0-ring)} \\ 0.00500 \text{ in. (20" 0-ring)} \end{cases}$$

Therefore, the inside diameter of the flange should be 5 + 0.00418 in. for the 5" 0-ring and 20 + 0.00500 for the 20" 0-ring.

When an internal pressure of 300 psig is now applied, the outside diameter of the 0-ring would tend to increase if it were not restrained by the flange. Since the flange is much stiffer than the 0-ring, we may assume that these would-be expansions of the 0-ring are completely suppressed. The result is that there is a circumferential pressure R lb/in between the 0-ring and the flange (or back-up ring) as well as an increase ΔF of the 0-ring compressions. The forces R and ΔF can be determined from the condition that

$$\delta_H = \delta_V = 0$$

due to the combined action of R, ΔF and the 300 psig internal pressure.

We have already found

$$\left(\delta_V\right)_{300 \text{ psig}} = \begin{cases} -0.0152 \text{ in. (5" 0-ring)} \\ -0.0172 \text{ in. (20" 0-ring)} \end{cases}$$

From Eq. (37b) we have

$$\left(\delta_H\right)_{300 \text{ psig}} = \frac{a^2(300)\left[0.636 - \dfrac{1.18}{1 + 14/\mu^2}\right]}{30 \times 10^6 (0.012)}$$

$$= \begin{cases} 0.00227 \text{ in. (5" 0-ring)} \\ 0.0518 \text{ in. (20" 0-ring)} \end{cases}$$

Also

$$(\delta_v)_{\Delta F} = \begin{cases} \Delta F/18800 \text{ (5" 0-ring)} \\ \Delta F/16400 \text{ (20" 0-ring)} \end{cases}$$

and from Eq. (11b)

$$(\delta_H)_{\Delta F} = \frac{(\Delta F)b^3\left[0.137 - \dfrac{0.141}{1 + 14.4/\mu^2}\right]}{4.75}$$

$$= \begin{cases} \Delta F/21500 \text{ (5" 0-ring)} \\ \Delta F/18000 \text{ (20" 0-ring)} \end{cases}$$

Similarly from Eqs. (27) we obtain

$$(\delta_v)_R = -\frac{R(1/8)^3\left[0.193 - \dfrac{0.199}{1 + 14.4/\mu^2} + \left(\dfrac{0.3}{3.3\pi\mu}\right)\left(\dfrac{0.012}{0.125}\right)\right]}{4.75}$$

$$= \begin{cases} -R/15400 \text{ (5" 0-ring)} \\ -R/13200 \text{ (20" 0-ring)} \end{cases}$$

$$(\delta_H)_R = -\frac{0.318 + 2/(1 + 14/\mu^2)}{30 \times 10^6 (0.012)(1/8)/a^2}$$

$$= \begin{cases} -R/10800 \text{ (5" 0-ring)} \\ -R/1330 \text{ (20" 0-ring)} \end{cases}$$

Therefore, from the equations

$$(\delta_v)_{300 \text{ psig}} + (\delta_v)_{\Delta F} + (\delta_v)_R = 0$$

$$(\delta_H)_{300 \text{ psig}} + (\delta_H)_{\Delta F} + (\delta_H)_R = 0$$

we obtain

$$R = 732 \text{ lb/in}$$

$$\Delta F = 1180 \text{ lb/in}$$

for the 5" 0-ring and

$$R = 98.5 \text{ lb/in}$$

$$\Delta F = 404 \text{ lb/in}$$

for the 20" 0-ring.

Of course, the 0-ring would have failed under such heavy load. The result indicates

(1) The use of a back-up ring is desirable since it increases the O-ring compression.

(2) Clearance between the O-ring and back-up ring may be needed to avoid overstressing.

(3) As far as increasing the O-ring compression is concerned, the reaction of the back-up ring is more effective than the internal pressure. This indicates that, for sealing against external pressure, the tendency of the external pressure to relieve the O-ring compression is more than compensated by the reaction of the back-up ring. Therefore, O-rings can be used to seal against external pressure, provided a back-up ring is used.

52.3 Some Considerations of the Plastic Behavior of Hollow Metallic O-rings

Most of the hollow metallic O-rings currently in use operate in the plastic range. A satisfactory elasto-plastic analysis is very complicated. Some consideration of their plastic behavior are presented in this section based on very much simplified assumptions. The results obtained include:

1. A conservative estimate of sealing force.
2. An estimate of the decrease of the sealing force when the flanges tend to separate as a result of differential thermal expansion, external loads, etc.
3. An estimate of the area of contact between the O-ring and the flange.

They seem to correlate well with the limited experimental data available.

52.3.1 Yielding Load and Estimate of Sealing Force

At the beginning of the process of tightening the connector, the compression is small and the O-ring behaves elastically. The elastic solution presented in Section 52.2 is valid. It was shown that the predominating stresses are bending stresses. Therefore, for simplicity we shall neglect the membrane stresses completely. The maximum bending moments occur at the outer and inner surfaces of the top and bottom of the O-ring.

$$M_\phi = \frac{Fb}{\pi}$$
$$M_\theta = \nu M_\phi \qquad (40)$$

The corresponding maximum stresses are

$$\sigma_\phi = \frac{6Fb}{\pi h^2}$$
$$\sigma_\theta = \nu \sigma_\phi \qquad (41)$$

where

F is the compressive force
b is the tube radius of O-ring
h is the wall thickness of O-ring
ν is Poisson's ratio of O-ring material

According to Mises' yield criterion, initial yielding at these points begins when

$$\sigma_\phi \sqrt{1-\nu+\nu^2} = \text{yield strength of material in tension test, Y} \qquad (42)$$

or, the installation force causing the O-ring to begin yielding as

$$F_{yield} = \frac{\pi h^2 Y}{6b\sqrt{1-\nu+\nu^2}} \qquad (43)$$

Further increase of load will spread the plastic zone both outward and in depth. The load deflection curve will begin to deviate from a straight-line. The deflection will still remain small since the plastic deformation will be contained by the neighboring elastic material. With further increase in load the plastic zone will finally penetrate the wall thickness at the top and the bottom of the O-ring. The material at these points will have very small bending rigidity and behaves more or less like a hinge. It can be easily shown

that the bending moment causing the hinge to occur is 3/2 times the moment of initial yielding if the small effect of work-hardening is neglected, i.e.

$$M_{hinge} = 1.5M_{yield} = \frac{1.5b}{\pi}F_{yield} = \frac{h^2Y}{4\sqrt{1-\nu+\nu^2}} \tag{44}$$

We shall call the load at which the plastic hinge occurs the hinge load. It should be expected that for loads greater than the hinge load, the deflection of the O-ring increases very much faster even though unrestricted deflection still does not occur because one hinge alone does not transform the O-ring to a "mechanism". Referring to a typical load deflection curve we are saying that F_{hinge} corresponds to the point A

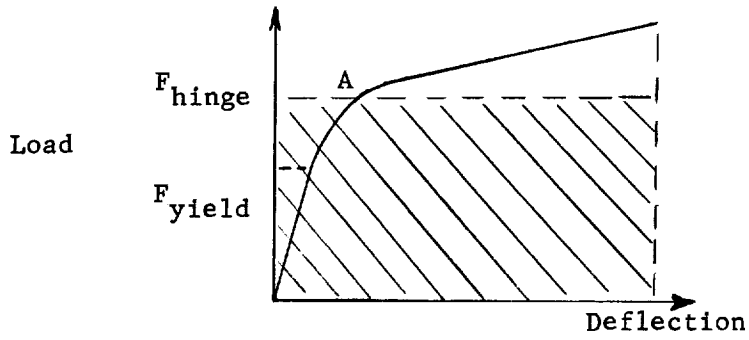

Fig. 52.6 Load-Deflection Curve of an O-ring

A rough estimate of F_{hinge} can be made that, similar to the bending moment

$$F_{hinge} = 1.5\ F_{yield} = \frac{\pi h^2Y}{4b\sqrt{1-\nu+\nu^2}} \tag{45}$$

Referring to Fig. 52.6, it can be seen that F_{hinge} as given above serves as a good lower estimate of the sealing force for most O-ring applications.

A load-deflection diagram for a 1/8 in. tube size, 0.010 in. wall, type 321 stainless steel O-ring is given in Reference 1. It shows that the load-deflection curve begins to deviate from a straight line at a load of approximately 75 lb/in and large deflection begins to occur around a load of 120 lb/in. If we take F_{yield} as 75 lb/in, Eq. (43) gives us the yield limit of the material in tension as:

$$Y = \frac{(75)(6)(1/16)\sqrt{1-0.3+(0.3)(0.3)}}{\pi(0.01)^2} \cong 80{,}000 \text{ psi}$$

If we take 120 lb/in as F_{hinge}, then

$$F_{hinge} = 120/75\ F_{yield} = 1.6\ F_{yield}$$

which seems to correlate well with Eq. (45).

52.3.2 Spring Constant of O-ring When Flanges are Separating

After the O-ring is installed a conservative estimate of the sealing force is given by Eq. (45) The sealing force decreases if the flanges tend to separate from each other due to differential thermal expansion, adverse external loads, etc. The amount of decrease of the sealing force depends on the resilience of the O-ring. If the effect of the change of the geometry of the O-ring is negligible then it is a fundamental hypothesis of the theory of plasticity that the spring constant of the O-ring during unloading is approximately the same as the elastic spring constant of the O-ring. Indeed, this fact is substantiated by the load-deflection diagram of Reference 1. The elastic spring constant of most O-rings is given by Eq. (11a). For a non-pressure-energized O-ring the decrease in sealing force due to separating of flanges is therefore

(spring constant of O-ring as given by Eq.(11a)) x (amount of separation)

52.3.3 Area of Contact Between O-Ring and Flange

In the following we shall present a simple method of estimating the area of contact between the O-ring and the flanges based on energy considerations. The work done by the compressive load can be approximated by the shaded area in Fig. 52.6, i.e.

$$(F_{hinge}) \times (\text{O-ring compression, } \delta) \qquad (46)$$

Assume that all this work is done in flattening a portion of the O-ring and that in the flattened portion, the moment is at the fully plastic moment (M_{hinge}). This part of the work is given approximately as

$$2M_{hinge}\theta \cong 4M_{hinge}\sin^{-1}\frac{c}{2b} \qquad (47)$$

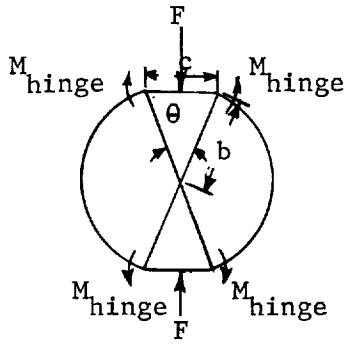

Equating the work given by Eqs. (46) and (47) and making use of Eqs. (44) and (45) we obtain the following relation between the width of the area of contact c and the amount of 0-ring compression δ

$$\frac{c}{2b} = \sin\left(\frac{\delta}{b}\right)\left(\frac{\pi}{4}\right) \tag{48}$$

For a 1/8 in. tube diameter 0-ring compressed 0.035 in , the width of area of contact is

$$c = 1/8 \sin \left(\frac{0.035}{1/16}\right)\left(\frac{\pi}{4}\right)$$

$$= 0.053 \text{ in.}$$

which seems to correlate well with the measured value of

$$c \tilde{=} 3/64 \text{ in.} \tilde{=} 0.047 \text{ in.}$$

on one of the 0-rings available to us.

The average sealing stress is of course the sealing force divided by the area of contact. However, the sealing stress is far from being uniform over the area of contact and the maximum sealing stress is much greater than the average stress. The distribution of sealing stress has the general shape of the shaded area in the following figure.

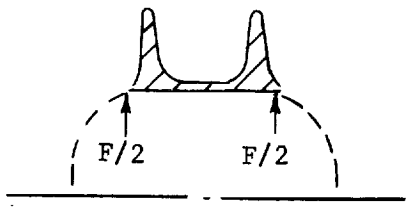

This is necessary because the flattened portion of the 0-ring is at approximately constant moment and in order to maintain a constant moment the sealing force has to concentrate near the edges of the area of contact.

52.4 Appendix - Elastic Analysis of Hollow Metallic O-Rings

52.4.0 Introduction

The hollow metallic O-rings used as static seals are made of metal tubing formed into rings by welding the two ends together. The three basic types of O-rings (Ref. 1) are shown in Fig. 52.1. Essentially they are shells under axi-symmetric loading. As a first step toward the general analysis, they will be treated as elastic thin shells under axi-symmetric loading. Specifically excluded from the present analysis are stability, large deflection, plasticity and thick-shell effects.

The appropriate equations were given by Clark (Ref. 2). Much the same formulation and symbols shall be used here. Fig. 52.7 shows the dimensions of an O-ring and the coordinate axes. Also shown are our conventions about positive senses of the stress resultants and load intensities.

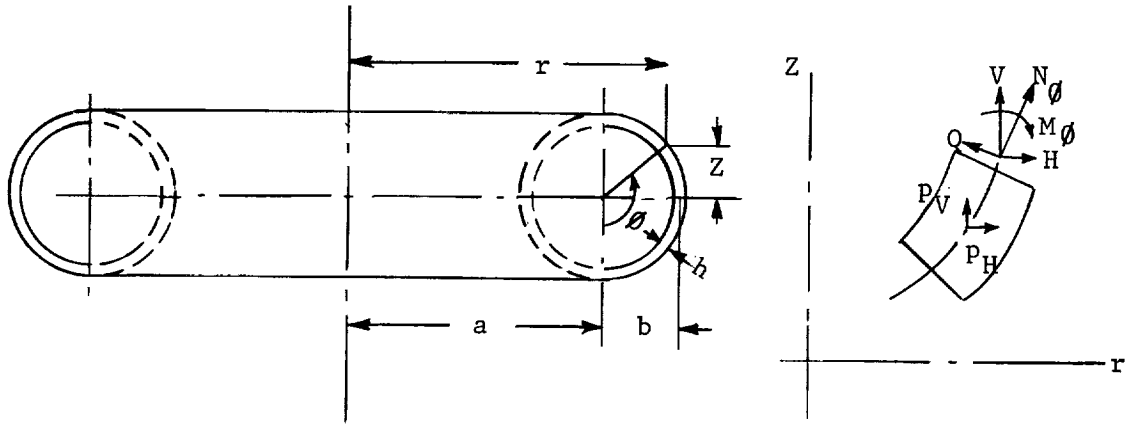

FIGURE 52.7

Co-ordinates for Elastic Analysis of O-Ring

For most O-rings the ratio of tube diameter and ring diameter is small and can be neglected in comparison with unity ($b/a \ll 1$). This makes the outer half and inner half of the O-ring structurally symmetric. It can be shown from Ref. 2 that now the governing equations for an O-ring assume the following simple form

$$\frac{d^2\beta}{d\phi^2} + \mu\psi \sin \phi = \mu\Omega \cos \phi \qquad (1a)$$

$$\frac{d^2\psi}{d\phi^2} - \mu\beta \sin \phi = -\frac{dP_H}{d\phi} \qquad (1b)$$

where $\beta = \phi_{original} - \phi_{deformed}$ = rotation of shell

$\psi = \frac{ma}{Eh^2} H$ = non-dimensionalized horizontal stress resultant

$\Omega = \frac{ma}{Eh^2} V = \frac{-mab}{Eh^2} \int p_v d\phi$ = non-dimensionalized vertical stress resultant

$P_H = \frac{mab}{Eh^2} p_H$ = non-dimensionalized horizontal load intensity

$\mu = \frac{mb^2}{ah}$

$m = \sqrt{12(1 - \nu^2)}$

ν = Poisson's ratio

E = Young's modulus

h = wall thickness of 0-ring

When the rotation of the shell β and the stress function ψ are known, the stress and moment resultants are given by

$$N_\phi = \frac{Eh^2}{ma} \left[\psi \cos \phi + \Omega \sin \phi\right] \tag{2a}$$

$$N_\theta = \frac{Eh^2}{mb} \left[\frac{d\psi}{d\phi} + P_H\right] \tag{2b}$$

$$Q = \frac{Eh^2}{ma} \left[-\psi \sin \phi + \Omega \cos \phi\right] \tag{2c}$$

$$M_\phi = \frac{Eh^3}{m^2 b} \frac{d\beta}{d\phi} \tag{2d}$$

$$M_\theta = \nu M_\phi \tag{2e}$$

and the displacement components in the vertical and horizontal directions by

$$w = -b \int (\beta \cos \phi - \epsilon_\phi \sin \phi) d\phi \tag{3a}$$

$$u = b \int (\beta \sin \phi + \epsilon_\phi \cos \phi) d\phi \tag{3b}$$

or alternatively

$$u = a(N_\theta - \nu N_\phi)/Eh \tag{3c}$$

where the meridianal membrane strain

$$\epsilon_\phi = (N_\phi - \nu N_\theta)/Eh \tag{3d}$$

Our aim is to find solutions of Eqs. (1) which satisfy the prescribed stress boundary conditions and are periodic in ϕ with period 2π.

Referring to Fig. 52.1, we see that the load on the 0-rings consists of four basic types. The solution for each will be given in the following. Proper combination of these gives us the solutions for the three types of 0-rings.

52.4.1 Solutions for Loading (a) - Uniform Axial Compression

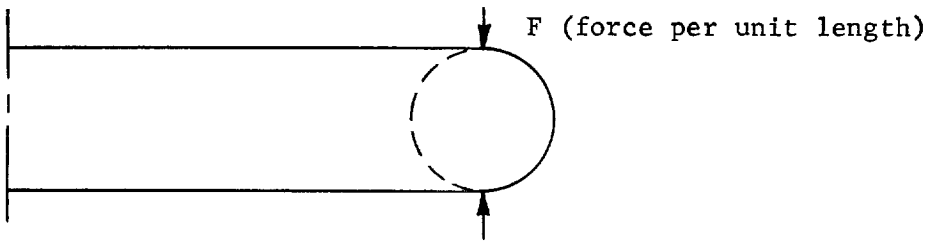

This loading is typified by the initial seating compression.

For this loading $P_H = 0$

$$\Omega = -\frac{ma}{Eh^2}\frac{F}{2} \qquad 0<\phi<\pi$$

$$\Omega = +\frac{ma}{Eh^2}\frac{F}{2} \qquad -\pi<\phi<0$$

We can expand the right-hand side of Eq. (1a) as a convergent Fourier Series.

$$\mu\Omega\cos\phi = -\frac{\mu maF}{Eh^2}\frac{4}{\pi}\sum_{1}^{\infty}\frac{n}{4n^2-1}\sin 2n\phi$$

The solutions of Eq. (1) can be shown to be

$$\beta = \frac{\mu maF}{Eh^2}\sum_{1}^{\infty}A_{2n}\sin 2n\phi \tag{4a}$$

$$\psi = -\frac{\mu}{2}\frac{\mu maF}{Eh^2}\sum_{1}^{\infty}\frac{1}{(2n-1)^2}\left[A_{2n} - A_{2(n-1)}\right]\cos(2n-1)\phi \tag{4b}$$

where $$A_{2n} + \frac{\mu^2}{16n^2}\left[\frac{2(4n^2+1)}{(4n^2-1)^2}A_{2n} - \frac{A_{2(n+1)}}{(2n+1)^2} - \frac{A_{2(n-1)}}{(2n-1)^2}\right] = \frac{1}{n(4n^2-1)\pi}$$

$$(n = 1, 2, 3, \text{---}) \tag{5}$$

$$A_0 = 0$$

It is interesting to consider first the limiting case $\mu\to 0$. As is well-known from the study of the bending of curved tubes (Refs 3, 4), this implies that the flattening of the tube cross-section introduces negligible strain in the circumferential fibres of the O-ring. Therefore, the solution should agree with the corresponding case of the bending of a thin ring by equal and opposite forces (Ref. 5) if the plate bending rigidity is replaced by the beam bending rigidity. Indeed, it can be easily shown from Eqs. (4) that

$$\psi_{\mu\to 0} = 0 \tag{6a}$$

$$\beta_{\mu\to 0} = \frac{Fb^2}{\pi D}\sum_{1}^{\infty}\frac{\sin 2n\phi}{n(4n^2-1)}$$

$$= \begin{cases} \frac{Fb^2}{\pi D}\left[\frac{\pi}{2}(\cos\phi - 1) + \phi\right] & 0 \le \phi \le \pi \\ \frac{Fb^2}{\pi D}\left[\frac{\pi}{2}(1 - \cos\phi) + \phi\right] & -\pi \le \phi \le 0 \end{cases} \qquad (6b)$$

where the bending rigidity $D = Eh^3/12(1-\nu^2)$.

This result is not only interesting in itself but also helps us to improve the convergence of our solution, Eq. (4). We can rewrite Eq. (4a) as:

$$\beta = \beta_{\mu\to 0} + \bar{\beta} \qquad (7)$$

where

$$\bar{\beta} = \frac{\mu maF}{Eh^2}\sum_{1}^{\infty}\left[A_{2n} - \frac{1}{n(4n^2-1)\pi}\right]\sin 2n\phi \qquad (8a)$$

$$= \left(\frac{\mu maF}{Eh^2}\right)\left(-\frac{\mu^2}{16}\right)\sum_{1}^{\infty}\frac{1}{n^2}\left[\frac{2(4n^2+1)}{(4n^2-1)^2}A_{2n} - \frac{A_{2(n+1)}}{(2n+1)^2} - \frac{A_{2(n-1)}}{(2n-1)^2}\right]\sin 2n\phi \qquad (8b)$$

The alternate form (8b) for $\bar{\beta}$ demonstrates its superior convergence to Eq. (4a) for β. The form (8a) is more direct for the actual numerical evaluation of the series. Eq. (7) admits the following interpretation. $\beta_{\mu\to 0}$ represents the solution for a fictatious 0-ring with the same dimensions as the original 0-ring but with the parameter $\mu\to 0$; $\bar{\beta}$ represents a correction for the finite value of the parameter μ. This representation is particularly advantageous at large μ when the convergence of Eq. (4a) becomes rather slow.

We can also improve the convergence of Eq. (4b) for ψ by integrating Eq. (1b) with β as given by Eq. (7). This is not attempted here because Eq. (4b) for ψ is already a faster converging series than Eq. (4a) for β and because the transformation would devoid of a simple physical interpretation as Eq. (7).

For most 0-rings $\mu^2 < 10$, and results of engineering accuracy can be obtained by keeping one term of the series expansion for $\bar{\beta}$ and two terms of the series expansion for ψ. By neglecting A_6 in Eq. (5) for n = 1 and n = 2 and noting that $\mu^2 < 10$, we obtain approximately

$$A_2 \cong \frac{1}{3\pi(1 + \mu^2/14.4)} \qquad (9a)$$

$$A_4 \cong \frac{1}{30\pi} + \frac{1}{120\pi(1 + 14.4/\mu^2)} \qquad (9b)$$

$$\bar{\beta} \cong -\frac{Fb^2}{D}\frac{\sin 2\phi}{3\pi(1 + 14.4/\mu^2)} \qquad (9c)$$

$$\psi \cong -\frac{maF}{Eh^2}\frac{2.4}{\pi(1+14.4/\mu^2)}\left[\cos\phi - \frac{1}{9}\left(1 - \frac{1+14.4/\mu^2}{144/\mu^2}\right)\cos 3\phi\right] \tag{9d}$$

The stress and moment resultants can be obtained by substituting Eqs. (6b),, (7), (9c) and (9d)into Eqs. (2). For this loading the bending moments are the predominating stress resultants.

$$M_\phi = \begin{cases} Fb\left[-\frac{1}{2}\sin\phi + \frac{1}{\pi} - \frac{2\cos 2\phi}{3\pi(1+14.4/\mu^2)}\right] & 0\leq\phi\leq\pi \\ Fb\left[\frac{1}{2}\sin\phi + \frac{1}{\pi} - \frac{2\cos 2\phi}{3\pi(1+14.4/\mu^2}\right] & -\pi\leq\phi\leq 0 \end{cases} \tag{10a}$$

$$M_\theta = \nu M_\phi \tag{10b}$$

Other quantities of interest are the shortening of the vertical diameter of tube δ_v and extension of the outside diameter of the ring δ_H. From Eqs. (3) we obtain

$$\delta_v = w(0) - w(\pi) = F\left\{\frac{b^3}{D}\left[\frac{\pi}{4} - \frac{2}{\pi} - \frac{4}{9\pi(1+14.4/\mu^2)}\right]\right\} \tag{11a}$$

$$\delta_H = 2\left[u\left(\frac{\pi}{2}\right) - u(0)\right] = F\left\{\frac{b^3}{D}\left[\frac{2}{\pi} - \frac{1}{2} - \frac{4}{9\pi(1+14.4/\mu^2)}\right]\right\} \tag{11b}$$

The first equation defines the spring constant of the 0-ring

$$\frac{F}{\delta_v} = \frac{D}{b^3}\Big/\left[\frac{\pi}{4} - \frac{2}{\pi} - \frac{4}{9\pi(1+14.4/\mu^2)}\right] \tag{12}$$

which is of primary importance in the application of 0-rings. Notice that the spring constant increases with μ. This is as expected, since for larger μ, more of the work done by the compressive force is stored in the form of strain energy of extension of circumferential fibres rather than flattening of the cross-section.

52.4.2 Solutions for Loading (b) - Uniform Lateral Compression

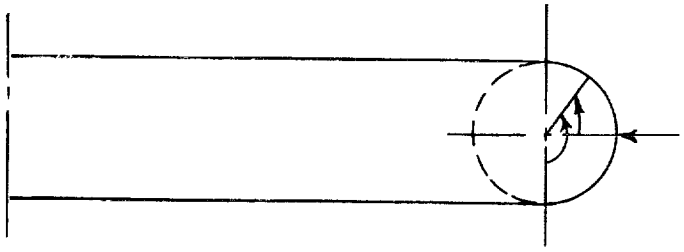

This loading results from the reaction of the back-up ring. To take advantage of symmetry, it is more convenient to replace the independent variable ϕ by the new variable

$$\gamma = \phi - \frac{\pi}{2}$$

For the present loading $\Omega = 0$ and

$$\frac{dp_H}{d\gamma} = 0 \text{ except at } \gamma = 0 \tag{13}$$

Eqs. (1) become

$$\begin{aligned} &\frac{d^2\beta}{d\gamma^2} + \mu\psi \cos\gamma = 0 \\ &\frac{d^2\psi}{d\gamma^2} - \mu\beta \cos\gamma = 0 \end{aligned} \tag{14}$$

together with the jump condition

$$\psi_{+0} - \psi_{-0} = \frac{ma}{Eh^2} R \tag{15}$$

We could express β and ψ as convergent Fourier series and determine the Fourier coefficients from Eqs. (14) and (15). The difficulty here is, however, since ψ is discontinuous at $\gamma = 0$, if we should differentiate the Fourier series representation of ψ, the result will not converge to $d\psi/d\gamma$ which is needed to calculate stresses and strains. In order to get around this difficulty, we shall replace Eqs. (14) and (15) by the following equivalent system.

$$\beta = \beta_{\mu\to 0} + \bar{\beta} \tag{16a}$$

$$\psi = \psi_{\mu\to 0} + \bar{\psi} \tag{16b}$$

$$\frac{d^2\beta_{\mu\to 0}}{d\gamma^2} + (\mu\psi)_{\mu\to 0} \cos\gamma = 0 \tag{17a}$$

$$\frac{d^2\psi_{\mu\to 0}}{d\gamma^2} = 0 \tag{17b}$$

$$(\psi_{\mu\to 0})_{\gamma=+0} - (\psi_{\mu\to 0})_{\gamma=-0} = \left(\frac{ma}{Eh^2}\right) R \tag{17c}$$

$$\frac{d^2\beta}{d\gamma^2} + \mu\bar{\psi} \cos\gamma = -\mu\psi_{\mu\to 0} \cos\gamma \tag{18a}$$

$$\frac{d^2\bar{\psi}}{d\gamma^2} - \mu\beta \cos\gamma = 0 \tag{18b}$$

$$(\bar{\psi})_{\gamma=+0} = (\bar{\psi})_{\gamma=-0} \tag{18c}$$

The solutions of Eqs. (17) can be shown to be

$$\beta_{\mu\to 0} = \begin{cases} + \dfrac{\mu maR}{2\pi Eh^2}\left[2\sin\gamma + (\gamma - \pi)(1 - \cos\gamma)\right] & 0 \le \gamma \le \pi \quad (19a) \\ + \dfrac{\mu maR}{2\pi Eh^2}\left[2\sin + (\gamma + \pi)(1 - \cos\gamma)\right] & -\pi \le \gamma \le 0 \quad (19b) \end{cases}$$

$$\bar{\psi}_{\mu\to 0} = \begin{cases} - \dfrac{maR}{2\pi Eh^2}\left[\gamma - \pi\right] & 0 < \gamma \le \pi \quad (20a) \\ - \dfrac{maR}{2\pi Eh^2}\left[\gamma + \pi\right] & -\pi \le \gamma < 0 \quad (20b) \end{cases}$$

Now $\bar{\psi}_{\mu\to 0}$ can be expanded as the following convergent Fourier series

$$\bar{\psi}_{\mu\to 0} = \frac{maR}{\pi Eh^2} \sum_1^\infty \frac{\sin n\gamma}{n}$$

Therefore, Eqs. (18) become

$$\frac{d^2\beta}{d\gamma^2} + \mu\bar{\psi}\cos\gamma = -\mu\bar{\psi}_{\mu\to 0}\cos\gamma$$

$$= -\frac{\mu maR}{\pi Eh^2}\left[\frac{1}{4}\sin\gamma + \sum_2^\infty \frac{n}{n^2 - 1}\sin n\gamma\right]$$

$$\frac{d^2\bar{\psi}}{d\gamma^2} - \mu\beta\cos\gamma = 0$$

which admit the solution

$$\beta = \frac{\mu maR}{\pi Eh^2}\sum_1^\infty A_n \sin n\gamma \quad (21a)$$

$$\bar{\psi} = -\frac{\mu}{2}\frac{\mu maR}{\pi Eh^2}\sum_1^\infty \frac{1}{n^2}(A_{n+1} + A_{n-1})\sin n\gamma \quad (21b)$$

where $A_0 = 0$

$$A_1 + \frac{\mu^2}{16}(A_1 + A_3) = 1/4$$

$$A_n + \frac{\mu^2}{4n^2}\left[\frac{2(n^2+1)}{(n^2-1)^2}A_n + \frac{A_{n-2}}{(n-1)^2} + \frac{A_{n+2}}{(n+1)^2}\right] = \frac{1}{n(n^2-1)} \quad (21c)$$

$$(n = 2, 3, 4, \text{---})$$

Again, as in loading condition (a), we can write

$$\beta = \beta_{\mu\to 0} + \bar{\beta} \tag{22}$$

where

$$\bar{\beta} = \frac{\mu maR}{\pi Eh^2}\left[(A_1 - 1/4)\sin\gamma + \sum_2^{\infty}\left(A_n - \frac{1}{n(n^2-1)}\right)\sin n\gamma\right] \tag{23}$$

By neglecting $(A_n)_{n\geq 4}$ in Eq. (21c) and noting that for practical 0-rings $\mu^2<10$ we obtain approximately

$$\begin{aligned} A_1 &\cong 1/4(1 + \mu^2/14) \\ A_2 &\cong 1/6(1 + \mu^2/14.4) \\ A_3 &\cong (1 + \mu^2/48)/24(1 + \mu^2/14) \\ A_4 &\cong (1 + \mu^2/19.2)/60(1 + \mu^2/14.4) \end{aligned} \tag{24}$$

Keeping three terms in the series for $\bar{\beta}$ and $\bar{\psi}$ and simplifying the resulting expressions by limiting to 5% accuracy, we obtain, approximately

$$\bar{\beta} \cong -\frac{\mu maR}{Eh^2}\frac{1}{2\pi(1 + 14/\mu^2)}\left[\frac{1}{2}\sin\gamma + \frac{1}{3}\sin 2\gamma + \frac{1}{17}\sin 3\gamma\right] \tag{25a}$$

$$\bar{\psi} \cong -\frac{maR}{Eh^2}\frac{1}{2\pi(1 + 14/\mu^2)}\left[3.5\sin\gamma + \sin 2\gamma + \frac{1}{3.75}\sin 3\gamma\right] \tag{25b}$$

The predominating stress resultants are

$$N_\theta = -\frac{R}{2\pi}\left(\frac{a}{b}\right)\left[1 + \frac{1}{1 + 14/\mu^2}(3.5\cos\gamma + 2\cos 2\gamma + 0.8\cos 3\gamma)\right] \tag{26a}$$

$$M_\phi = \begin{cases} \dfrac{Rb}{2\pi}\left[-(\pi - \gamma)\sin\gamma + \cos\gamma + 1 - \dfrac{1}{1 + 14/\mu^2}\left(\dfrac{1}{2}\cos\gamma + \dfrac{2}{3}\cos 2\gamma + \dfrac{3}{17}\cos 3\gamma\right)\right] & 0\leq\gamma\leq\pi \\ \dfrac{Rb}{2\pi}\left[(\pi + \gamma)\sin\gamma + \cos\gamma + 1 - \dfrac{1}{1 + 14/\mu^2}\left(\dfrac{1}{2}\cos\gamma + \dfrac{2}{3}\cos 2\gamma + \dfrac{3}{17}\cos 3\gamma\right)\right] & \pi\leq\gamma\leq 0 \end{cases} \tag{26b}$$

$$M_\theta = \nu M_\phi \tag{26c}$$

Notice that the first term in N_θ represents the "hoop tension." The other terms represent the correction for the finite value of μ and are anti-symmetric with respect to the vertical tube diameter. Notice also when finite μ is considered, M_ϕ no longer vanishes at the inner edge ($\gamma = \pi$) of the ring. From

Eqs. (26a) and (26b) it can be shown that for the present loading

$$\frac{\text{bending stress, } 6\,M_\phi/h^2}{\text{membrane stress, } N_\phi/h} = 0\ (\mu)$$

The extension of the vertical diameter of tube and shortening of the outside diameter of the ring are

$$-\delta_v = w(\tfrac{\pi}{2}) - w(-\tfrac{\pi}{2}) = \frac{b^3 R}{\pi D}\left[1 - \frac{\pi}{8} - \frac{0.625}{1 + 14/\mu^2} + \left(\frac{\nu}{\mu m}\right)\left(\frac{h}{b}\right)\right] \tag{27a}$$

$$-\delta_H = -2u(0) = \frac{R}{\pi Eh}\left(\frac{a}{b}\right)(a)\left[1 + 6.3/(1 + 14/\mu^2)\right] \tag{27b}$$

52.4.3 Solutions for Loading (c) - Uniform Internal Pressure on Half of Ring

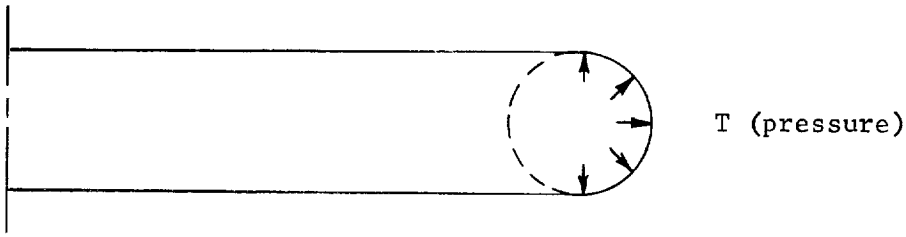

This loading is represented by the internal pressure on a "pressure-energized" O-ring. For this loading

$$\Omega = \frac{mabT}{Eh^2}\sin\phi \qquad 0 \le \phi \le \pi$$

$$= 0 \qquad -\pi \le \phi \le 0$$

$$P_H = \frac{mabT}{Eh^2}\sin\phi \qquad 0 \le \phi \le \pi$$

$$= 0 \qquad -\pi \le \phi \le 0$$

The right-hand side of Eqs. (1) can be expanded as the following convergent Fourier series

$$\mu\Omega\cos\phi = \frac{\mu mabT}{Eh^2}\left[\frac{1}{4}\sin 2\phi - \frac{2}{\pi}\sum_1^\infty \frac{\cos(2n-1)\phi}{(2n+1)(2n-3)}\right] \tag{28a}$$

$$-\frac{dP_H}{d\phi} = -\frac{mabT}{Eh^2}\left[\frac{1}{2}\cos\phi + \frac{2}{\pi}\sum_1^\infty \frac{2n}{4n^2-1}\sin 2n\phi\right] \tag{28b}$$

It can be shown then that Eqs. (1) have the following solution

$$\beta = \frac{\mu mabT}{Eh^2}\sum_1^\infty A_{2n-1}\cos(2n-1)\phi \tag{29a}$$

$$\psi = \frac{mabT}{Eh^2}\left\{\left[\frac{1}{2}\cos\phi + \frac{1}{\pi}\sum_1^\infty \frac{\sin 2n\phi}{n(4n^2-1)}\right] - \frac{\mu^2}{8}\sum_1^\infty \frac{A_{2n-1} - A_{2n+1}}{n^2}\sin 2n\phi\right\} \tag{29b}$$

where

$$A_1 + \frac{\mu^2}{16}(A_1 - A_3) = \frac{-1}{2\pi}$$

$$A_n + \frac{\mu^2}{4n^2}\left[\frac{2(n^2+1)}{(n^2-1)^2}A_n - \frac{A_{n+2}}{(n+1)^2} - \frac{A_{n-2}}{(n-1)^2}\right] = \frac{2}{\pi(n^2-1)n^2} \tag{30}$$

$$(n = 3, 5, 7, \text{---})$$

It is easy to show that the solution converges to the following for the limiting case of $\mu \to 0$

$$\psi_{\mu\to 0} = \begin{cases} \frac{mabT}{Eh^2}\left[\frac{\phi}{\pi} + \frac{1}{2}\right] & -\pi \le \phi \le 0 \\ \frac{mabT}{Eh^2}\left[\cos\phi + \frac{\phi}{\pi} - \frac{1}{2}\right] & 0 \le \phi \le \pi \end{cases} \tag{31a}$$

$$\beta_{\mu\to 0} = \begin{cases} \frac{\mu mabT}{Eh^2}\left[\frac{1}{2}\sin\phi - \frac{\phi}{2} + \frac{\phi}{\pi}\sin\phi + \frac{2}{\pi}\cos\phi - \frac{\pi}{4}\right] & -\pi \le \phi \le 0 \\ \frac{\mu mabT}{Eh^2}\left[-\frac{1}{2}\sin\phi + \frac{\phi}{2} + \frac{\phi}{\pi}\sin\phi + \frac{2}{\pi}\cos\phi - \frac{\pi}{4}\right] & 0 \le \phi \le \pi \end{cases} \tag{31b}$$

Therefore we can rewrite Eqs. (29) as

$$\beta = \beta_{\mu\to 0} + \bar{\beta} \tag{32a}$$

$$\psi = \psi_{\mu\to 0} + \bar{\psi} \tag{32b}$$

where

$$\bar{\beta} = \frac{\mu mabT}{Eh^2}\left[(A_1 + 1/2\pi)\cos\phi + \sum_{n=3,5,7\cdots}\left(A_n - \frac{2}{\pi(n^2-1)n^2}\right)\cos n\phi\right] \tag{33a}$$

$$\bar{\psi} = -\left(\frac{\mu^2}{8}\right)\left(\frac{mabT}{Eh^2}\right)\sum_1^\infty \frac{1}{n^2}(A_{2n-1} - A_{2n+1})\sin 2n\phi \tag{33b}$$

By neglecting $(A_n)_{n>3}$ in Eq. (30) and noting that for practical O-rings $\mu^2 < 10$ we obtain approximately

$$A_1 \cong -\frac{1 + \mu^2/192}{2\pi(1 + \mu^2/14)}$$

$$A_3 \cong \frac{1 - \mu^2/16}{36\pi(1 + \mu^2/14)} \tag{34}$$

Keeping two terms in the series for $\bar{\beta}$ and one term for $\bar{\Psi}$, we obtain, approximately

$$\bar{\beta} \cong \left(\frac{\mu mabT}{Eh^2}\right)\left(\frac{1}{2\pi(1 + 14/\mu^2)}\right)(0.927 \cos \phi - 0.104 \cos 3\phi) \tag{35a}$$

$$\bar{\Psi} \cong \left(\frac{mabT}{Eh^2}\right)\left(\frac{1.85 \sin 2\phi}{2\pi(1 + 14/\mu^2)}\right) \tag{35b}$$

The predominating stress resultants are

$$N_\theta = \frac{aT}{\pi}\left[1 + \frac{1.85 \cos 2\phi}{(1 + 14/\mu^2)}\right] \tag{36a}$$

$$M_\phi = \begin{cases} b^2T\left[\frac{1}{2}\cos\phi - \frac{1}{2} + \frac{\phi}{\pi}\cos\phi - \frac{1}{\pi}\sin\phi \right. \\ \qquad \left. - \frac{1}{2\pi(1 + 14/\mu^2)}(0.927 \sin\phi - 0.312 \sin 3\phi)\right] & -\pi \le \phi \le 0 \\ b^2T\left[-\frac{1}{2}\cos\phi + \frac{1}{2} + \frac{\phi}{\pi}\cos\phi - \frac{1}{\pi}\sin\phi \right. \\ \qquad \left. - \frac{1}{2\pi(1 + 14/\mu^2)}(0.927 \sin\phi - 0.312 \sin 3\phi)\right] & 0 \le \phi \le \pi \end{cases} \tag{36b}$$

$$M_\theta = \nu M_\phi \tag{36c}$$

The extensions of the vertical diameter of tube and outside diameter of ring are

$$-\delta_v = w(\pi) - w(0) = \frac{b^4T}{4D}\left[1 - 0.927/(1 + 14/\mu^2) - \left(\frac{8}{\pi}\right)\left(\frac{h}{b}\right)\left(\frac{\nu}{\mu m}\right)\right] \tag{37a}$$

$$\delta_H = 2\left[u\left(\frac{\pi}{2}\right)\right] = \frac{2a^2T}{\pi Eh}\left[1 - 1.85/(1 + 14/\mu^2)\right] \tag{37b}$$

Eq. (37a) shows that if the parameter μ is sufficiently small, the vertical diameter of the tube may actually decrease, resulting in a decrease in the sealing pressure between the O-ring and the flange surface. This may seem to be somewhat surprising since it corresponds to a negative pressure-energizing effect. However, if the O-ring is backed up by a retaining ring, then a reactive force R would exist between the O-ring and the retaining ring under the pressure T. It can be shown from Eqs. (27a), (27b) and (37b) that now the vertical diameter of the tube always increases, resulting in a pressure-energizing effect.

52.4.4 Solutions for Loading (d) - Uniform Internal Pressure

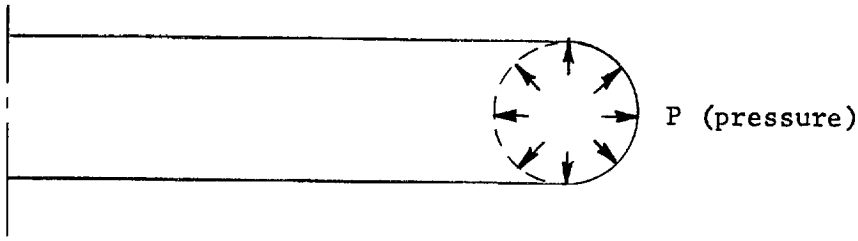

For this loading we have the well-known membrane solution

$$N_{\phi} = Pb \frac{1 + \frac{1}{2}\frac{b}{a}\sin\phi}{1 + \frac{b}{a}\sin\phi} \cong Pb$$

$$N_{\theta} = Pb/2 \qquad (38)$$

$$\beta = M_{\phi} = M_{\theta} = 0$$

The corresponding increase in the outside diameter of the ring is

$$\delta_H = 2a\epsilon_{\theta} = 2a\left(\frac{N_{\theta}}{Eh} - \nu\frac{N_{\phi}}{Eh}\right) = a\frac{Pb}{Eh}(1 - 2\nu) \qquad (39a)$$

and the increase in tube diameter

$$-\delta_V = 2b\frac{Pb}{Eh}\left(1 - \frac{\nu}{2}\right) = \frac{Pb}{Eh}(b)(2 - \nu) \qquad (39b)$$

Notice that in order to get $N_{\theta} = Pb/2$, we have to solve the unsimplified version of Eqs. (1) for ψ with accuracy to the order of b/a. This is necessary wheneve N_{ϕ} is of the same order of magnitude as N_{θ}. The reason for this is explained very clearly in Ref. 6.

Notice that the stresses and deformations under this loading are much smaller than those under loading (c). The implication of this result is the equivalence of the following loading conditions:

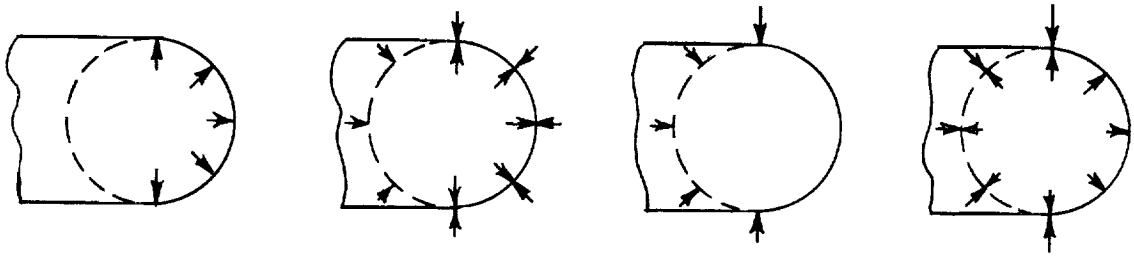

(1) (2) (3)

These figures represent the internal pressure on (1) "pressure energized" O-ring, (2) standard O-ring, and (3) "pressure filled" O-ring. They show that within the elastic theory all three types of O-rings behave essentially the same.

52.4.5 Discussion and Conclusion

(1) The solutions of ring shells have been presented as the sum of

(a) The solution for a fictitious ring with the same dimensions but with the parameter $\mu \to 0$. Physically for μ to approach zero we must have the ring diameter very much greater than the tube diameter.

(b) An auxiliary solution which represents the corrections for the finite value of μ.

The advantages of this representation are:

(a) The solutions for the fictitious ring are obtainable in closed form.

(b) The auxiliary solution converges faster than the formal Fourier series solution, particularly when the parameter μ gets larger.

(c) Singularities in loading which give trouble to the formal Fourier series solution are removed.

In order to illustrate the superior convergence of the auxiliary solution, the moment M_ϕ at the top and bottom of the O-ring for loading condition (a) is computed for two cases: $\mu^2 = 10$ and $\mu^2 = 400$. For $\mu^2 = 10$, the coefficients A_{2n}'s are determined from Eq. (5) by cutting off at $n>10$. The auxiliary series solution converges so fast that the fifth term is only about 0.0015% as large as the leading term. Eq. (10a) which keeps only the leading term of the series has a 2% accuracy. Yet ten terms of the original series only have a 7% accuracy. For $\mu^2 = 400$, the coefficients A_{2n}'s are determined from Eq. (5) by cutting off at $n>20$. The auxiliary series solution converges fast. The fifth term is smaller than 0.03% of the leading term. The real merit of the auxiliary solution, however, is not in its fast convergence when accurate values of A_{2n}'s are known, but that the accurate solution can be obtained without having to solve the some twenty simultaneous equations (5) for $A_{2n}(n \leq 20)$. Taking an extreme case for example, let $A_4, A_6, \cdots = 0$, in Eq. (5), we obtain $A_2 = 3.687 \times 10^{-3}$ immediately. Using this value of A_2 and keeping only the leading term in the auxiliary series, we obtain a solution which is only 8% in error. This is remarkable indeed since we know that the more accurate value of the coefficients A_{2n}'s are

$$A_2 = 4.404 \times 10^{-3}$$
$$A_4 = 7.464 \times 10^{-3}$$
$$A_6 = 3.368 \times 10^{-3}$$
$$\vdots$$

On the other hand, five terms of the original series give a 28% error. Even the sum of all twenty terms still has an 8% error.

(2) Simple expressions for the stresses in O-rings and for the load-deflection relations are obtained. The spring constant of the O-ring is given by Eq. (11a). From this the O-ring squeeze needed for a given seating pressure can be determined. Designers would wish to know the variation of sealing pressure with internal pressure. The load-deflection relations, Eqs (11), (27) and (37), enable us to determine the sealing pressure when the internal pressure is given.

Within the assumptions of the present elastic theory, all three types of O-rings behave similarly. The use of a back-up ring is desirable, since in addition to its principal function of retaining, it also helps to increase the sealing pressure.

(3) It seems that in the current applications, O-rings are squeezed to such an extent that plasticity and large deflection effects are important. These problems are extremely complicated. For most O-rings the parameter μ is small. The approximation $\mu \to 0$ simplifies the problem a great deal and gives promise to solutions that take these complicating factors into consideration.

The essential simplifications are:

(a) Under axial compression (loading (a)) the flattening of the tube cross-section introduces negligible circumferential extension. The problem goes over to that of a cylinder.

(b) Under circumferential loads the circumferential stress resultants N_θ of all the fibres are the same and equal to the "hoop tension", the magnitude of which can be determined readily. The O-ring now becomes statically determinate. The other stress resultants can be determined from the equations of equilibrium and the deformation found from the appropriate stress-strain laws.

52.5 References

1. United Aircraft Products, Inc., Handbook of United Metallic O-Rings, Bulletin No. 59619A, Dayton, Ohio, 1959.

2. R.A. Clark, "On the Theory of Thin Elastic Toroidal Shells," J. Math. and Phys., Vol. 29, 1950, pp. 146-178.

3. R.A. Clark and E. Reissner, "Bending of Curved Tubes," Advances in Applied Mechanics, Vol. II, Academic Press, 1950.

4. T. von Karman, "Über die Formänderung dünnwandiger Rohre, insbesondere federnder Ausgleichsrohre," VDI Zeitschrift, Vol. 55, 1911, pp. 1889-1895.

5. S. Timoshenko, Strength of Materials, Part II, pp. 81-83, Second Ed., Van Nostrand, 1941.

6. W.R. Dean, "The Distortion of a Curved Tube Due to Internal Pressure," Philosophical Mag., Serial 7, Vol. 8, 1939, pp. 452-464

53. COMPARISONS AND CONCLUSIONS

by

B. T. Fang

Pressure-energized cantilever-type and metallic O-ring seals are analyzed in Sections 51 and 52, respectively. As compared with some other types of seals they are characterized by the following advantages:

(1) High resiliency

(2) High localized sealing stress

(3) External load taken by other components of the connector.

(4) Lower clamping pressure needed, thus lighter flanges.

(5) Compatibility to extreme temperatures and to most fluids.

(6) Ability to seal at high pressure

Possible disadvantages are:

(1) Since the seal is formed by hard metal-to-metal mating, a smooth surface finish is required if a coating material is not used. When a soft coating material is used, there is the difficulty of forming a good coating, particularly at extreme temperatures.

(2) Because of the lighter cross-section and lower total sealing force, relative motion between the gasket and the flanges is more likely to occur as a result of internal pressure, differential thermal expansion and vibrations. The ability to reseal is of importance.

In Section 51 a detailed study of several common types of pressure-energized seals is made, and design procedures are given. Characteristics of seals are shown which give the increase of sealing force and change of maximum stress with internal pressure. Since the sealing force increases with the fluid pressure, it may occur that a not-too-well-designed seal may function properly at high pressures but leak at low pressure. Among the different types of seal legs considered, the tapered leg with a lip on the end is the best design. It gives greater sealing force at low pressures and is subjected to lower bending stresses, while its high-pressure sealing ability is only insignificantly inferior to that of the uniform-leg design. Possible relative radial and rotational motions of the seal and the flanges are also studied in Section 51. Since, when under pressure, the sealing force is much greater than the initial sealing compression, there seems to be no reason why reseal cannot be effected after relative motion has happened. Further experimental work is desired to see if there are any yet unknown factors which prevent this reseal. The sealing-force-versus-pressure

characteristics in Section 51 are obtained without considering the separation of flanges due to pressure. The gross flange deformation is treated in Section 41. The consideration of the seal characteristics as well as the gross flange deformation is illustrated by design example in Section 13.2.

In Section 52 the hollow metallic O-rings are investigated. A general elastic analysis is made. It is found that the standard and pressure-filled type O-rings also have some pressure-energizing effect. As compared with the standard O-rings, the pressure-filled O-rings can withstand higher pressure without buckling. The pressure-energizing effect of the pressure-energized type O-rings should be greater than the corresponding effect of the other two types of O-rings. Unfortunately because of the plasticity and large deformation effects, reliable quantitative information is lacking. Further experimental work in this respect is needed. In general, since the O-rings operate in the plastic range, their behavior is less well defined than that of the pressure-energized seals discussed in Section 51. The result of O-ring analysis is illustrated by a design example in Section 13.1 for a flanged connector sealed by an O-ring.

As to the relative merits of the cantilever-type seals treated in Section 51 and the hollow metallic O-rings in Section 52, the following general conclusions can be made:

(1) For a well-designed cantilever-type seal, the seal stays in the elastic range. The variation of sealing force with pressure in the system is accurately known. The gasket is reusable. The O-ring is compressed to the extent that large plastic deformation occurs. The sealing force is less accurately known and the O-ring is not reusable.

(2) When the O-ring is compressed, it expands radially and rests on the mechanical back-up provided. Part of the radial pressure is taken by the mechanical back-up rather than as hoop tension of the O-ring. For the cantilever-type seal, the radial pressure is mainly taken by hoop tension in the web. More critical tolerances on the dimensions of the seal and the mechanical back-up are required if we should want to design the cantilever-type seal in such a way that the radial pressure is taken by the mechanical back-up.

(3) Rotation of the seal cross-section is less a problem with the O-ring than with the cantilever-type pressure-energized seal when there is differential radial growth of the two flange faces.

DISTRIBUTION LIST FOR REPORTS ON CONTRACT NAS 8-4012

NASA Headquarters, Washington 25, D.C.

Mr. Henry Burlage, Jr.
Chief, Liquid Propulsion Systems, RPL (3)

Mr. A.O. Tischler
Assistant Director for Propulsion, MLP (1)

NASA, Marshall Space Flight Center, Huntsville, Alabama

Mr. Charles Wood (M-P&VE-PT), Technical Manager (24)
Office of Technical Information, M-MS-IPC
Contracting Officer, M-P&C-C
Patent Office, M-PAT

NASA Other Locations

Technical & Scientific Information Facility
Attention: NASA Representative, Code CRT
P.O. Box 5700, Bethesda, Maryland (24)

Attention: Technical Librarian

Ames Research Center
Moffett Field, California (2)

Goddard Space Flight Center
Greenbelt, Maryland (2)

Jet Propulsion Laboratory
California Institute of Technology
4800 Oak Grove Drive
Pasadena, California (2)

Langley Research Center
Langley Field, Virginia (2)

Lewis Research Center
21000 Brookpark Road
Cleveland 35, Ohio (2)

Marshall Space Flight Center
Huntsville, Alabama (2)

Manned Spacecraft Center
Houston, Texas (2)

Advanced Research Projects Agency
Pentagon, Room 3D154
Washington 25, D.C.

Aeronautical Systems Division
Air Force Systems Command
Wright-Patterson Air Force Base, Ohio

Attention: Technical Librarian

Air Force Missile Development Center
Holloman Air Force Base, New Mexico

Air Force Missile Test Center
Patrick Air Force Base, Florida

Air Force Systems Command, Dyna-Soar
Air Force Unit Post Office
Los Angeles 45, California

Army Ordnance Missile Command
Redstone Arsenal, Alabama

Armed Services Technical Information Agency
Arlington Hall Station
Arlington 12, Virginia

Arnold Engineering Development Center
A.E.O.R.
Tullahoma, Tennessee

Bureau of Naval Weapons
Department of the Navy
Washington 25, D.C.

Central Intelligence Agency
2430 E. Street, N.W.
Washington 25, D.C.

Headquarters, United States Air Force
Washington 25, D.C.

Office of Naval Research
Washington 25, D.C.

Attention: Technical Librarian

Picatinny Arsenal
Dover, New Jersey

Rocket Research Laboratories
Edwards Air Force Base, California

U.S. Naval Ordnance Test Station
China Lake, California

U.S. Atomic Energy Commission
Technical Information Services
Box 62
Oak Ridge, Tennessee

Liquid Propellant Information Agency
Johns Hopkins University
Applied Physics Laboratory
8621 Georgia Avenue
Silver Spring, Maryland

Aerojet-General Corporation
P.O. Box 296
Azusa, California

Aerojet-General Corporation
P. O. Box 1947
Sacramento 9, California

Aeronutronic
A Division of Ford Motor Company
Ford Road
Newport Beach, California

Aerospace Corporation
2400 East El Segundo Boulevard
El Segundo, California

Arthur D. Little, Inc.
Acorn Park
Cambridge 40, Massachusetts

Astropower, Inc., Subsidiary of Douglas
Aircraft Company, Inc.
2968 Randolph Avenue
Costa Mesa, California

Astrosystems, Inc.
82 Naylon Avenue
Livingston, New Jersey

Atlantic Research Corporation
Edsall Road and Shirley Highway
Alexandria, Virginia

Attention: Technical Librarian

Beech Aircraft Corporation
Boulder Facility
Box 631
Boulder, Colorado

Bell Aerosystems Company
P. O. Box 1
Buffalo 5, New York

Bendix Systems Division
Bendix Corporation
Ann Arbor, Michigan

Boeing Company
P. O. Box 3707
Seattle 24, Washington

Convair (Astronautics)
Division of General Dynamics Corporation
P. O. Box 2672
San Diego 12, California

Curtiss-Wright Corporation
Wright Aeronautical Division
Wood-ridge, New Jersey

Douglas Aircraft Company, Inc.
Missile and Space Systems Division
3000 Ocean Park Boulevard
Santa Monica, California

Fairchild Stratos Corporation
Aircraft Missiles Division
Hagerstown, Maryland

General Electric Company
Missile and Space Vehicle Department
Box 8555
Philadelphia, Pennsylvania

General Electric Company
Rocket Propulsion Units
Building 300
Cincinnati 15, Ohio

Grumman Aircraft Engineering Corporation
Bethpage, Long Island, New York

Kidde Aero-Space Division
Walter Kidde and Company, Inc.
675 Main Street
Belleville 9, New Jersey

Attention: Technical Librarian

Lockheed Aircraft Corporation
Missile and Space Division
Sunnyvale, California

Lockheed Propulsion Company
P.O. Box 111
Redlands, California

Marquardt Corporation
16555 Saticoy Street
Box 2013 - South Annex
Van Nuys, California

Martin Division
Martin Marietta Corporation
Baltimore 3, Maryland

Martin Denver Division
Martin Marietta Corporation
Denver, Colorado

McDonnell Aircraft Corporation
P. O. Box 6101
Lambert Field, Missouri

North American Aviation, Inc.
Space & Information Systems Division
Downey, California

Northrup Corporation
1001 East Broadway
Hawthorne, California

Pratt & Whitney Aircraft Corporation
Florida Research & Development Center
West Palm Beach, Florida

Radio Corporation of America
Astro-Electronics Division
Defense Electronic Products
Princeton, New Jersey

Reaction Motors Division
Thiokol Chemical Corporation
Denville, New Jersey

Republic Aviation Corporation
Farmingdale
Long Island, New York

Attention: Technical Librarian

Rocketdyne (Library Dept. 586-306)
Division of North American Aviation, Inc.
6633 Canoga Avenue
Canoga Park, California

Space General Corporation
9200 Flair Avenue
El Monte, California

Space Technology Laboratories
P. O. Box 95001
Airport Station
Los Angeles 45, California

Stanford Research Institute
333 Ravenswood Avenue
Menlo Park, California

TAPCO Division
Thompson-Ramo-Wooldridge, Inc.
23555 Euclid Avenue
Cleveland 17, Ohio

Thiokol Chemical Corporation
Redstone Division
Huntsville, Alabama

United Aircraft Corporation
East Hartford Plant
400 Main Street
Hartford, Connecticut

United Technology Corporation
587 Methilda Avenue
Sunnyvale, California

Vought Astronautics
Box 5907
Dallas 22, Texas

Armour Research Foundation
Illinois Institute of Technology
10 West 35th Street
Chicago 16, Illinois

Battelle Memorial Institute
505 King Avenue
Columbus 1, Ohio

National Bureau of Standards
Cryogenic Engineering Laboratory
Boulder, Colorado